Copyrighted Materials
Copyright © 2005 John Wiley & Sons Retrieved from www.knovel.com

CHAPTER 4

Linear Wire Antennas

4.1 INTRODUCTION

Wire antennas, linear or curved, are some of the oldest, simplest, cheapest, and in many cases the most versatile for many applications. It should not then come as a surprise to the reader that we begin our analysis of antennas by considering some of the oldest, simplest, and most basic configurations. Initially we will try to minimize the complexity of the antenna structure and geometry to keep the mathematical details to a minimum.

4.2 INFINITESIMAL DIPOLE

An infinitesimal linear wire ($l \ll \lambda$) is positioned symmetrically at the origin of the coordinate system and oriented along the z axis, as shown in Figure 4.1(a). Although infinitesimal dipoles are not very practical, they are used to represent capacitor-plate (also referred to as *top-hat-loaded*) antennas. In addition, they are utilized as building blocks of more complex geometries. The end plates are used to provide capacitive loading in order to maintain the current on the dipole nearly uniform. Since the end plates are assumed to be small, their radiation is usually negligible. The wire, in addition to being very small ($l \ll \lambda$), is very thin ($a \ll \lambda$). The spatial variation of the current is assumed to be constant and given by

$$\mathbf{I}(z') = \hat{\mathbf{a}}_z I_0 \tag{4-1}$$

where $I_0 =$ constant.

4.2.1 Radiated Fields

To find the fields radiated by the current element, the two-step procedure of Figure 3.1 is used. It will be required to determine first **A** and **F** and then find the **E** and **H**. The functional relation between **A** and the source **J** is given by (3-49), (3-51), or (3-53). Similar relations are available for **F** and **M**, as given by (3-50), (3-52), and (3-54).

Antenna Theory: Analysis Design, Third Edition, by Constantine A. Balanis
ISBN 0-471-66782-X Copyright © 2005 John Wiley & Sons, Inc.

Since the source only carries an electric current $\mathbf{I}_e, \mathbf{I}_m$ and the potential function $\mathbf{F}$ are zero. To find $\mathbf{A}$ we write

$$\mathbf{A}(x, y, z) = \frac{\mu}{4\pi} \int_C \mathbf{I}_e(x', y', z') \frac{e^{-jkR}}{R} dl' \tag{4-2}$$

where (x, y, z) represent the observation point coordinates, (x', y', z') represent the coordinates of the source, R is the distance from any point on the source to the observation point, and path C is along the length of the source. For the problem of Figure 4.1

$$\mathbf{I}_e(x', y', z') = \hat{\mathbf{a}}_z I_0 \tag{4-3a}$$

$$x' = y' = z' = 0 \text{ (infinitesimal dipole)} \tag{4-3b}$$

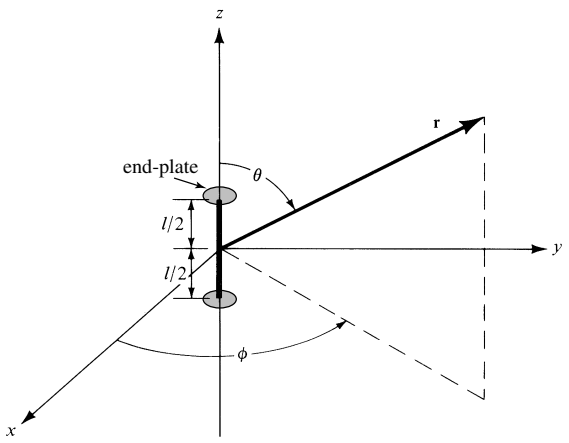

(a) Infinitesimal dipole

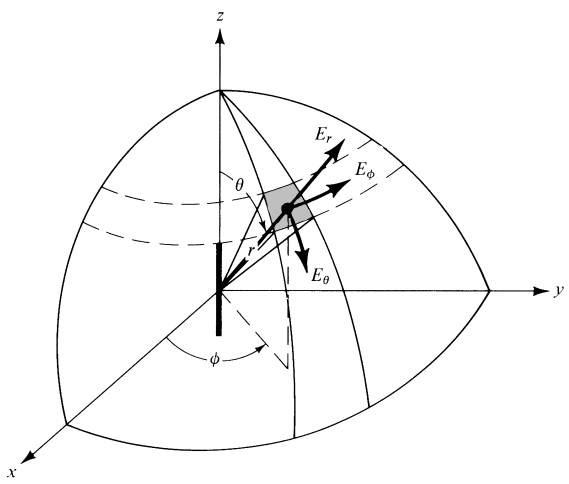

(b) Electric field orientation

Figure 4.1 Geometrical arrangement of an infinitesimal dipole and its associated electric-field components on a spherical surface.

$$R = \sqrt{(x-x')^2 + (y-y')^2 + (z-z')^2} = \sqrt{x^2+y^2+z^2}$$
$$= r = \text{constant} \tag{4-3c}$$
$$dl' = dz' \tag{4-3d}$$

so we can write (4-2) as

$$\boxed{\mathbf{A}(x,y,z) = \hat{\mathbf{a}}_z \frac{\mu I_0}{4\pi r} e^{-jkr} \int_{-l/2}^{+l/2} dz' = \hat{\mathbf{a}}_z \frac{\mu I_0 l}{4\pi r} e^{-jkr}} \tag{4-4}$$

The next step of the procedure is to find $\mathbf{H}_A$ using (3-2a) and then $\mathbf{E}_A$ using (3-15) or (3-10) with $\mathbf{J} = 0$. To do this, it is often much simpler to transform (4-4) from rectangular to spherical components and then use (3-2a) and (3-15) or (3-10) in spherical coordinates to find $\mathbf{H}$ and $\mathbf{E}$.

The transformation between rectangular and spherical components is given, in matrix form, by (VII-12a) (see Appendix VII)

$$\begin{bmatrix} A_r \\ A_\theta \\ A_\phi \end{bmatrix} = \begin{bmatrix} \sin\theta\cos\phi & \sin\theta\sin\phi & \cos\theta \\ \cos\theta\cos\phi & \cos\theta\sin\phi & -\sin\theta \\ -\sin\phi & \cos\phi & 0 \end{bmatrix} \begin{bmatrix} A_x \\ A_y \\ A_z \end{bmatrix} \tag{4-5}$$

For this problem, $A_x = A_y = 0$, so (4-5) using (4-4) reduces to

$$A_r = A_z \cos\theta = \frac{\mu I_0 l e^{-jkr}}{4\pi r} \cos\theta \tag{4-6a}$$
$$A_\theta = -A_z \sin\theta = -\frac{\mu I_0 l e^{-jkr}}{4\pi r} \sin\theta \tag{4-6b}$$
$$A_\phi = 0 \tag{4-6c}$$

Using the symmetry of the problem (no ϕ variations), (3-2a) can be expanded in spherical coordinates and written in simplified form as

$$\mathbf{H} = \hat{\mathbf{a}}_\phi \frac{1}{\mu r} \left[\frac{\partial}{\partial r}(r A_\theta) - \frac{\partial A_r}{\partial \theta} \right] \tag{4-7}$$

Substituting (4-6a)–(4-6c) into (4-7) reduces it to

$$\boxed{\begin{aligned} H_r &= H_\theta = 0 \qquad (4\text{-}8a) \\ H_\phi &= j\frac{k I_0 l \sin\theta}{4\pi r}\left[1 + \frac{1}{jkr}\right] e^{-jkr} \qquad (4\text{-}8b) \end{aligned}}$$

The electric field $\mathbf{E}$ can now be found using (3-15) or (3-10) with $\mathbf{J} = 0$. That is,

$$\mathbf{E} = \mathbf{E}_A = -j\omega\mathbf{A} - j\frac{1}{\omega\mu\epsilon}\nabla(\nabla \cdot \mathbf{A}) = \frac{1}{j\omega\epsilon}\nabla \times \mathbf{H} \tag{4-9}$$

Substituting (4-6a)–(4-6c) or (4-8a)–(4-8b) into (4-9) reduces it to

$$E_r = \eta \frac{I_0 l \cos\theta}{2\pi r^2}\left[1 + \frac{1}{jkr}\right] e^{-jkr} \tag{4-10a}$$

$$E_\theta = j\eta \frac{k I_0 l \sin\theta}{4\pi r}\left[1 + \frac{1}{jkr} - \frac{1}{(kr)^2}\right] e^{-jkr} \tag{4-10b}$$

$$E_\phi = 0 \tag{4-10c}$$

The **E**- and **H**-field components are valid everywhere, except on the source itself, and they are sketched in Figure 4.1(b) on the surface of a sphere of radius r. It is a straightforward exercise to verify Equations (4-10a)–(4-10c), and this is left as an exercise to the reader (Prob. 4.13).

4.2.2 Power Density and Radiation Resistance

The input impedance of an antenna, which consists of real and imaginary parts, was discussed in Section 2.13. For a lossless antenna, the real part of the input impedance was designated as radiation resistance. It is through the mechanism of the radiation resistance that power is transferred from the guided wave to the free-space wave. To find the input resistance for a lossless antenna, the Poynting vector is formed in terms of the **E**- and **H**-fields radiated by the antenna. By integrating the Poynting vector over a closed surface (usually a sphere of constant radius), the total power radiated by the source is found. The real part of it is related to the input resistance.

For the infinitesimal dipole, the complex Poynting vector can be written using (4-8a)–(4-8b) and (4-10a)–(4-10c) as

$$\begin{aligned}\mathbf{W} &= \tfrac{1}{2}(\mathbf{E} \times \mathbf{H}^*) = \tfrac{1}{2}(\hat{\mathbf{a}}_r E_r + \hat{\mathbf{a}}_\theta E_\theta) \times (\hat{\mathbf{a}}_\phi H_\phi^*) \\ &= \tfrac{1}{2}(\hat{\mathbf{a}}_r E_\theta H_\phi{}^* - \hat{\mathbf{a}}_\theta E_r H_\phi{}^*)\end{aligned} \tag{4-11}$$

whose radial W_r and transverse W_θ components are given, respectively, by

$$W_r = \frac{\eta}{8}\left|\frac{I_0 l}{\lambda}\right|^2 \frac{\sin^2\theta}{r^2}\left[1 - j\frac{1}{(kr)^3}\right] \tag{4-12a}$$

$$W_\theta = j\eta \frac{k|I_0 l|^2 \cos\theta \sin\theta}{16\pi^2 r^3}\left[1 + \frac{1}{(kr)^2}\right] \tag{4-12b}$$

The complex power moving in the radial direction is obtained by integrating (4-11)–(4-12b) over a closed sphere of radius r. Thus it can be written as

$$P = \oiint_S \mathbf{W} \cdot d\mathbf{s} = \int_0^{2\pi}\int_0^{\pi} (\hat{\mathbf{a}}_r W_r + \hat{\mathbf{a}}_\theta W_\theta) \cdot \hat{\mathbf{a}}_r r^2 \sin\theta \, d\theta \, d\phi \tag{4-13}$$

which reduces to

$$P = \int_0^{2\pi}\int_0^{\pi} W_r r^2 \sin\theta \, d\theta \, d\phi = \eta\frac{\pi}{3}\left|\frac{I_0 l}{\lambda}\right|^2\left[1 - j\frac{1}{(kr)^3}\right] \tag{4-14}$$

The transverse component W_θ of the power density does not contribute to the integral. Thus (4-14) does not represent the total complex power radiated by the antenna. Since W_θ, as given by (4-12b), is purely imaginary, it will not contribute to any real radiated power. However, it does contribute to the imaginary (reactive) power which along with the second term of (4-14) can be used to determine the total reactive power of the antenna. *The reactive power density, which is most dominant for small values of kr, has both radial and transverse components. It merely changes between outward and inward directions to form a standing wave at a rate of twice per cycle. It also moves in the transverse direction as suggested by (4-12b).*

Equation (4-13), which gives the real and imaginary power that is moving outwardly, can also be written as

$$P = \frac{1}{2}\iint_S \mathbf{E} \times \mathbf{H}^* \cdot d\mathbf{s} = \eta\left(\frac{\pi}{3}\right)\left|\frac{I_0 l}{\lambda}\right|^2\left[1 - j\frac{1}{(kr)^3}\right]$$

$$= P_{\text{rad}} + j2\omega(\tilde{W}_m - \tilde{W}_e) \tag{4-15}$$

where

P = power (in radial direction)
P_{rad} = time-average power radiated
$\tilde{W}_m$ = time-average magnetic energy density (in radial direction)
$\tilde{W}_e$ = time-average electric energy density (in radial direction)
$2\omega(\tilde{W}_m - \tilde{W}_e)$ = time-average imaginary (reactive) power (in radial direction)

From (4-14)

$$P_{\text{rad}} = \eta\left(\frac{\pi}{3}\right)\left|\frac{I_0 l}{\lambda}\right|^2 \tag{4-16}$$

and

$$2\omega(\tilde{W}_m - \tilde{W}_e) = -\eta\left(\frac{\pi}{3}\right)\left|\frac{I_0 l}{\lambda}\right|^2 \frac{1}{(kr)^3} \tag{4-17}$$

It is clear from (4-17) that the radial electric energy must be larger than the radial magnetic energy. For large values of kr ($kr \gg 1$ or $r \gg \lambda$), the reactive power diminishes and vanishes when $kr = \infty$.

Since the antenna radiates its real power through the radiation resistance, for the infinitesimal dipole it is found by equating (4-16) to

$$\boxed{P_{\text{rad}} = \eta\left(\frac{\pi}{3}\right)\left|\frac{I_0 l}{\lambda}\right|^2 = \frac{1}{2}|I_0|^2 R_r} \tag{4-18}$$

where R_r is the radiation resistance. Equation (4-18) reduces to

$$\boxed{R_r = \eta\left(\frac{2\pi}{3}\right)\left(\frac{l}{\lambda}\right)^2 = 80\pi^2\left(\frac{l}{\lambda}\right)^2} \tag{4-19}$$

for a free-space medium ($\eta \simeq 120\pi$). It should be pointed out that the radiation resistance of (4-19) represents the total radiation resistance since (4-12b) does not contribute to it.

For a wire antenna to be classified as an infinitesimal dipole, its overall length must be very small (usually $l \leq \lambda/50$).

Example 4.1

Find the radiation resistance of an infinitesimal dipole whose overall length is $l = \lambda/50$.

Solution: Using (4-19)

$$R_r = 80\pi^2 \left(\frac{l}{\lambda}\right)^2 = 80\pi^2 \left(\frac{1}{50}\right)^2 = 0.316 \text{ ohms}$$

Since the radiation resistance of an infinitesimal dipole is about 0.3 ohms, it will present a very large mismatch when connected to practical transmission lines, many of which have characteristic impedances of 50 or 75 ohms. The reflection efficiency (e_r) and hence the overall efficiency (e_0) will be very small.

The reactance of an infinitesimal dipole is capacitive. This can be illustrated by considering the dipole as a flared open-circuited transmission line, as discussed in Section 1.4. Since the input impedance of an open-circuited transmission line a distance $l/2$ from its open end is given by $Z_{in} = -jZ_c \cot(\beta l/2)$, where Z_c is its characteristic impedance, it will always be negative (capacitive) for $l \ll \lambda$.

4.2.3 Radian Distance and Radian Sphere

The **E**- and **H**-fields for the infinitesimal dipole, as represented by (4-8a)–(4-8b) and (4-10a)–(4-10c), are valid everywhere (except on the source itself). An inspection of these equations reveals the following:

(a) At a distance $r = \lambda/2\pi$ (or $kr = 1$), which is referred to as the *radian distance*, the magnitude of the first and second terms within the brackets of (4-8b) and (4-10a) is the same. Also at the radian distance the magnitude of all three terms within the brackets of (4-10b) is identical; the only term that contributes to the total field is the second, because the first and third terms cancel each other. This is illustrated in Figure 4.2.

(b) At distances less than the radian distance $r < \lambda/2\pi$ ($kr < 1$), the magnitude of the second term within the brackets of (4-8b) and (4-10a) is greater than the first term and begins to dominate as $r \ll \lambda/2\pi$. For (4-10b) and $r < \lambda/2\pi$, the magnitude of the third term within the brackets is greater than the magnitude of the first and second terms while the magnitude of the second term is greater than that of the first one; each of these terms begins to dominate as $r \ll \lambda/2\pi$. This is illustrated in Figure 4.2. The region $r < \lambda/2\pi$ ($kr < 1$) is referred to as the *near-field* region, and the energy in that region is basically imaginary (stored).

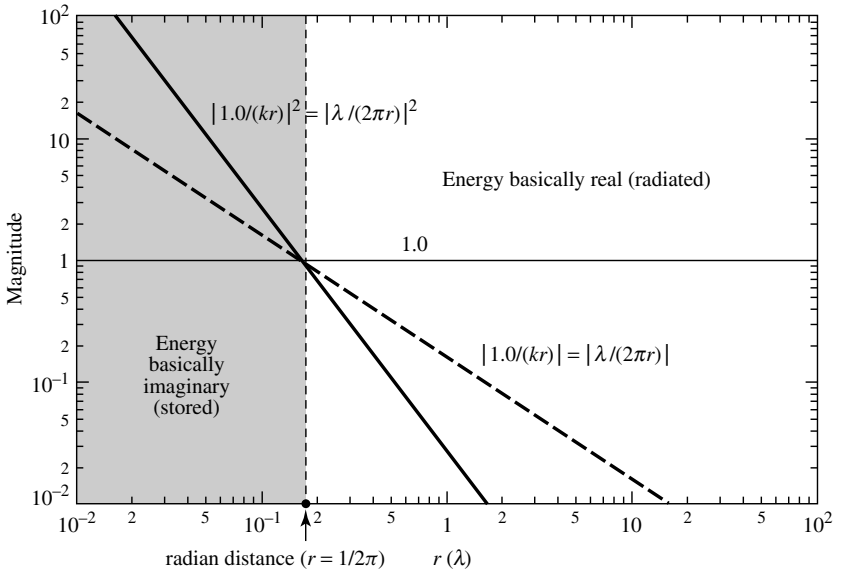

Figure 4.2 Magnitude variation, as a function of the radial distance, of the field terms radiated by an infinitesimal dipole.

(c) At distances greater than the radian distance $r > \lambda/2\pi$ $(kr > 1)$, the first term within the brackets of (4-8b) and (4-10a) is greater than the magnitude of the second term and begins to dominate as $r \gg \lambda/2\pi$ $(kr \gg 1)$. For (4-10b) and $r > \lambda/2\pi$, the first term within the brackets is greater than the magnitude of the second and third terms while the magnitude of the second term is greater than that of the third; each of these terms begins to dominate as $r \gg \lambda/2\pi$. This is illustrated in Figure 4.2. The region $r > \lambda/2\pi$ $(kr > 1)$ is referred to as the *intermediate-field* region while that for $r \gg \lambda/2\pi$ $(kr \gg 1)$ is referred to as the *far-field* region, and the energy in that region is basically real (radiated).

(d) The sphere with radius equal to the radian distance $(r = \lambda/2\pi)$ is referred as the *radian sphere*, and it defines the region within which the reactive power density is greater than the radiated power density [1]–[3]. For an antenna, the radian sphere represents the volume occupied mainly by the stored energy of the antenna's electric and magnetic fields. Outside the radian sphere the radiated power density is greater than the reactive power density and begins to dominate as $r \gg \lambda/2\pi$. *Therefore the radian sphere can be used as a reference, and it defines the transition between stored energy pulsating primarily in the $\pm\theta$ direction [represented by (4-12b)] and energy radiating in the radial (r) direction [represented by the first term of (4-12a); the second term represents stored energy pulsating inwardly and outwardly in the radial (r) direction].* Similar behavior, where the power density near the antenna is primarily reactive and far away is primarily real, is exhibited by all antennas, although not exactly at the radian distance.

4.2.4 Near-Field ($kr \ll 1$) Region

An inspection of (4-8a)–(4-8b) and (4-10a)–(4-10c) reveals that for $kr \ll \lambda$ or $r \ll \lambda/2\pi$ they can be reduced in much simpler form and can be approximated by

$$\left.\begin{aligned} E_r &\simeq -j\eta \frac{I_0 l e^{-jkr}}{2\pi kr^3} \cos\theta && \text{(4-20a)} \\ E_\theta &\simeq -j\eta \frac{I_0 l e^{-jkr}}{4\pi kr^3} \sin\theta && \text{(4-20b)} \\ E_\phi &= H_r = H_\theta = 0 && \text{(4-20c)} \\ H_\phi &\simeq \frac{I_0 l e^{-jkr}}{4\pi r^2} \sin\theta && \text{(4-20d)} \end{aligned}\right\} \quad kr \ll 1$$

The **E**-field components, E_r and E_θ, are in time-phase but they are in time-phase quadrature with the **H**-field component H_ϕ; therefore there is no time-average power flow associated with them. This is demonstrated by forming the time-average power density as

$$\mathbf{W}_{\text{av}} = \tfrac{1}{2}\text{Re}[\mathbf{E} \times \mathbf{H}^*] = \tfrac{1}{2}\text{Re}[\hat{\mathbf{a}}_r E_\theta H^*{}_\phi - \hat{\mathbf{a}}_\theta E_r H^*{}_\phi] \tag{4-21}$$

which by using (4-20a)–(4-20d) reduces to

$$\mathbf{W}_{\text{av}} = \frac{1}{2}\text{Re}\left[-\hat{\mathbf{a}}_r j\frac{\eta}{k}\left|\frac{I_0 l}{4\pi}\right|^2 \frac{\sin^2\theta}{r^5} + \hat{\mathbf{a}}_\theta j\frac{\eta}{k}\frac{|I_0 l|^2}{8\pi^2}\frac{\sin\theta\cos\theta}{r^5}\right] = 0 \tag{4-22}$$

The condition of $kr \ll 1$ can be satisfied at moderate distances away from the antenna provided that the frequency of operation is very low. Equations (4-20a) and (4-20b) are similar to those of a static electric dipole and (4-20d) to that of a static current element. Thus we usually refer to (4-20a)–(4-20d) as the *quasistationary fields*.

4.2.5 Intermediate-Field ($kr > 1$) Region

As the values of kr begin to increase and become greater than unity, the terms that were dominant for $kr \ll 1$ become smaller and eventually vanish. For moderate values of kr the **E**-field components lose their in-phase condition and approach time-phase quadrature. Since their magnitude is not the same, in general, they form a rotating vector whose extremity traces an ellipse. This is analogous to the polarization problem except that the vector rotates in a plane parallel to the direction of propagation and is usually referred to as the *cross field*. At these intermediate values of kr, the E_θ and H_ϕ components approach time-phase, which is an indication of the formation of time-average power flow in the outward (radial) direction (radiation phenomenon).

As the values of kr become moderate ($kr > 1$), the field expressions can be approximated again but in a different form. In contrast to the region where $kr \ll 1$, the first term within the brackets in (4-8b) and (4-10a) becomes more dominant and the second term can be neglected. The same is true for (4-10b) where the second and third terms

become less dominant than the first. Thus we can write for $kr > 1$

$$\left.\begin{aligned} E_r &\simeq \eta \frac{I_0 l e^{-jkr}}{2\pi r^2} \cos\theta && \text{(4-23a)} \\ E_\theta &\simeq j\eta \frac{k I_0 l e^{-jkr}}{4\pi r} \sin\theta && \text{(4-23b)} \\ E_\phi &= H_r = H_\theta = 0 && \text{(4-23c)} \\ H_\phi &\simeq j \frac{k I_0 l e^{-jkr}}{4\pi r} \sin\theta && \text{(4-23d)} \end{aligned}\right\} \quad kr > 1$$

The total electric field is given by

$$\mathbf{E} = \hat{\mathbf{a}}_r E_r + \hat{\mathbf{a}}_\theta E_\theta \tag{4-24}$$

whose magnitude can be written as

$$|\mathbf{E}| = \sqrt{|E_r|^2 + |E_\theta|^2} \tag{4-25}$$

4.2.6 Far-Field ($kr \gg 1$) Region

Since (4-23a)–(4-23d) are valid only for values of $kr > 1$ ($r > \lambda$), then E_r will be smaller than E_θ because E_r is inversely proportional to r^2 where E_θ is inversely proportional to r. In a region where $kr \gg 1$, (4-23a)–(4-23d) can be simplified and approximated by

$$\left.\begin{aligned} E_\theta &\simeq j\eta \frac{k I_0 l e^{-jkr}}{4\pi r} \sin\theta && \text{(4-26a)} \\ E_r &\simeq E_\phi = H_r = H_\theta = 0 && \text{(4-26b)} \\ H_\phi &\simeq j \frac{k I_0 l e^{-jkr}}{4\pi r} \sin\theta && \text{(4-26c)} \end{aligned}\right\} \quad kr \gg 1$$

The ratio of E_θ to H_ϕ is equal to

$$Z_w = \frac{E_\theta}{H_\phi} \simeq \eta \tag{4-27}$$

where

Z_w = wave impedance

η = intrinsic impedance ($377 \simeq 120\pi$ ohms for free-space)

The **E**- and **H**-field components are perpendicular to each other, transverse to the radial direction of propagation, and the r variations are separable from those of θ and ϕ. The shape of the pattern is not a function of the radial distance r, and the fields form a *T*ransverse *E*lectro*M*agnetic (TEM) wave whose wave impedance is equal to the intrinsic impedance of the medium. As it will become even more evident in

later chapters, *this relationship is applicable in the far-field region of all antennas of finite dimensions*. Equations (4-26a)–(4-26c) can also be derived using the procedure outlined and relationships developed in Section 3.6. This is left as an exercise to the reader (Prob. 4.15).

Example 4.2

For an infinitesimal dipole determine and interpret the vector effective length [see Section 2.15, Figure 2.29(a)]. At what incidence angle does the open-circuit maximum voltage occurs at the output terminals of the dipole if the electric-field intensity of the incident wave is 10 mV/m? The length of the dipole is 10 cm.

Solution: Using (4-26a) and the effective length as defined by (2-92), we can write that

$$E_\theta = j\eta \frac{kI_0 l e^{-jkr}}{4\pi r} \sin\theta = -\hat{\mathbf{a}}_\theta j\eta \frac{kI_0 e^{-jkr}}{4\pi r} \cdot (-\hat{\mathbf{a}}_\theta l \sin\theta)$$
$$= -\hat{\mathbf{a}}_\theta j\eta \frac{kI_0 e^{-jkr}}{4\pi r} \cdot \boldsymbol{\ell}_e$$

Therefore, the effective length is

$$\boldsymbol{\ell}_e = -\hat{\mathbf{a}}_\theta l \sin\theta$$

whose maximum value occurs when $\theta = 90^\circ$, and it is equal to l. Therefore, to achieve maximum output the wave must be incident upon the dipole at a normal incidence angle ($\theta = 90^\circ$).

The open-circuit maximum voltage is equal to

$$V_{oc}|_{\max} = |\mathbf{E}^i \cdot \boldsymbol{\ell}_e|_{\max} = |\hat{\mathbf{a}}_\theta 10 \times 10^{-3} \cdot (-\hat{\mathbf{a}}_\theta l \sin\theta)|_{\max}$$
$$= 10 \times 10^{-3} l = 10^{-3} \text{ volts}$$

4.2.7 Directivity

The real power P_{rad} radiated by the dipole was found in Section 4.2.2, as given by (4-16). The same expression can be obtained by first forming the average power density, using (4-26a)–(4-26c). That is,

$$\mathbf{W}_{\text{av}} = \frac{1}{2}\text{Re}(\mathbf{E} \times \mathbf{H}^*) = \hat{\mathbf{a}}_r \frac{1}{2\eta}|E_\theta|^2 = \hat{\mathbf{a}}_r \frac{\eta}{2}\left|\frac{kI_0 l}{4\pi}\right|^2 \frac{\sin^2\theta}{r^2} \tag{4-28}$$

Integrating (4-28) over a closed sphere of radius r reduces it to (4-16). This is left as an exercise to the reader (Prob. 4.14).

Associated with the average power density of (4-28) is a radiation intensity U which is given by

$$U = r^2 \, W_{\text{av}} = \frac{\eta}{2}\left(\frac{kI_0 l}{4\pi}\right)^2 \sin^2\theta = \frac{r^2}{2\eta}|E_\theta(r, \theta, \phi)|^2 \tag{4-29}$$

and it conforms with (2-12a). The normalized pattern of (4-29) is shown in Figure 4.3. The maximum value occurs at $\theta = \pi/2$ and it is equal to

$$U_{\max} = \frac{\eta}{2}\left(\frac{kI_0 l}{4\pi}\right)^2 \tag{4-30}$$

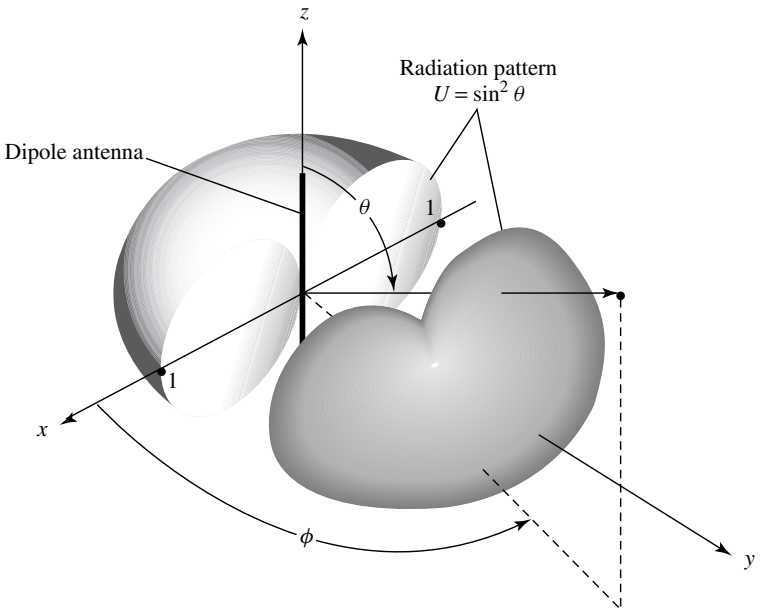

Figure 4.3 Three-dimensional radiation pattern of infinitesimal dipole.

Using (4-16) and (4-30), the directivity reduces to

$$\boxed{D_0 = 4\pi \frac{U_{\max}}{P_{\text{rad}}} = \frac{3}{2}} \tag{4-31}$$

and the maximum effective aperture to

$$\boxed{A_{em} = \left(\frac{\lambda^2}{4\pi}\right) D_0 = \frac{3\lambda^2}{8\pi}} \tag{4-32}$$

The radiation resistance of the dipole can be obtained by the definition of (4-18). Since the radiated power obtained by integrating (4-28) over a closed sphere is the same as that of (4-16), the radiation resistance using it will also be the same as obtained previously and given by (4-19).

Integrating the complex Poynting vector over a closed sphere, as was done in (4-13), results in the power (real and imaginary) directed in the radial direction. Any transverse components of power density, as given by (4-12b), will not be captured by the integration even though they are part of the overall power. *Because of this limitation, this method cannot be used to derive the input reactance of the antenna.*

The procedure that can be used to derive the far-zone electric and magnetic fields radiated by an antenna, along with some of the most important parameters/figures of merit that are used to describe the performance of an antenna, are summarized in Table 4.1.

TABLE 4.1 Summary of Procedure to Determine the Far-Field Radiation Characteristics of an Antenna

1. Specify electric and/or magnetic current densities **J, M** [physical or equivalent (see Chapter 3, Figure 3.1)]
2. Determine vector potential components $A_\theta,\ A_\phi$ and/or $F_\theta,\ F_\phi$ using (3-46)–(3-54) in far field
3. Find far-zone **E** and **H** radiated fields ($E_\theta,\ E_\phi;\ H_\theta,\ H_\phi$) using (3-58a)–(3-58b)
4. Form either

   a. $$\mathbf{W}_{\text{rad}}(r,\theta,\phi) = \mathbf{W}_{\text{av}}(r,\theta,\phi) = \frac{1}{2}\text{Re}[\mathbf{E}\times\mathbf{H}^*]$$
   $$\simeq \frac{1}{2}\text{Re}\ [(\hat{a}_\theta E_\theta + \hat{a}_\phi E_\phi)\times(\hat{a}_\theta H_\theta^* + \hat{a}_\phi H_\phi^*)]$$
   $$\mathbf{W}_{\text{rad}}(r,\theta,\phi) = \hat{a}_r\frac{1}{2}\left[\frac{|E_\theta|^2+|E_\phi|^2}{\eta}\right] = \hat{a}_r\frac{1}{r^2}|f(\theta,\phi)|^2$$

   or

   b. $U(\theta,\phi) = r^2\ W_{\text{rad}}(r,\theta,\phi) = |f(\theta,\phi)|^2$
5. Determine either

   a. $$P_{\text{rad}} = \int_0^{2\pi}\int_0^{\pi} W_{\text{rad}}(r,\theta,\phi)r^2\sin\theta\,d\theta\,d\phi$$

   or

   b. $$P_{\text{rad}} = \int_0^{2\pi}\int_0^{\pi} U(\theta,\phi)\sin\theta\,d\theta\,d\phi$$
6. Find directivity using
$$D(\theta,\phi) = \frac{U(\theta,\phi)}{U_0} = \frac{4\pi U(\theta,\phi)}{P_{\text{rad}}}$$
$$D_0 = D_{\max} = D(\theta,\phi)|_{\max} = \frac{U(\theta,\phi)|_{\max}}{U_0} = \frac{4\pi U(\theta,\phi)|_{\max}}{P_{\text{rad}}}$$
7. Form *normalized* power amplitude pattern:
$$P_n(\theta,\phi) = \frac{U(\theta,\phi)}{U_{\max}}$$
8. Determine radiation and input resistance:
$$R_r = \frac{2P_{\text{rad}}}{|I_0|^2};\qquad R_{in} = \frac{R_r}{\sin^2\left(\dfrac{kl}{2}\right)}$$
9. Determine maximum effective area
$$A_{em} = \frac{\lambda^2}{4\pi}D_0$$

4.3 SMALL DIPOLE

The creation of the current distribution on a thin wire was discussed in Section 1.4, and it was illustrated with some examples in Figure 1.16. The radiation properties of an infinitesimal dipole, which is usually taken to have a length $l \le \lambda/50$, were discussed

in the previous section. Its current distribution was assumed to be constant. Although a constant current distribution is not realizable (other than top-hat-loaded elements), it is a mathematical quantity that is used to represent actual current distributions of antennas that have been incremented into many small lengths.

A better approximation of the current distribution of wire antennas, whose lengths are usually $\lambda/50 < l \leq \lambda/10$, is the triangular variation of Figure 1.16(a). The sinusoidal variations of Figures 1.16(b)–(c) are more accurate representations of the current distribution of any length wire antenna.

The most convenient geometrical arrangement for the analysis of a dipole is usually to have it positioned symmetrically about the origin with its length directed along the z-axis, as shown in Figure 4.4(a). This is not necessary, but it is usually the most convenient. The current distribution of a small dipole ($\lambda/50 < l \leq \lambda/10$) is shown in

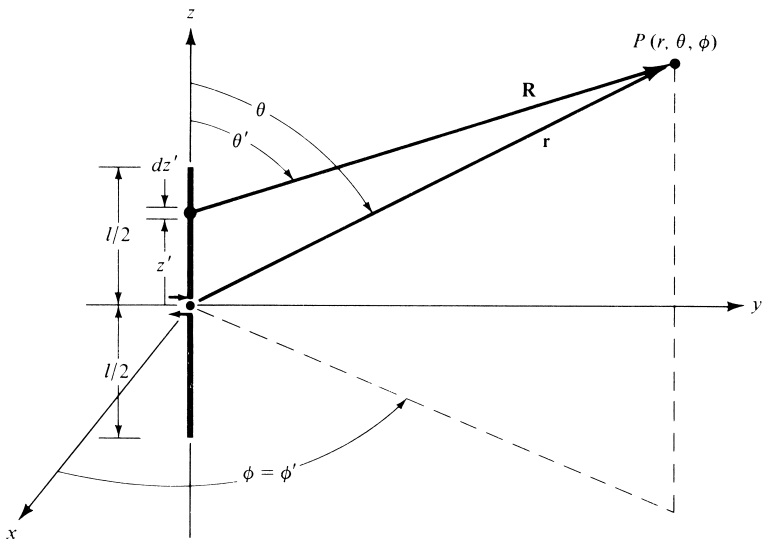

(a) Dipole and geometry

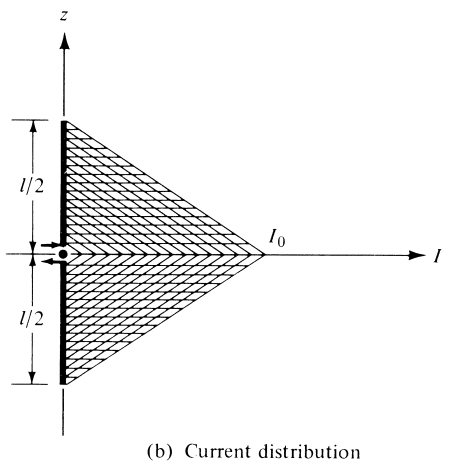

(b) Current distribution

Figure 4.4 Geometrical arrangement of dipole and current distribution.

Figure 4.4(b), and it is given by

$$\mathbf{I}_e(x', y', z') = \begin{cases} \hat{\mathbf{a}}_z I_0 \left(1 - \dfrac{2}{l} z'\right), & 0 \le z' \le l/2 \\ \hat{\mathbf{a}}_z I_0 \left(1 + \dfrac{2}{l} z'\right), & -l/2 \le z' \le 0 \end{cases} \tag{4-33}$$

where $I_0 =$ constant.

Following the procedure established in the previous section, the vector potential of (4-2) can be written using (4-33) as

$$\begin{aligned} \mathbf{A}(x, y, z) = \frac{\mu}{4\pi} \Bigg[& \hat{\mathbf{a}}_z \int_{-l/2}^{0} I_0 \left(1 + \frac{2}{l} z'\right) \frac{e^{-jkR}}{R} \, dz' \\ & + \hat{\mathbf{a}}_z \int_{0}^{l/2} I_0 \left(1 - \frac{2}{l} z'\right) \frac{e^{-jkR}}{R} \, dz' \Bigg] \end{aligned} \tag{4-34}$$

Because the overall length of the dipole is very small (usually $l \le \lambda/10$), the values of R for different values of z' along the length of the wire ($-l/2 \le z' \le l/2$) are not much different from r. Thus R can be approximated by $R \simeq r$ throughout the integration path. The maximum phase error in (4-34) by allowing $R = r$ for $\lambda/50 < l \le \lambda/10$, will be $kl/2 = \pi/10$ rad $= 18^\circ$ for $l = \lambda/10$. Smaller values will occur for the other lengths. As it will be shown in the next section, this amount of phase error is usually considered negligible and has very little effect on the overall radiation characteristics. Performing the integration, (4-34) reduces to

$$\mathbf{A} = \hat{\mathbf{a}}_z A_z = \hat{\mathbf{a}}_z \frac{1}{2} \left[\frac{\mu I_0 l e^{-jkr}}{4\pi r} \right] \tag{4-35}$$

which is one-half of that obtained in the previous section for the infinitesimal dipole and given by (4-4).

The potential function given by (4-35) becomes a more accurate approximation as $kr \to \infty$. This is also the region of most practical interest, and it has been designated as the *far-field* region. Since the potential function for the triangular distribution is one-half of the corresponding one for the constant (uniform) current distribution, the corresponding fields of the former are one-half of the latter. Thus we can write the **E**- and **H**-fields radiated by a small dipole as

$$\left.\begin{aligned} E_\theta &\simeq j\eta \frac{k I_0 l e^{-jkr}}{8\pi r} \sin\theta \qquad \text{(4-36a)} \\ E_r &\simeq E_\phi = H_r = H_\theta = 0 \qquad \text{(4-36b)} \\ H_\phi &\simeq j \frac{k I_0 l e^{-jkr}}{8\pi r} \sin\theta \qquad \text{(4-36c)} \end{aligned}\right\} \quad kr \gg 1$$

with the wave impedance equal, as before, to (4-27).

Since the directivity of an antenna is controlled by the relative shape of the field or power pattern, the directivity, and maximum effective area of this antenna are the

same as the ones with the constant current distribution given by (4-31) and (4-32), respectively.

The radiation resistance of the antenna is strongly dependent upon the current distribution. Using the procedure established for the infinitesimal dipole, it can be shown that for the small dipole its radiated power is one-fourth ($\frac{1}{4}$) of (4-18). Thus the radiation resistance reduces to

$$\boxed{R_r = \frac{2P_{\text{rad}}}{|I_0|^2} = 20\pi^2 \left(\frac{l}{\lambda}\right)^2} \tag{4-37}$$

which is also one-fourth ($\frac{1}{4}$) of that obtained for the infinitesimal dipole as given by (4-19). Their relative patterns (shapes) are the same and are shown in Figure 4.3.

4.4 REGION SEPARATION

Before we attempt to solve for the fields radiated by a finite dipole of any length, it would be very desirable to discuss the separation of the space surrounding an antenna into three regions; namely, the *reactive near-field, radiating near-field* (*Fresnel*) and the *far-field* (*Fraunhofer*) which were introduced briefly in Section 2.2.4. This is necessary because for a dipole antenna of any length and any current distribution, it will become increasingly difficult to solve for the fields everywhere. Approximations can be made, especially for the far-field (Fraunhofer) region, which is usually the one of most practical interest, to simplify the formulation to yield closed form solutions. The same approximations used to simplify the formulation of the fields radiated by a finite dipole are also used to formulate the fields radiated by most practical antennas. So it will be very important to introduce them properly and understand their implications upon the solution.

The difficulties in obtaining closed form solutions that are valid everywhere for any practical antenna stem from the inability to perform the integration of

$$\mathbf{A}(x, y, z) = \frac{\mu}{4\pi} \int_C \mathbf{I}_e(x', y', z') \frac{e^{-jkR}}{R}\, dl' \tag{4-38}$$

where

$$R = \sqrt{(x - x')^2 + (y - y')^2 + (z - z')^2} \tag{4-38a}$$

For a finite dipole with sinusoidal current distribution, the integral of (4-38) can be reduced to a closed form that is valid everywhere! This will be shown in Chapter 8. The length R is defined as the distance from any point on the source to the observation point. The integral of (4-38) was used to solve for the fields of infinitesimal and small dipoles in Sections 4.1 and 4.2. However in the first case (infinitesimal dipole) $R = r$ and in the second case (small dipole) R was approximated by $r (R \simeq r)$ because the length of the dipole was restricted to be $l \leq \lambda/10$. The major simplification of (4-38) will be in the approximation of R.

A very thin dipole of finite length l is symmetrically positioned about the origin with its length directed along the z-axis, as shown in Figure 4.5(a). Because the wire is assumed to be very thin ($x' = y' = 0$), we can write (4-38) as

$$R = \sqrt{(x - x')^2 + (y - y')^2 + (z - z')^2} = \sqrt{x^2 + y^2 + (z - z')^2} \tag{4-39}$$

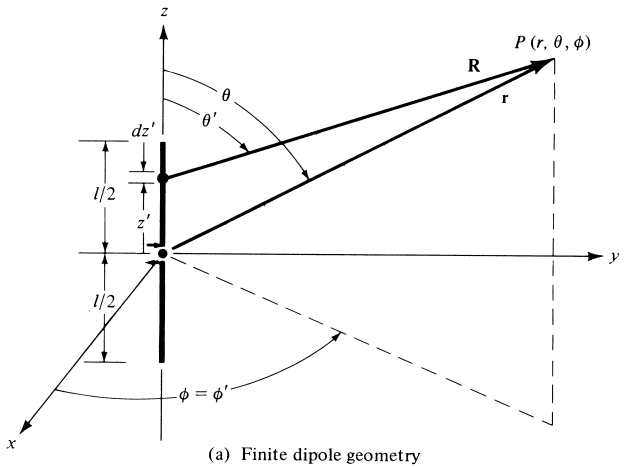

(a) Finite dipole geometry

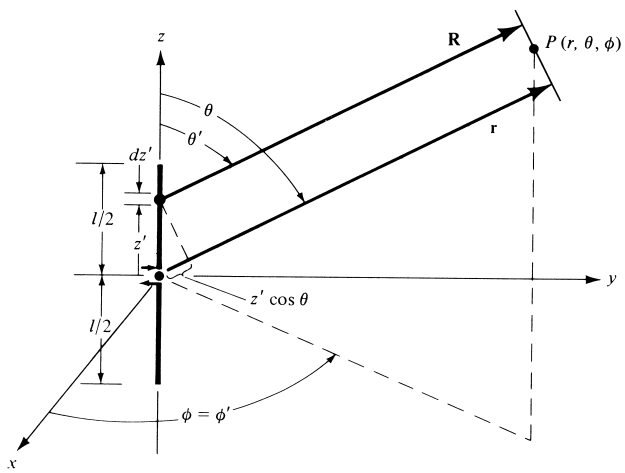

(b) Geometrical arrangement for far-field approximations

Figure 4.5 Finite dipole geometry and far-field approximations.

which when expanded can be written as

$$R = \sqrt{(x^2 + y^2 + z^2) + (-2zz' + z'^2)} = \sqrt{r^2 + (-2rz'\cos\theta + z'^2)} \tag{4-40}$$

where

$$r^2 = x^2 + y^2 + z^2 \tag{4-40a}$$

$$z = r\cos\theta \tag{4-40b}$$

Using the binomial expansion, we can write (4-40) in a series as

$$R = r - z'\cos\theta + \frac{1}{r}\left(\frac{z'^2}{2}\sin^2\theta\right) + \frac{1}{r^2}\left(\frac{z'^3}{2}\cos\theta\sin^2\theta\right) + \cdots \tag{4-41}$$

whose higher order terms become less significant provided $r \gg z'$.

4.4.1 Far-Field (Fraunhofer) Region

The most convenient simplification of (4-41), other than $R \simeq r$, will be to approximate it by its first two terms, or

$$R \simeq r - z' \cos\theta \tag{4-42}$$

The most significant neglected term of (4-41) is the third whose maximum value is

$$\frac{1}{r}\left(\frac{z'^2}{2}\sin^2\theta\right)_{\max} = \frac{z'^2}{2r} \qquad \text{when } \theta = \pi/2 \tag{4-43}$$

When (4-43) attains its maximum value, the fourth term of (4-41) vanishes because $\theta = \pi/2$. It can be shown that the higher order terms not shown in (4-41) also vanish. Therefore approximating (4-41) by (4-42) introduces a *maximum* error given by (4-43).

It has been shown by many investigators through numerous examples that for most practical antennas, *with overall lengths greater than a wavelength* ($l > \lambda$), a maximum total phase error of $\pi/8$ rad (22.5°) is not very detrimental in the analytical formulations. Using that as a criterion we can write, using (4-43), that the maximum phase error should always be

$$\frac{k(z')^2}{2r} \leq \frac{\pi}{8} \tag{4-44}$$

which for $-l/2 \leq z' \leq l/2$ reduces to

$$r \geq 2\left(\frac{l^2}{\lambda}\right) \tag{4-45}$$

Equation (4-45) simply states that to maintain the maximum phase error of an antenna equal to or less than $\pi/8$ rad (22.5°), the observation distance r must equal or be greater than $2l^2/\lambda$ where l is the largest* dimension of the antenna structure. The usual simplification for the far-field region is to approximate the R in the exponential (e^{-jkR}) of (4-38) by (4-42) and the R in the denominator of (4-38) by $R \simeq r$. These simplifications are designated as the far-field approximations and are usually denoted in the literature as

Far-field Approximations

$$\begin{aligned} R &\simeq r - z'\cos\theta \qquad \text{for phase terms} \\ R &\simeq r \qquad\qquad\qquad\ \ \text{for amplitude terms} \end{aligned} \tag{4-46}$$

provided r satisfies (4-45).

It may be advisable to illustrate the approximation (4-46) geometrically. For $R \simeq r - z'\cos\theta$, where θ is the angle measured from the z-axis, the radial vectors $\mathbf{R}$ and $\mathbf{r}$ must be parallel to each other, as shown in Figure 4.5(b). For any other antenna whose maximum dimension is D, the approximation of (4-46) is valid provided the observations are made at a distance

$$r \geq 2\frac{D^2}{\lambda} \tag{4-47}$$

For an aperture antenna the maximum dimension is taken to be its diagonal.

*Provided the overall length (l) of the antenna is large compared to the wavelength [see IEEE Standard Definitions of Terms for Antennas, IEEE Std (145-1983)].

For most practical antennas, whose overall length is large compared to the wavelength, these are adequate approximations which have been shown by many investigators through numerous examples to give valid results in pattern predictions. Some discrepancies are evident in regions of low intensity (usually below -25 dB). This is illustrated in Figure 2.9 where the patterns of a paraboloidal antenna for $R = \infty$ and $R = 2D^2/\lambda$ differ at levels below -25 dB. Allowing R to have a value of $R = 4D^2/\lambda$ gives better results.

It would seem that the approximation of R in (4-46) for the amplitude is more severe than that for the phase. However a close observation reveals this is not the case. Since the observations are made at a distance where r is very large, any small error in the approximation of the denominator (amplitude) will not make much difference in the answer. However, because of the periodic nature of the phase (repeats every 2π rad), it can be a major fraction of a period. The best way to illustrate it will be to consider an example.

Example 4.3

For an antenna with an overall length $l = 5\lambda$, the observations are made at $r = 60\lambda$. Find the errors in phase and amplitude using (4-46).

Solution: For $\theta = 90^\circ$, $z' = 2.5\lambda$, and $r = 60\lambda$, (4-40) reduces to

$$R_1 = \lambda\sqrt{(60)^2 + (2.5)^2} = 60.052\lambda$$

and (4-46) to

$$R_2 = r = 60\lambda$$

Therefore the phase difference is

$$\Delta\phi = k\Delta R = \frac{2\pi}{\lambda}(R_1 - R_2) = 2\pi(0.052) = 0.327 \text{ rad} = 18.74^\circ$$

which is an appreciable fraction ($\simeq \frac{1}{20}$) of a full period (360°).

The difference of the inverse values of R is

$$\frac{1}{R_2} - \frac{1}{R_1} = \frac{1}{\lambda}\left(\frac{1}{60} - \frac{1}{60.052}\right) = \frac{1.44 \times 10^{-5}}{\lambda}$$

which should always be a very small value in amplitude.

4.4.2 Radiating Near-Field (Fresnel) Region

If the observation point is chosen to be smaller than $r = 2l^2/\lambda$, the maximum phase error by the approximation of (4-46) is greater than $\pi/8$ rad (22.5°) which may be undesirable in many applications. If it is necessary to choose observation distances smaller than (4-45), another term (the third) in the series solution of (4-41) must be retained to maintain a maximum phase error of $\pi/8$ rad (22.5°). Doing this, the infinite series of (4-41) can be approximated by

$$R \simeq r - z'\cos\theta + \frac{1}{r}\left(\frac{z'^2}{2}\sin^2\theta\right) \tag{4-48}$$

The most significant term that we are neglecting from the infinite series of (4-41) is the fourth. To find the maximum phase error introduced by the omission of the next most significant term, the angle θ at which this occurs must be found. To do this, the neglected term is differentiated with respect to θ and the result is set equal to zero. Thus

$$\frac{\partial}{\partial\theta}\left[\frac{1}{r^2}\left(\frac{z'^3}{2}\cos\theta\sin^2\theta\right)\right] = \frac{z'^3}{2r^2}\sin\theta[-\sin^2\theta + 2\cos^2\theta] = 0 \tag{4-49}$$

The angle $\theta = 0$ is not chosen as a solution because for that value the fourth term is equal to zero. In other words, $\theta = 0$ gives the minimum error. The maximum error occurs when the second term of (4-49) vanishes; that is when

$$[-\sin^2\theta + 2\cos^2\theta]_{\theta=\theta_1} = 0 \tag{4-50}$$

or

$$\theta_1 = \tan^{-1}(\pm\sqrt{2}) \tag{4-50a}$$

If the maximum phase error is allowed to be equal or less than $\pi/8$ rad, the distance r at which this occurs can be found from

$$\frac{kz'^3}{2r^2}\cos\theta\sin^2\theta\Big|_{\substack{z'=l/2\\ \theta=\tan^{-1}\sqrt{2}}} = \frac{\pi}{\lambda}\frac{l^3}{8r^2}\left(\frac{1}{\sqrt{3}}\right)\left(\frac{2}{3}\right) = \frac{\pi}{12\sqrt{3}}\left(\frac{l^3}{\lambda r^2}\right) \le \frac{\pi}{8} \tag{4-51}$$

which reduces to

$$r^2 \ge \frac{2}{3\sqrt{3}}\left(\frac{l^3}{\lambda}\right) = 0.385\left(\frac{l^3}{\lambda}\right) \tag{4-52}$$

or

$$r \ge 0.62\sqrt{l^3/\lambda} \tag{4-52a}$$

A value of r greater than that of (4-52a) will lead to an error less than $\pi/8$ rad (22.5°). Thus the region where the first three terms of (4-41) are significant, and the omission of the fourth introduces a maximum phase error of $\pi/8$ rad (22.5°), is defined by

$$2l^2/\lambda > r \ge 0.62\sqrt{l^3/\lambda} \tag{4-53}$$

where l is the length of the antenna. This region is designated as *radiating near-field* because the radiating power density is greater than the reactive power density and the field pattern (its shape) is a function of the radial distance r. This region is also called the *Fresnel region* because the field expressions in this region reduce to Fresnel integrals.

The discussion has centered around the finite length antenna of length l with the observation considered to be a point source. If the antenna is not a line source, l in (4-53) must represent the largest dimension of the antenna (which for an aperture is the diagonal). *Also if the transmitting antenna has maximum length l_t and the receiving antenna has maximum length l_r, then the sum of l_t and l_r must be used in place of l in (4-53).*

The boundaries for separating the far-field (Fraunhofer), the radiating near-field (Fresnel), and the reactive near-field regions are not very rigid. Other criteria have also been established [4] but the ones introduced here are the most "popular." Also the fields, as the boundaries from one region to the other are crossed, do not change abruptly but undergo a very gradual transition.

4.4.3 Reactive Near-Field Region

If the distance of observation is smaller than the inner boundary of the Fresnel region, this region is usually designated as *reactive near-field* with inner and outer boundaries defined by

$$0.62\sqrt{l^3/\lambda} > r > 0 \tag{4-54}$$

where l is the length of the antenna. In this region the reactive power density predominates, as was demonstrated in Section 4.1 for the infinitesimal dipole.

In summary, the space surrounding an antenna is divided into three regions whose boundaries are determined by

$$\text{reactive near-field } [0.62\sqrt{D^3/\lambda} > r > 0] \tag{4-55a}$$

$$\text{radiating near-field (Fresnel) } [2D^2/\lambda > r \geq 0.62\sqrt{D^3/\lambda}] \tag{4-55b}$$

$$\text{far-field (Fraunhofer) } [\infty \geq r \geq 2D^2/\lambda] \tag{4-55c}$$

where D is the largest dimension of the antenna ($D = l$ for a wire antenna).

4.5 FINITE LENGTH DIPOLE

The techniques that were developed previously can also be used to analyze the radiation characteristics of a linear dipole of any length. To reduce the mathematical complexities, it will be assumed in this chapter that the dipole has a negligible diameter (ideally zero). This is a good approximation provided the diameter is considerably smaller than the operating wavelength. Finite radii dipoles will be analyzed in Chapters 8 and 9.

4.5.1 Current Distribution

For a very thin dipole (ideally zero diameter), the current distribution can be written, to a good approximation, as

$$\mathbf{I}_e(x'=0, y'=0, z') = \begin{cases} \hat{\mathbf{a}}_z I_0 \sin\left[k\left(\dfrac{l}{2} - z'\right)\right], & 0 \leq z' \leq l/2 \\ \hat{\mathbf{a}}_z I_0 \sin\left[k\left(\dfrac{l}{2} + z'\right)\right], & -l/2 \leq z' \leq 0 \end{cases} \tag{4-56}$$

This distribution assumes that the antenna is *center-fed and the current vanishes at the end points* ($z' = \pm l/2$). Experimentally it has been verified that the current in a center-fed wire antenna has sinusoidal form with nulls at the end points. For $l = \lambda/2$

and $\lambda/2 < l < \lambda$ the current distribution of (4-56) is shown plotted in Figures 1.16(b) and 1.12(c), respectively. The geometry of the antenna is that shown in Figure 4.5.

4.5.2 Radiated Fields: Element Factor, Space Factor, and Pattern Multiplication

For the current distribution of (4-56) it will be shown in Chapter 8 that closed form expressions for the **E**- and **H**-fields can be obtained which are valid in all regions (any observation point except on the source itself). In general, however, this is not the case. Usually we are limited to the far-field region, because of the mathematical complications provided in the integration of the vector potential **A** of (4-2). Since closed form solutions, which are valid everywhere, cannot be obtained for many antennas, the observations will be restricted to the far-field region. This will be done first in order to illustrate the procedure. In some cases, even in that region it may become impossible to obtain closed form solutions.

The finite dipole antenna of Figure 4.5 is subdivided into a number of infinitesimal dipoles of length $\Delta z'$. As the number of subdivisions is increased, each infinitesimal dipole approaches a length dz'. For an infinitesimal dipole of length dz' positioned along the z-axis at z', the electric and magnetic field components in the far field are given, using (4-26a)–(4-26c), as

$$dE_\theta \simeq j\eta \frac{kI_e(x', y', z')e^{-jkR}}{4\pi R} \sin\theta \, dz' \tag{4-57a}$$

$$dE_r \simeq dE_\phi = dH_r = dH_\theta = 0 \tag{4-57b}$$

$$dH_\phi \simeq j \frac{kI_e(x', y', z')e^{-jkR}}{4\pi R} \sin\theta \, dz' \tag{4-57c}$$

where R is given by (4-39) or (4-40).

Using the far-field approximations given by (4-46), (4-57a) can be written as

$$dE_\theta \simeq j\eta \frac{kI_e(x', y', z')e^{-jkr}}{4\pi r} \sin\theta e^{+jkz'\cos\theta} \, dz' \tag{4-58}$$

Summing the contributions from all the infinitesimal elements, the summation reduces, in the limit, to an integration. Thus

$$\boxed{E_\theta = \int_{-l/2}^{+l/2} dE_\theta = j\eta \frac{ke^{-jkr}}{4\pi r} \sin\theta \left[\int_{-l/2}^{+l/2} I_e(x', y', z')e^{jkz'\cos\theta} \, dz' \right]} \tag{4-58a}$$

The factor outside the brackets is designated as the *element factor* and that within the brackets as the *space factor*. For this antenna, the element factor is equal to the field of a unit length infinitesimal dipole located at a reference point (the origin). In general, the element factor depends on the type of current and its direction of flow while the space factor is a function of the current distribution along the source.

The total field of the antenna is equal to the product of the element and space factors. This is referred to as *pattern multiplication* for continuously distributed sources (see also Chapter 7), and it can be written as

$$\boxed{\text{total field} = (\text{element factor}) \times (\text{space factor})} \tag{4-59}$$

The pattern multiplication for continuous sources is analogous to the pattern multiplication of (6-5) for discrete-element antennas (arrays).

For the current distribution of (4-56), (4-58a) can be written as

$$E_\theta \simeq j\eta \frac{kI_0 e^{-jkr}}{4\pi r} \sin\theta \left\{ \int_{-l/2}^{0} \sin\left[k\left(\frac{l}{2} + z'\right)\right] e^{+jkz'\cos\theta}\, dz' + \int_{0}^{+l/2} \sin\left[k\left(\frac{l}{2} - z'\right)\right] e^{+jkz'\cos\theta}\, dz' \right\} \tag{4-60}$$

Each one of the integrals in (4-60) can be integrated using

$$\int e^{\alpha x} \sin(\beta x + \gamma)\, dx = \frac{e^{\alpha x}}{\alpha^2 + \beta^2} [\alpha \sin(\beta x + \gamma) - \beta \cos(\beta x + \gamma)] \tag{4-61}$$

where

$$\alpha = \pm jk\cos\theta \tag{4-61a}$$

$$\beta = \pm k \tag{4-61b}$$

$$\gamma = kl/2 \tag{4-61c}$$

After some mathematical manipulations, (4-60) takes the form of

$$\boxed{E_\theta \simeq j\eta \frac{I_0 e^{-jkr}}{2\pi r} \left[\frac{\cos\left(\frac{kl}{2}\cos\theta\right) - \cos\left(\frac{kl}{2}\right)}{\sin\theta} \right]} \tag{4-62a}$$

In a similar manner, or by using the established relationship between the E_θ and H_ϕ in the far field as given by (3-58b) or (4-27), the total H_ϕ component can be written as

$$\boxed{H_\phi \simeq \frac{E_\theta}{\eta} \simeq j \frac{I_0 e^{-jkr}}{2\pi r} \left[\frac{\cos\left(\frac{kl}{2}\cos\theta\right) - \cos\left(\frac{kl}{2}\right)}{\sin\theta} \right]} \tag{4-62b}$$

4.5.3 Power Density, Radiation Intensity, and Radiation Resistance

For the dipole, the average Poynting vector can be written as

$$\mathbf{W}_{\text{av}} = \frac{1}{2}\text{Re}[\mathbf{E} \times \mathbf{H}^*] = \frac{1}{2}\text{Re}[\hat{\mathbf{a}}_\theta E_\theta \times \hat{\mathbf{a}}_\phi H_\phi^*] = \frac{1}{2}\text{Re}\left[\hat{\mathbf{a}}_\theta E_\theta \times \hat{\mathbf{a}}_\phi \frac{E_\theta^*}{\eta}\right]$$

$$\mathbf{W}_{\text{av}} = \hat{\mathbf{a}}_r W_{\text{av}} = \hat{\mathbf{a}}_r \frac{1}{2\eta}|E_\theta|^2 = \hat{\mathbf{a}}_r \eta \frac{|I_0|^2}{8\pi^2 r^2}\left[\frac{\cos\left(\frac{kl}{2}\cos\theta\right) - \cos\left(\frac{kl}{2}\right)}{\sin\theta}\right]^2 \quad (4\text{-}63)$$

and the radiation intensity as

$$U = r^2\ W_{\text{av}} = \eta \frac{|I_0|^2}{8\pi^2}\left[\frac{\cos\left(\frac{kl}{2}\cos\theta\right) - \cos\left(\frac{kl}{2}\right)}{\sin\theta}\right]^2 \quad (4\text{-}64)$$

The normalized (to 0 dB) elevation power patterns, as given by (4-64) for $l = \lambda/4, \lambda/2, 3\lambda/4$, and λ are shown plotted in Figure 4.6. The current distribution of each is given by (4-56). The power patterns for an infinitesimal dipole $l \ll \lambda$ ($U \sim \sin^2\theta$) is also included for comparison. As the length of the antenna increases, the beam becomes narrower. Because of that, the directivity should also increase with length. It is found that the 3-dB beamwidth of each is equal to

$l \ll \lambda$	3-dB beamwidth $= 90^\circ$
$l = \lambda/4$	3-dB beamwidth $= 87^\circ$
$l = \lambda/2$	3-dB beamwidth $= 78^\circ$
$l = 3\lambda/4$	3-dB beamwidth $= 64^\circ$
$l = \lambda$	3-dB beamwidth $= 47.8^\circ$

(4-65)

As the length of the dipole increases beyond one wavelength ($l > \lambda$), the number of lobes begin to increase. The normalized power pattern for a dipole with $l = 1.25\lambda$ is shown in Figure 4.7. In Figure 4.7(a) the three-dimensional pattern is illustrated using the software from [5], while in Figure 4.7(b) the two-dimensional (elevation pattern) is depicted. For the three-dimensional illustration, a 90° angular section of the pattern has been omitted to illustrate the elevation plane directional pattern variations. The current distribution for the dipoles with $l = \lambda/4, \lambda/2, \lambda, 3\lambda/2$, and 2λ, as given by (4-56), is shown in Figure 4.8.

To find the total power radiated, the average Poynting vector of (4-63) is integrated over a sphere of radius r. Thus

$$P_{\text{rad}} = \oiint_S \mathbf{W}_{\text{av}} \cdot d\mathbf{s} = \int_0^{2\pi}\int_0^{\pi} \hat{\mathbf{a}}_r W_{\text{av}} \cdot \hat{\mathbf{a}}_r r^2 \sin\theta\, d\theta\, d\phi$$

$$= \int_0^{2\pi}\int_0^{\pi} W_{\text{av}} r^2 \sin\theta\, d\theta\, d\phi \quad (4\text{-}66)$$

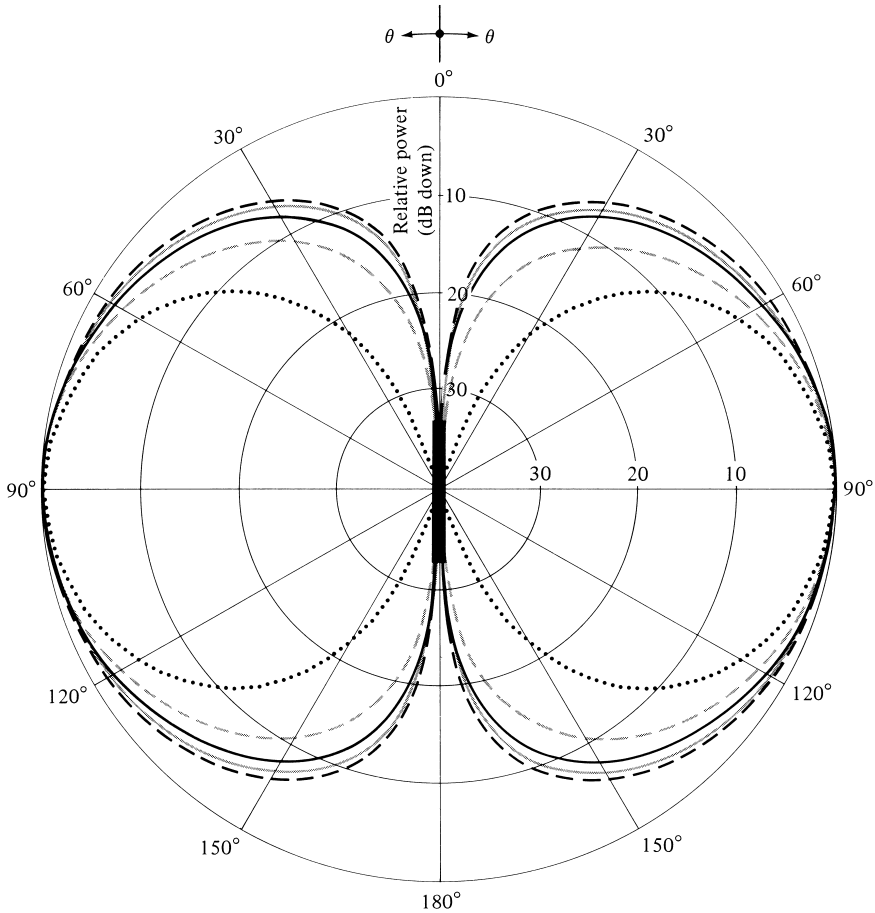

Figure 4.6 Elevation plane amplitude patterns for a thin dipole with sinusoidal current distribution ($l = \lambda/50, \lambda/4, \lambda/2, 3\lambda/4, \lambda$).

Using (4-63), we can write (4-66) as

$$P_{\text{rad}} = \int_0^{2\pi} \int_0^{\pi} W_{\text{av}} r^2 \sin\theta \, d\theta \, d\phi$$

$$= \eta \frac{|I_0|^2}{4\pi} \int_0^{\pi} \frac{\left[\cos\left(\frac{kl}{2}\cos\theta\right) - \cos\left(\frac{kl}{2}\right)\right]^2}{\sin\theta} d\theta \tag{4-67}$$

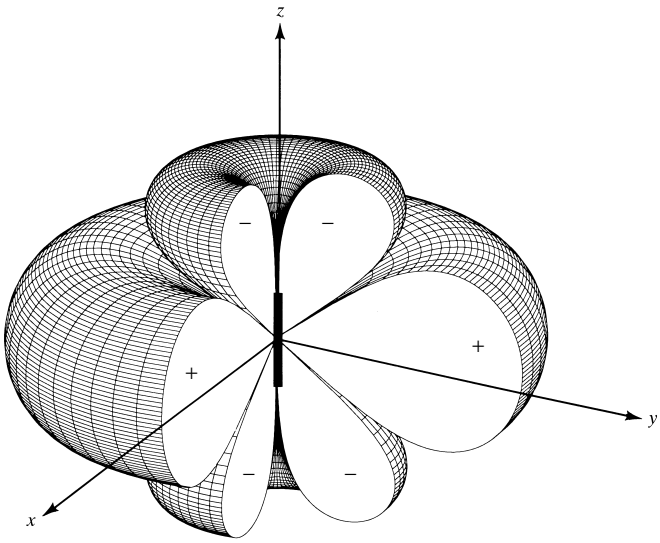

(a) Three-dimensional

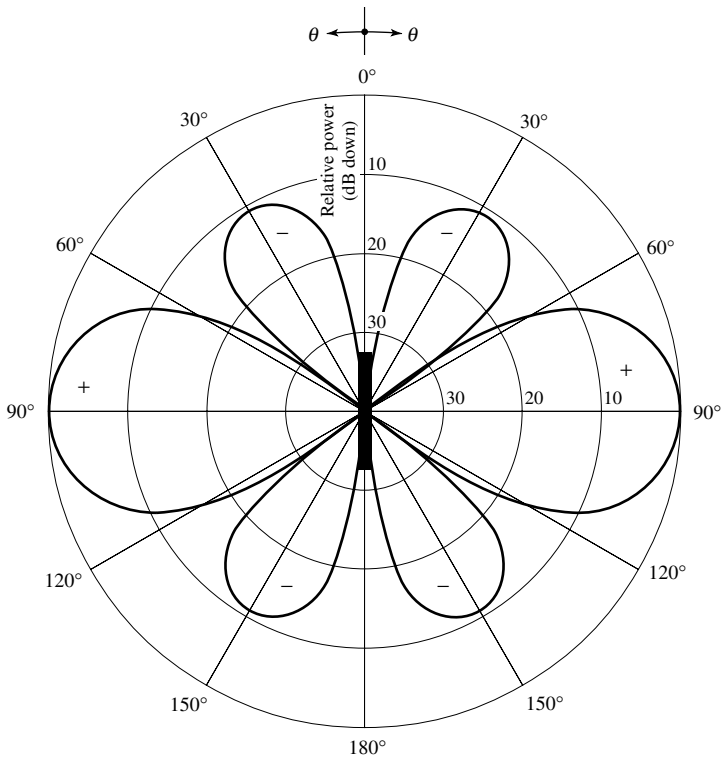

(b) Two-dimensional

Figure 4.7 Three- and two-dimensional amplitude patterns for a thin dipole of $l = 1.25\lambda$ and sinusoidal current distribution.

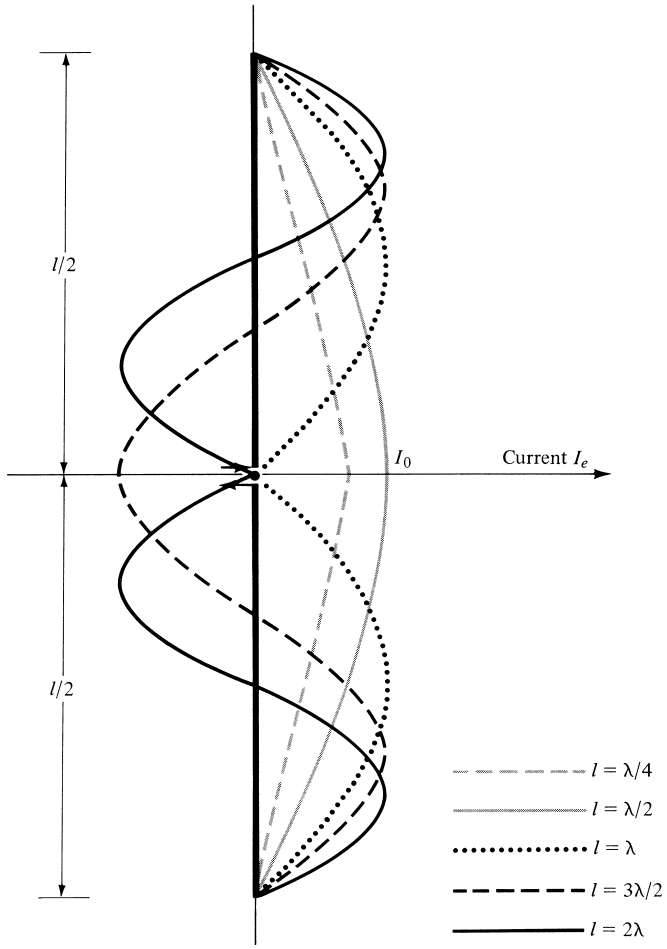

Figure 4.8 Current distributions along the length of a linear wire antenna.

After some extensive mathematical manipulations, it can be shown that (4-67) reduces to

$$P_{\text{rad}} = \eta \frac{|I_0|^2}{4\pi}\{C + \ln(kl) - C_i(kl) + \tfrac{1}{2}\sin(kl)[S_i(2kl) - 2S_i(kl)] + \tfrac{1}{2}\cos(kl)[C + \ln(kl/2) + C_i(2kl) - 2C_i(kl)]\} \tag{4-68}$$

where $C = 0.5772$ (Euler's constant) and $C_i(x)$ and $S_i(x)$ are the cosine and sine integrals (see Appendix III) given by

$$C_i(x) = -\int_x^\infty \frac{\cos y}{y}\,dy = \int_\infty^x \frac{\cos y}{y}\,dy \tag{4-68a}$$

$$S_i(x) = \int_0^x \frac{\sin y}{y}\,dy \tag{4-68b}$$

The derivation of (4-68) from (4-67) is assigned as a problem at the end of the chapter (Prob. 4.21). $C_i(x)$ is related to $C_{in}(x)$ by

$$\begin{aligned} C_{in}(x) &= \ln(\gamma x) - C_i(x) = \ln(\gamma) + \ln(x) - C_i(x) \\ &= 0.5772 + \ln(x) - C_i(x) \end{aligned} \tag{4-69}$$

where

$$C_{in}(x) = \int_0^x \left(\frac{1-\cos y}{y}\right) dy \tag{4-69a}$$

$C_i(x)$, $S_i(x)$ and $C_{in}(x)$ are tabulated in Appendix III.

The radiation resistance can be obtained using (4-18) and (4-68) and can be written as

$$\begin{aligned} R_r = \frac{2P_{\text{rad}}}{|I_0|^2} = \frac{\eta}{2\pi}\{&C + \ln(kl) - C_i(kl) \\ &+ \tfrac{1}{2}\sin(kl) \times [S_i(2kl) - 2S_i(kl)] \\ &+ \tfrac{1}{2}\cos(kl) \times [C + \ln(kl/2) + C_i(2kl) - 2C_i(kl)]\} \end{aligned} \tag{4-70}$$

Shown in Figure 4.9 is a plot of R_r as a function of l (in wavelengths) when the antenna is radiating into free-space ($\eta \simeq 120\pi$).

The imaginary part of the impedance cannot be derived using the same method as the real part because, as was explained in Section 4.2.2, the integration over a closed sphere in (4-13) does not capture the imaginary power contributed by the transverse component W_θ of the power density. Therefore, the EMF method is used in Chapter 8 as

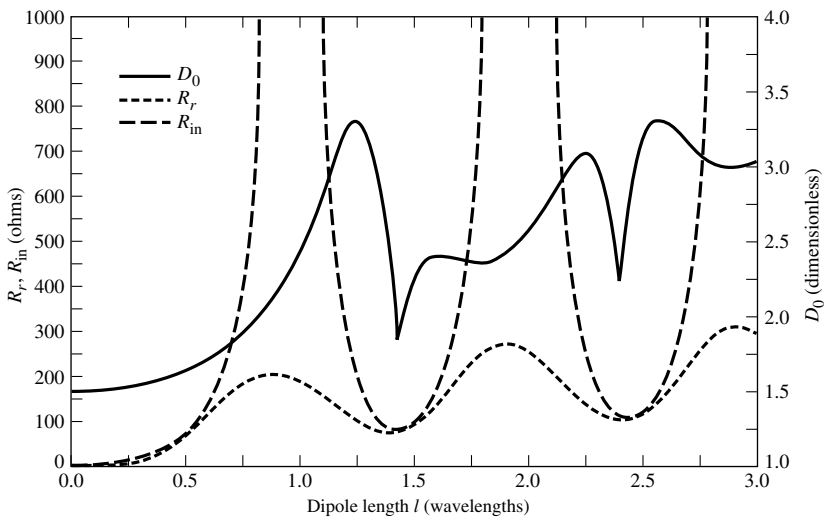

Figure 4.9 Radiation resistance, input resistance and directivity of a thin dipole with sinusoidal current distribution.

an alternative approach. Using the EMF method, the imaginary part of the impedance, relative to the current maximum, is given by (8-60b) or

$$X_m = \frac{\eta}{4\pi}\left\{2S_i(kl) + \cos(kl)[2S_i(kl) - S_i(2kl)] - \sin(kl)\left[2C_i(kl) - C_i(2kl) - C_i\left(\frac{2ka^2}{l}\right)\right]\right\} \tag{4-70a}$$

An approximate form of (4-60b) for small dipoles is given by (8-62).

4.5.4 Directivity

As was illustrated in Figure 4.6, the radiation pattern of a dipole becomes more directional as its length increases. When the overall length is greater than one wavelength, the number of lobes increases and the antenna loses its directional properties. The parameter that is used as a "figure of merit" for the directional properties of the antenna is the directivity which was defined in Section 2.6.

The directivity was defined mathematically by (2-22), or

$$D_0 = 4\pi \frac{F(\theta,\phi)|_{\max}}{\displaystyle\int_0^{2\pi}\int_0^{\pi} F(\theta,\phi)\sin\theta\, d\theta\, d\phi} \tag{4-71}$$

where $F(\theta,\phi)$ is related to the radiation intensity U by (2-19), or

$$U = B_0 F(\theta,\phi) \tag{4-72}$$

From (4-64), the dipole antenna of length l has

$$F(\theta,\phi) = F(\theta) = \left[\frac{\cos\left(\frac{kl}{2}\cos\theta\right) - \cos\left(\frac{kl}{2}\right)}{\sin\theta}\right]^2 \tag{4-73}$$

and

$$B_0 = \eta\frac{|I_0|^2}{8\pi^2} \tag{4-73a}$$

Because the pattern is not a function of ϕ, (4-71) reduces to

$$D_0 = \frac{2F(\theta)|_{\max}}{\displaystyle\int_0^{\pi} F(\theta)\sin\theta\, d\theta} \tag{4-74}$$

Equation (4-74) can be written, using (4-67), (4-68), and (4-73), as

$$D_0 = \frac{2F(\theta)|_{\max}}{Q} \tag{4-75}$$

where

$$Q = \{C + \ln(kl) - C_i(kl) + \tfrac{1}{2}\sin(kl)[S_i(2kl) - 2S_i(kl)] + \tfrac{1}{2}\cos(kl)[C + \ln(kl/2) + C_i(2kl) - 2C_i(kl)]\} \tag{4-75a}$$

The maximum value of $F(\theta)$ varies and depends upon the length of the dipole.

Values of the directivity, as given by (4-75) and (4-75a), have been obtained for $0 < l \leq 3\lambda$ and are shown plotted in Figure 4.9. The corresponding values of the maximum effective aperture are related to the directivity by

$$A_{em} = \frac{\lambda^2}{4\pi} D_0 \tag{4-76}$$

4.5.5 Input Resistance

In Section 2.13 the input impedance was defined as "the ratio of the voltage to current at a pair of terminals or the ratio of the appropriate components of the electric to magnetic fields at a point." The real part of the input impedance was defined as the input resistance which for a lossless antenna reduces to the radiation resistance, a result of the radiation of real power.

In Section 4.2.2, the radiation resistance of an infinitesimal dipole was derived using the definition of (4-18). The radiation resistance of a dipole of length l with sinusoidal current distribution, of the form given by (4-56), is expressed by (4-70). By this definition, the radiation resistance is referred to the maximum current which for some lengths ($l = \lambda/4, 3\lambda/4, \lambda$, etc.) does not occur at the input terminals of the antenna (see Figure 4.8). To refer the radiation resistance to the input terminals of the antenna, the antenna itself is first assumed to be lossless ($R_L = 0$). Then the power at the input terminals is equated to the power at the current maximum.

Referring to Figure 4.10, we can write

$$\frac{|I_{in}|^2}{2} R_{in} = \frac{|I_0|^2}{2} R_r \tag{4-77}$$

or

$$R_{in} = \left[\frac{I_0}{I_{in}}\right]^2 R_r \tag{4-77a}$$

where

R_{in} = radiation resistance at input (feed) terminals
R_r = radiation resistance at current maximum Eq. (4-70)
I_0 = current maximum
I_{in} = current at input terminals

For a dipole of length l, the current at the input terminals (I_{in}) is related to the current maximum (I_0) referring to Figure 4.10, by

$$I_{in} = I_0 \sin\left(\frac{kl}{2}\right) \tag{4-78}$$

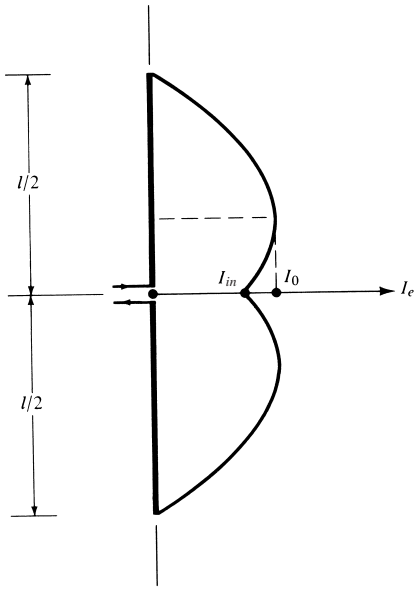

Figure 4.10 Current distribution of a linear wire antenna when current maximum does not occur at the input terminals.

Thus the input radiation resistance of (4-77a) can be written as

$$R_{in} = \frac{R_r}{\sin^2\left(\frac{kl}{2}\right)} \tag{4-79}$$

Values of R_{in} for $0 < l \leq 3\lambda$ are shown in Figure 4.9.

To compute the radiation resistance (in ohms), directivity (dimensionless and in dB), and input resistance (in ohms) for a dipole of length l, a MATLAB and FORTRAN computer program has been developed. The program is based on the definitions of each as given by (4-70), (4-71), and (4-79). The radiated power P_{rad} is computed by numerically integrating (over a closed sphere) the radiation intensity of (4-72)–(4-73a). The program, both in MATLAB and FORTRAN, is included in the computer disc made available with the book. The length of the dipole (in wavelengths) must be inserted as an input.

When the overall length of the antenna is a multiple of λ (i.e., $l = n\lambda, n = 1, 2, 3, \ldots$), it is apparent from (4-56) and from Figure 4.8 that $I_{in} = 0$. That is,

$$I_{in} = I_0 \sin\left[k\left(\frac{l}{2} \pm z'\right)\right]\Big|_{\substack{z'=0 \\ l=n\lambda, n=0,1,2,\ldots}} = 0 \tag{4-80}$$

which indicates that the input resistance at the input terminals, as given by (4-77a) or (4-79) is infinite. In practice this is not the case because the current distribution does not follow an exact sinusoidal distribution, especially at the feed point. It has, however, very high values. Two of the primary factors which contribute to the nonsinusoidal

current distribution on an actual wire antenna are the nonzero radius of the wire and finite gap spacing at the terminals.

The radiation resistance and input resistance, as predicted, respectively, by (4-70) and (4-79), are based on the ideal current distribution of (4-56) and do not account for the finite radius of the wire or the gap spacing at the feed. Although the radius of the wire does not strongly influence the resistances, the gap spacing at the feed does play a significant role especially when the current at and near the feed point is small.

4.5.6 Finite Feed Gap

To analytically account for a nonzero current at the feed point for antennas with a finite gap at the terminals, Schelkunoff and Friis [6] have changed the current of (4-56) by including a quadrature term in the distribution. The additional term is inserted to take into account the effects of radiation on the antenna current distribution. In other words, once the antenna is excited by the "ideal" current distribution of (4-56), electric and magnetic fields are generated which in turn disturb the "ideal" current distribution. This reaction is included by modifying (4-56) to

$$\mathbf{I}_e(x', y', z') = \begin{cases} \hat{\mathbf{a}}_z \left\{ I_0 \sin\left[k\left(\frac{l}{2} - z'\right)\right] + jpI_0\left[\cos(kz') - \cos\left(\frac{k}{2}l\right)\right]\right\}, \\ \qquad\qquad 0 \le z' \le l/2 \\ \hat{\mathbf{a}}_z \left\{ I_0 \sin\left[k\left(\frac{l}{2} + z'\right)\right] + jpI_0\left[\cos(kz') - \cos\left(\frac{k}{2}l\right)\right]\right\}, \\ \qquad\qquad -l/2 \le z' \le 0 \end{cases} \tag{4-81}$$

where p is a coefficient that is dependent upon the overall length of the antenna and the gap spacing at the terminals. The values of p become smaller as the radius of the wire and the gap decrease.

When $l = \lambda/2$,

$$\mathbf{I}_e(x', y', z') = \hat{\mathbf{a}}_z I_0(1 + jp)\cos(kz') \quad 0 \le |z'| \le \lambda/4 \tag{4-82}$$

and for $l = \lambda$

$$\mathbf{I}_e(x', y', z') = \begin{cases} \hat{\mathbf{a}}_z I_0\{\sin(kz') + jp[1 + \cos(kz')]\} & 0 \le z' \le \lambda/2 \\ \hat{\mathbf{a}}_z I_0\{-\sin(kz') + jp[1 + \cos(kz')]\} & -\lambda/2 \le z' \le 0 \end{cases} \tag{4-83}$$

Thus for $l = \lambda/2$ the shape of the current is not changed while for $l = \lambda$ it is modified by the second term which is more dominant for small values of z'.

The variations of the current distribution and impedances, especially of wire-type antennas, as a function of the radius of the wire and feed gap spacing can be easily taken into account by using advanced computational methods and numerical techniques, especially Integral Equations and Moment Method [7]–[12], which are introduced in Chapter 8.

To illustrate the point, the current distribution of an $l = \lambda/2$ and $l = \lambda$ dipole has been computed using an integral equation formulation with a moment method numerical solution, and it is shown in Figure 8.13(b) where it is compared with the ideal distribution of (4-56) and other available data. For the moment method solution, a gap at the feed has been inserted. As expected and illustrated in Figure 8.13(b), the current

distribution for the $l = \lambda/2$ dipole based on (4-56) is not that different from that based on the moment method. This is also illustrated by (4-82). Therefore the input resistance based on these two methods will not be that different. However, for the $l = \lambda$ dipole, the current distribution based on (4-56) is quite different, especially at and near the feed point, compared to that based on the moment method, as shown in Figure 8.13(b). This is expected since the current distribution based on the ideal current distribution is zero at the feed point; for practical antennas it is very small. Therefore the gap at the feed plays an important role on the current distribution at and near the feed point. In turn, the values of the input resistance based on the two methods will be quite different, since there is a significant difference in the current between the two methods. This is discussed further in Chapter 8.

4.6 HALF-WAVELENGTH DIPOLE

One of the most commonly used antennas is the half-wavelength ($l = \lambda/2$) dipole. Because its radiation resistance is 73 ohms, which is very near the 50-ohm or 75-ohm characteristic impedances of some transmission lines, its matching to the line is simplified especially at resonance. Because of its wide acceptance in practice, we will examine in a little more detail its radiation characteristics.

The electric and magnetic field components of a half-wavelength dipole can be obtained from (4-62a) and (4-62b) by letting $l = \lambda/2$. Doing this, they reduce to

$$E_\theta \simeq j\eta \frac{I_0 e^{-jkr}}{2\pi r} \left[\frac{\cos\left(\frac{\pi}{2}\cos\theta\right)}{\sin\theta} \right] \tag{4-84}$$

$$H_\phi \simeq j \frac{I_0 e^{-jkr}}{2\pi r} \left[\frac{\cos\left(\frac{\pi}{2}\cos\theta\right)}{\sin\theta} \right] \tag{4-85}$$

In turn, the time-average power density and radiation intensity can be written, respectively, as

$$W_{\text{av}} = \eta \frac{|I_0|^2}{8\pi^2 r^2} \left[\frac{\cos\left(\frac{\pi}{2}\cos\theta\right)}{\sin\theta} \right]^2 \simeq \eta \frac{|I_0|^2}{8\pi^2 r^2} \sin^3\theta \tag{4-86}$$

and

$$U = r^2\, W_{\text{av}} = \eta \frac{|I_0|^2}{8\pi^2} \left[\frac{\cos\left(\frac{\pi}{2}\cos\theta\right)}{\sin\theta} \right]^2 \simeq \eta \frac{|I_0|^2}{8\pi^2} \sin^3\theta \tag{4-87}$$

whose two-dimensional pattern is shown plotted in Figure 4.6 while the three-dimensional pattern is depicted in Figure 4.11. For the three-dimensional pattern of Figure 4.11, a 90° angular sector has been removed to illustrate the figure-eight elevation plane pattern variations.

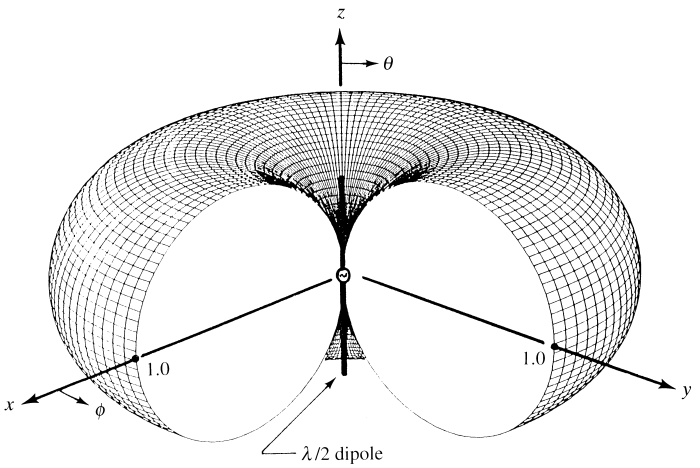

Figure 4.11 Three-dimensional pattern of a $\lambda/2$ dipole. (SOURCE: C. A. Balanis, "Antenna Theory: A Review" *Proc. IEEE*, Vol. 80, No 1. Jan. 1992. © 1992 IEEE).

The total power radiated can be obtained as a special case of (4-67), or

$$P_{\text{rad}} = \eta \frac{|I_0|^2}{4\pi} \int_0^{\pi} \frac{\cos^2\left(\frac{\pi}{2}\cos\theta\right)}{\sin\theta}\, d\theta \tag{4-88}$$

which when integrated reduces, as a special case of (4-68), to

$$P_{\text{rad}} = \eta \frac{|I_0|^2}{8\pi} \int_0^{2\pi} \left(\frac{1-\cos y}{y}\right) dy = \eta \frac{|I_0|^2}{8\pi} C_{in}(2\pi) \tag{4-89}$$

By the definition of $C_{in}(x)$, as given by (4-69), $C_{in}(2\pi)$ is equal to

$$C_{in}(2\pi) = 0.5772 + \ln(2\pi) - C_i(2\pi) = 0.5772 + 1.838 - (-0.02) \simeq 2.435 \tag{4-90}$$

where $C_i(2\pi)$ is obtained from the tables in Appendix III.

Using (4-87), (4-89), and (4-90), the maximum directivity of the half-wavelength dipole reduces to

$$\boxed{D_0 = 4\pi \frac{U_{\max}}{P_{\text{rad}}} = 4\pi \frac{U|_{\theta=\pi/2}}{P_{\text{rad}}} = \frac{4}{C_{in}(2\pi)} = \frac{4}{2.435} \simeq 1.643} \tag{4-91}$$

The corresponding maximum effective area is equal to

$$\boxed{A_{em} = \frac{\lambda^2}{4\pi} D_0 = \frac{\lambda^2}{4\pi}(1.643) \simeq 0.13\lambda^2} \tag{4-92}$$

and the radiation resistance, for a free-space medium ($\eta \simeq 120\pi$), is given by

$$\boxed{R_r = \frac{2P_{\text{rad}}}{|I_0|^2} = \frac{\eta}{4\pi} C_{in}(2\pi) = 30(2.435) \simeq 73} \tag{4-93}$$

The radiation resistance of (4-93) is also the radiation resistance at the input terminals (input resistance) since the current maximum for a dipole of $l = \lambda/2$ occurs at the input terminals (see Figure 4.8). As it will be shown in Chapter 8, the imaginary part (reactance) associated with the input impedance of a dipole is a function of its length (for $l = \lambda/2$, it is equal to $j42.5$). Thus the total input impedance for $l = \lambda/2$ is equal to

$$\boxed{Z_{in} = 73 + j42.5} \tag{4-93a}$$

To reduce the imaginary part of the input impedance to zero, the antenna is matched or reduced in length until the reactance vanishes. The latter is most commonly used in practice for half-wavelength dipoles.

Depending on the radius of the wire, the length of the dipole for first resonance is about $l = 0.47\lambda$ to 0.48λ; the thinner the wire, the closer the length is to 0.48λ. Thus, for thicker wires, a larger segment of the wire has to be removed from $\lambda/2$ to achieve resonance.

4.7 LINEAR ELEMENTS NEAR OR ON INFINITE PERFECT CONDUCTORS

Thus far we have considered the radiation characteristics of antennas radiating into an unbounded medium. The presence of an obstacle, especially when it is near the radiating element, can significantly alter the overall radiation properties of the antenna system. In practice the most common obstacle that is always present, even in the absence of anything else, is the ground. Any energy from the radiating element directed toward the ground undergoes a reflection. The amount of reflected energy and its direction are controlled by the geometry and constitutive parameters of the ground.

In general, the ground is a lossy medium ($\sigma \neq 0$) whose effective conductivity increases with frequency. Therefore it should be expected to act as a very good conductor above a certain frequency, depending primarily upon its composition and moisture content. To simplify the analysis, it will first be assumed that the ground is a perfect electric conductor, flat, and infinite in extent. The effects of finite conductivity and earth curvature will be incorporated later. The same procedure can also be used to investigate the characteristics of any radiating element near any other infinite, flat, perfect electric conductor. Although infinite structures are not realistic, the developed procedures can be used to simulate very large (electrically) obstacles. The effects that finite dimensions have on the radiation properties of a radiating element can be conveniently accounted for by the use of the Geometrical Theory of Diffraction (Chapter 12, Section 12.10) and/or the Moment Method (Chapter 8, Section 8.4).

4.7.1 Image Theory

To analyze the performance of an antenna near an infinite plane conductor, virtual sources (images) will be introduced to account for the reflections. As the name implies, these are not real sources but imaginary ones, which when combined with the real

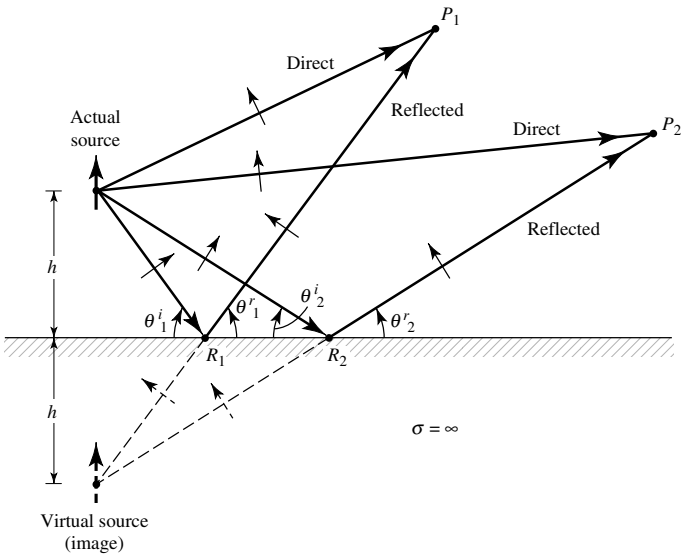

(a) Vertical electric dipole

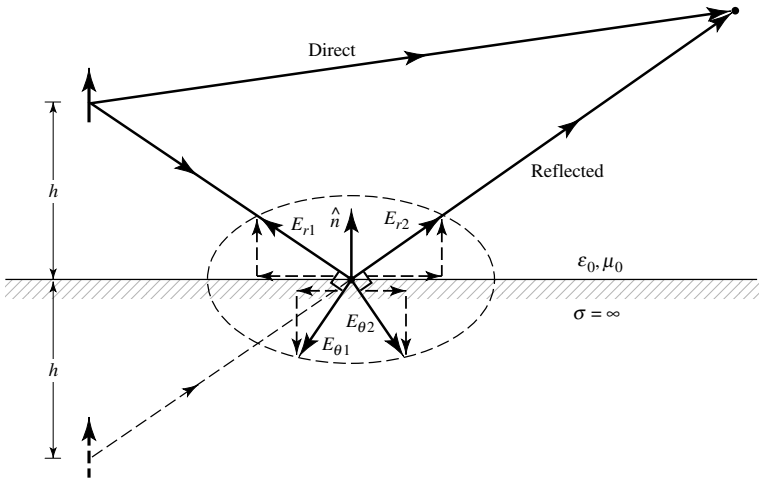

(b) Field components at point of reflection

Figure 4.12 Vertical electric dipole above an infinite, flat, perfect electric conductor.

sources, form an equivalent system. For analysis purposes only, the equivalent system gives the same radiated field on and above the conductor as the actual system itself. Below the conductor, the equivalent system does not give the correct field. However, in this region the field is zero and there is no need for the equivalent.

To begin the discussion, let us assume that a vertical electric dipole is placed a distance h above an infinite, flat, perfect electric conductor as shown in Figure 4.12(a). The arrow indicates the polarity of the source. Energy from the actual source is radiated in all directions in a manner determined by its unbounded medium directional properties. For an observation point P_1, there is a direct wave. In addition, a wave from the actual source radiated toward point R_1 of the interface undergoes a reflection.

The direction is determined by the law of reflection ($\theta_1^i = \theta_1^r$) which assures that the energy in homogeneous media travels in straight lines along the shortest paths. This wave will pass through the observation point P_1. By extending its actual path below the interface, it will seem to originate from a virtual source positioned a distance h below the boundary. For another observation point P_2 the point of reflection is R_2, but the virtual source is the same as before. The same is concluded for all other observation points above the interface.

The amount of reflection is generally determined by the respective constitutive parameters of the media below and above the interface. For a perfect electric conductor below the interface, the incident wave is completely reflected and the field below the boundary is zero. According to the boundary conditions, the tangential components of the electric field must vanish at all points along the interface. Thus for an incident electric field with vertical polarization shown by the arrows, the polarization of the reflected waves must be as indicated in the figure to satisfy the boundary conditions. To excite the polarization of the reflected waves, the virtual source must also be vertical and with a polarity in the same direction as that of the actual source (thus a reflection coefficient of $+1$).

Another orientation of the source will be to have the radiating element in a horizontal position, as shown in Figure 4.24. Following a procedure similar to that of the vertical dipole, the virtual source (image) is also placed a distance h below the interface but with a 180° polarity difference relative to the actual source (thus a reflection coefficient of -1).

In addition to electric sources, artificial equivalent "magnetic" sources and magnetic conductors have been introduced to aid in the analyses of electromagnetic boundary-value problems. Figure 4.13(a) displays the sources and their images for an electric plane conductor. The single arrow indicates an electric element and the double a magnetic one. The direction of the arrow identifies the polarity. Since many problems can be solved using duality, Figure 4.13(b) illustrates the sources and their images when the obstacle is an infinite, flat, perfect "magnetic" conductor.

4.7.2 Vertical Electric Dipole

The analysis procedure for vertical and horizontal electric and magnetic elements near infinite electric and magnetic plane conductors, using image theory, was illustrated graphically in the previous section. Based on the graphical model of Figure 4.12, the mathematical expressions for the fields of a vertical linear element near a perfect electric conductor will now be developed. For simplicity, only far-field observations will be considered.

Referring to the geometry of Figure 4.14(a), the far-zone direct component of the electric field of the infinitesimal dipole of length l, constant current I_0, and observation point P is given according to (4-26a) by

$$E_\theta^d = j\eta \frac{kI_0 l e^{-jkr_1}}{4\pi r_1} \sin\theta_1 \tag{4-94}$$

The reflected component can be accounted for by the introduction of the virtual source (image), as shown in Figure 4.14(a), and it can be written as

$$E_\theta^r = jR_v\eta \frac{kI_0 l e^{-jkr_2}}{4\pi r_2} \sin\theta_2 \tag{4-95}$$

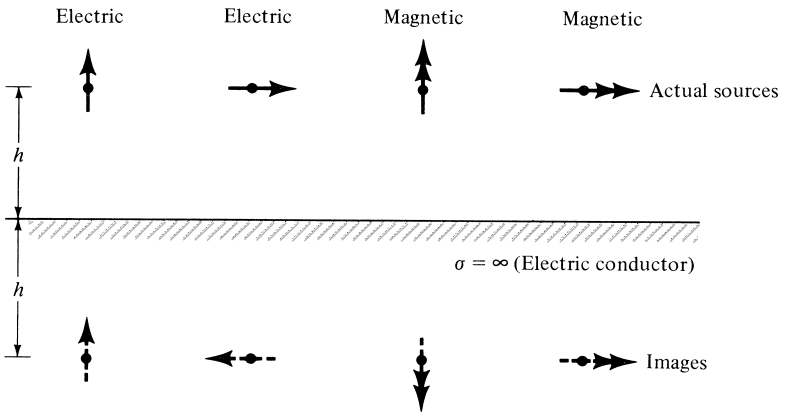

(a) Electric conductor

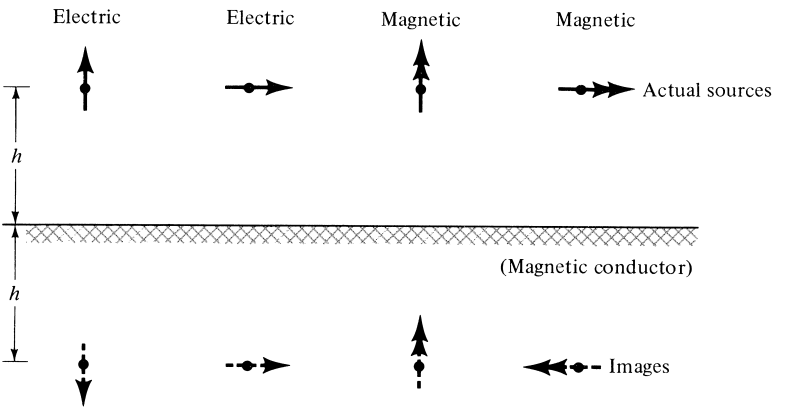

(b) Magnetic conductor

Figure 4.13 Electric and magnetic sources and their images near electric (PEC) and magnetic (PMC) conductors.

or

$$E_\theta^r = j\eta \frac{kI_0 l e^{-jkr_2}}{4\pi r_2} \sin\theta_2 \tag{4-95a}$$

since the reflection coefficient R_v is equal to unity.

The total field above the interface ($z \geq 0$) is equal to the sum of the direct and reflected components as given by (4-94) and (4-95a). Since a field cannot exist inside a perfect electric conductor, it is equal to zero below the interface. To simplify the expression for the total electric field, it is referred to the origin of the coordinate system ($z = 0$).

In general, we can write that

$$r_1 = [r^2 + h^2 - 2rh\cos\theta]^{1/2} \tag{4-96a}$$

$$r_2 = [r^2 + h^2 - 2rh\cos(\pi - \theta)]^{1/2} \tag{4-96b}$$

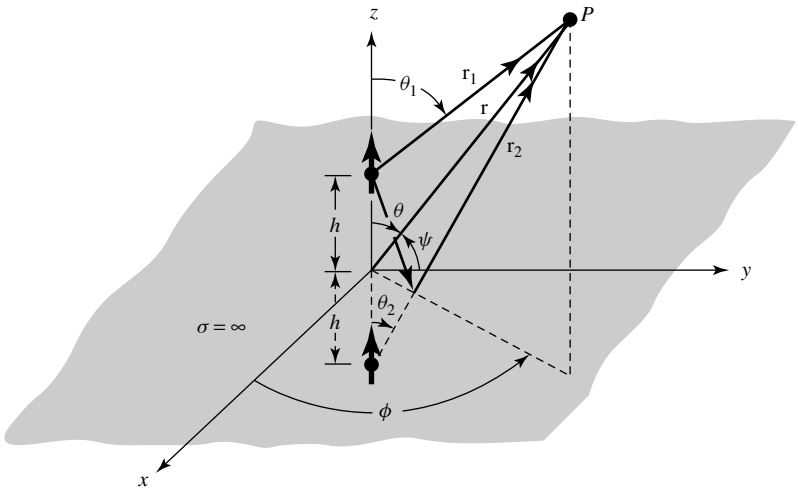

(a) Vertical electric dipole above ground plane

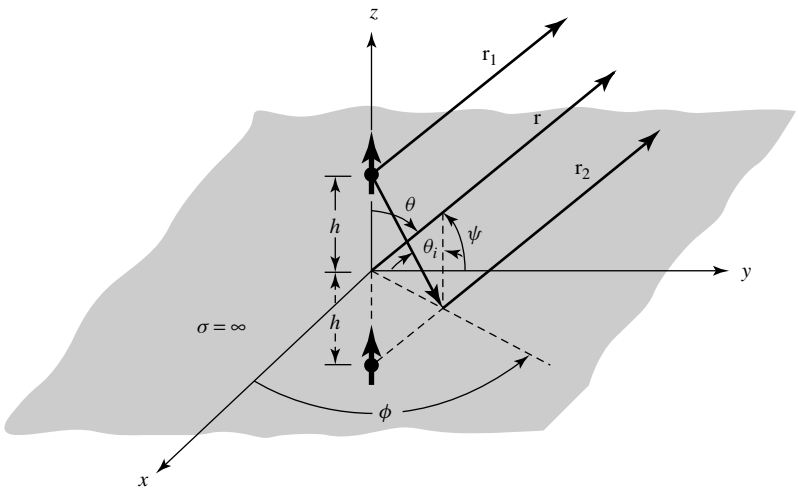

(b) Far-field observations

Figure 4.14 Vertical electric dipole above infinite perfect electric conductor.

For far-field observations ($r \gg h$), (4-96a) and (4-96b) reduce using the binomial expansion to

$$r_1 \simeq r - h\cos\theta \tag{4-97a}$$

$$r_2 \simeq r + h\cos\theta \tag{4-97b}$$

As shown in Figure 4.14(b), geometrically (4-97a) and (4-97b) represent parallel lines. Since the amplitude variations are not as critical

$$r_1 \simeq r_2 \simeq r \quad \text{for amplitude variations} \tag{4-98}$$

Using (4-97a)–(4-98), the sum of (4-94) and (4-95a) can be written as

$$\left.\begin{aligned} E_\theta &\simeq j\eta\frac{kI_0le^{-jkr}}{4\pi r}\sin\theta[2\cos(kh\cos\theta)] \quad z \geq 0 \\ E_\theta &= 0 \qquad\qquad\qquad\qquad\qquad\qquad\qquad\quad z < 0 \end{aligned}\right\} \tag{4-99}$$

It is evident that the total electric field is equal to the product of the field of a single source positioned symmetrically about the origin and a factor [within the brackets in (4-99)] which is a function of the antenna height (h) and the observation angle (θ). This is referred to as *pattern multiplication* and the factor is known as the *array factor* [see also (6-5)]. This will be developed and discussed in more detail and for more complex configurations in Chapter 6.

The shape and amplitude of the field is not only controlled by the field of the single element but also by the positioning of the element relative to the ground. To examine the field variations as a function of the height h, the normalized (to 0 dB) power patterns for $h = 0, \lambda/8, \lambda/4, 3\lambda/8, \lambda/2$, and λ have been plotted in Figure 4.15. Because of symmetry, only half of each pattern is shown. For $h > \lambda/4$ more minor lobes, in addition to the major ones, are formed. As h attains values greater than λ, an even greater number of minor lobes is introduced. These are shown in Figure 4.16 for $h = 2\lambda$ and 5λ. The introduction of the additional lobes in Figure 4.16 is usually called *scalloping*. In general, the total number of lobes is equal to the integer that is closest to

$$\boxed{\text{number of lobes } \simeq \frac{2h}{\lambda} + 1} \tag{4-100}$$

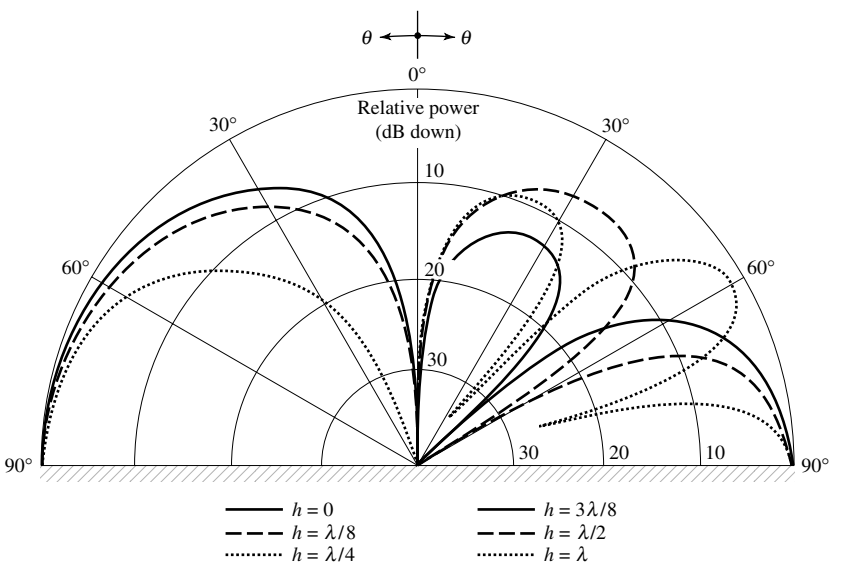

Figure 4.15 Elevation plane amplitude patterns of a vertical infinitesimal electric dipole for different heights above an infinite perfect electric conductor.

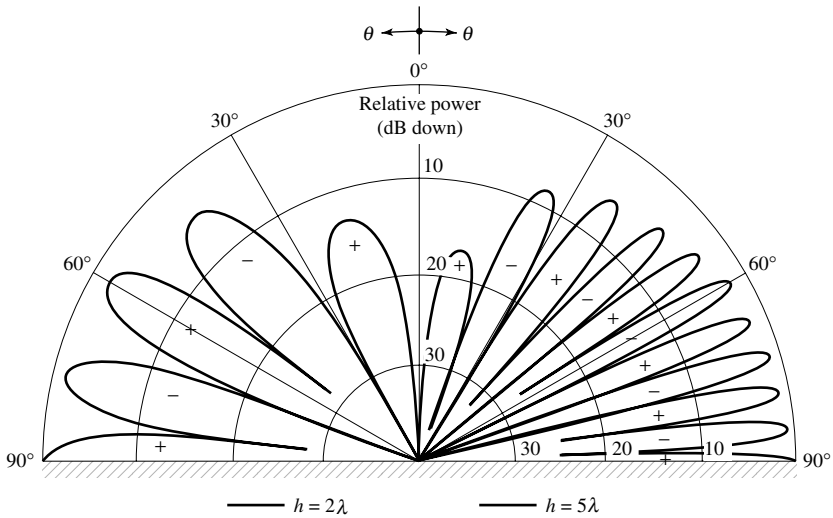

Figure 4.16 Elevation plane amplitude patterns of a vertical infinitesimal electric dipole for heights of 2λ and 5λ above an infinite perfect electric conductor.

Since the total field of the antenna system is different from that of a single element, the directivity and radiation resistance are also different. To derive expressions for them, we first find the total radiated power over the upper hemisphere of radius r using

$$P_{\text{rad}} = \oiint_S \mathbf{W}_{\text{av}} \cdot d\mathbf{s} = \frac{1}{2\eta} \int_0^{2\pi} \int_0^{\pi/2} |E_\theta|^2 r^2 \sin\theta \, d\theta \, d\phi$$

$$= \frac{\pi}{\eta} \int_0^{\pi/2} |E_\theta|^2 r^2 \sin\theta \, d\theta \tag{4-101}$$

which simplifies, with the aid of (4-99), to

$$P_{\text{rad}} = \pi\eta \left| \frac{I_0 l}{\lambda} \right|^2 \left[\frac{1}{3} - \frac{\cos(2kh)}{(2kh)^2} + \frac{\sin(2kh)}{(2kh)^3} \right] \tag{4-102}$$

As $kh \to \infty$ the radiated power, as given by (4-102), is equal to that of an isolated element. However, for $kh \to 0$, it can be shown by expanding the sine and cosine functions into series that the power is twice that of an isolated element. Using (4-99), the radiation intensity can be written as

$$U = r^2 \, W_{\text{av}} = r^2 \left(\frac{1}{2\eta} |E_\theta|^2 \right) = \frac{\eta}{2} \left| \frac{I_0 l}{\lambda} \right|^2 \sin^2\theta \cos^2(kh\cos\theta) \tag{4-103}$$

The maximum value of (4-103) occurs at $\theta = \pi/2$ and is given, excluding $kh \to \infty$, by

$$U_{\text{max}} = U|_{\theta=\pi/2} = \frac{\eta}{2} \left| \frac{I_0 l}{\lambda} \right|^2 \tag{4-103a}$$

which is four times greater than that of an isolated element. With (4-102) and (4-103a), the directivity can be written as

$$D_0 = \frac{4\pi U_{\max}}{P_{\text{rad}}} = \frac{2}{\left[\dfrac{1}{3} - \dfrac{\cos(2kh)}{(2kh)^2} + \dfrac{\sin(2kh)}{(2kh)^3}\right]} \tag{4-104}$$

whose value for $kh = 0$ is 3. The maximum value occurs when $kh = 2.881$ ($h = 0.4585\lambda$), and it is equal to 6.566 which is greater than four times that of an isolated element (1.5). The pattern for $h = 0.4585\lambda$ is shown plotted in Figure 4.17 while the directivity, as given by (4-104), is displayed in Figure 4.18 for $0 \le h \le 5\lambda$.

Using (4-102), the radiation resistance can be written as

$$R_r = \frac{2P_{\text{rad}}}{|I_0|^2} = 2\pi\eta\left(\frac{l}{\lambda}\right)^2\left[\frac{1}{3} - \frac{\cos(2kh)}{(2kh)^2} + \frac{\sin(2kh)}{(2kh)^3}\right] \tag{4-105}$$

whose value for $kh \to \infty$ is the same and for $kh = 0$ is twice that of the isolated element as given by (4-19). When $kh = 0$, the value of R_r as given by (4-105) is only one-half the value of an $l' = 2l$ isolated element according to (4-19). The radiation resistance, as given by (4-105), is plotted in Figure 4.18 for $0 \le h \le 5\lambda$ when $l = \lambda/50$ and the element is radiating into free-space ($\eta \simeq 120\pi$). It can be compared to the value of $R_r = 0.316$ ohms for the isolated element of Example 4.1.

In practice, a wide use has been made of a quarter-wavelength monopole ($l = \lambda/4$) mounted above a ground plane, and fed by a coaxial line, as shown in Figure 4.19(a). For analysis purposes, a $\lambda/4$ image is introduced and it forms the $\lambda/2$ equivalent of Figure 4.19(b). It should be emphasized that the $\lambda/2$ equivalent of Figure 4.19(b) gives

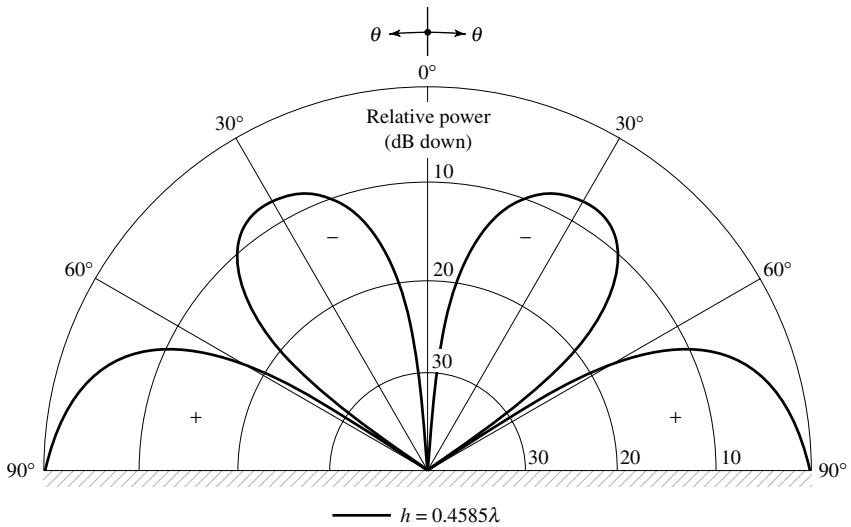

Figure 4.17 Elevation plane amplitude pattern of a vertical infinitesimal electric dipole at a height of 0.4585λ above an infinite perfect electric conductor.

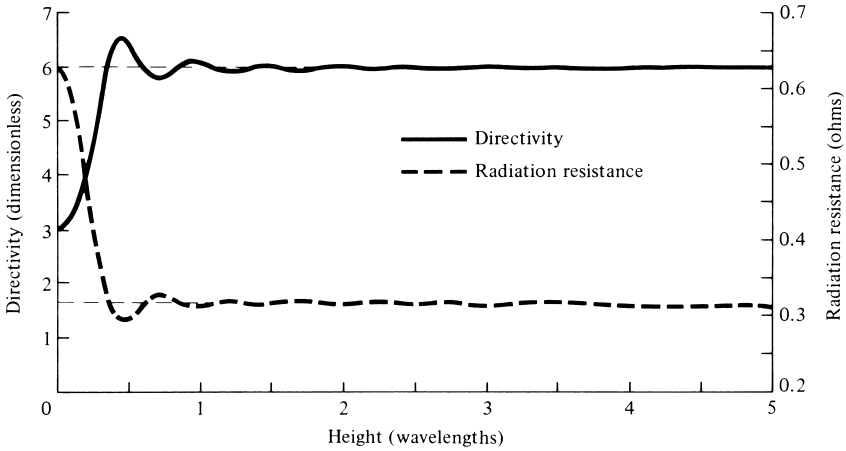

Figure 4.18 Directivity and radiation resistance of a vertical infinitesimal electric dipole as a function of its height above an infinite perfect electric conductor.

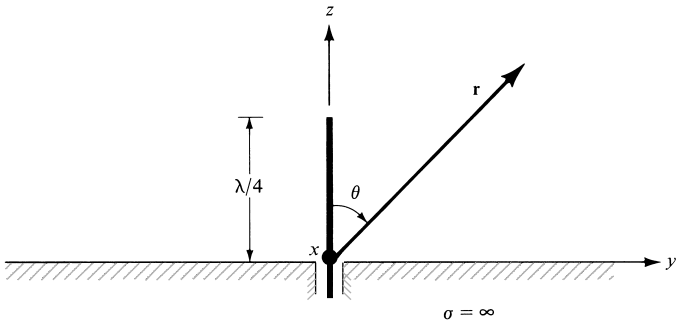

(a) λ/4 monopole on infinite electric conductor

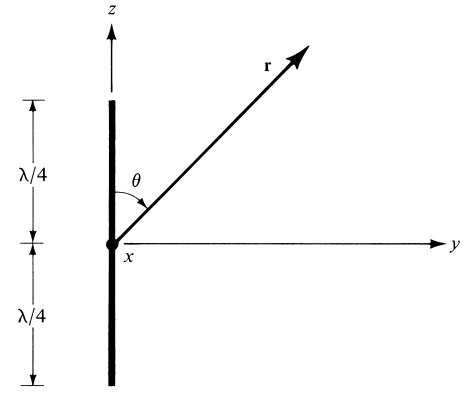

(b) Equivalent of λ/4 monopole on infinite electric conductor

Figure 4.19 Quarter-wavelength monopole on an infinite perfect electric conductor.

the correct field values for the actual system of Figure 4.19(a) only above the interface ($z \geq 0, 0 \leq \theta \leq \pi/2$). Thus, the far-zone electric and magnetic fields for the $\lambda/4$ monopole above the ground plane are given, respectively, by (4-84) and (4-85).

From the discussions of the resistance of an infinitesimal dipole above a ground plane for $kh = 0$, it follows that the input impedance of a $\lambda/4$ monopole above a ground plane is equal to one-half that of an isolated $\lambda/2$ dipole. Thus, referred to the current maximum, the input impedance Z_{im} is given by

$$Z_{im} \text{ (monopole)} = \tfrac{1}{2} Z_{im} \text{ (dipole)} = \tfrac{1}{2}[73 + j42.5] = 36.5 + j21.25 \qquad (4\text{-}106)$$

where $73 + j42.5$ is the input impedance (and also the impedance referred to the current maximum) of a $\lambda/2$ dipole as given by (4-93a).

The same procedure can be followed for any other length. The input impedance $Z_{im} = R_{im} + jX_{im}$ (referred to the current maximum) of a vertical $\lambda/2$ dipole placed near a flat lossy electric conductor, as a function of height above the ground plane, is plotted in Figure 4.20, for $0 \leq h \leq \lambda$. Conductivity values considered were 10^{-2}, 10^{-1}, 1, 10 S/m, and infinity (PEC). It is apparent that the conductivity does not strongly influence the impedance values. The conductivity values used are representative of dry to wet earth. It is observed that the values of the resistance and reactance approach, as the height increases, the corresponding ones of the isolated element (73 ohms for the resistance and 42.5 ohms for the reactance).

4.7.3 Approximate Formulas for Rapid Calculations and Design

Although the input resistance of a dipole of any length can be computed using (4-70) and (4-79), while that of the corresponding monopole using (4-106), very good answers

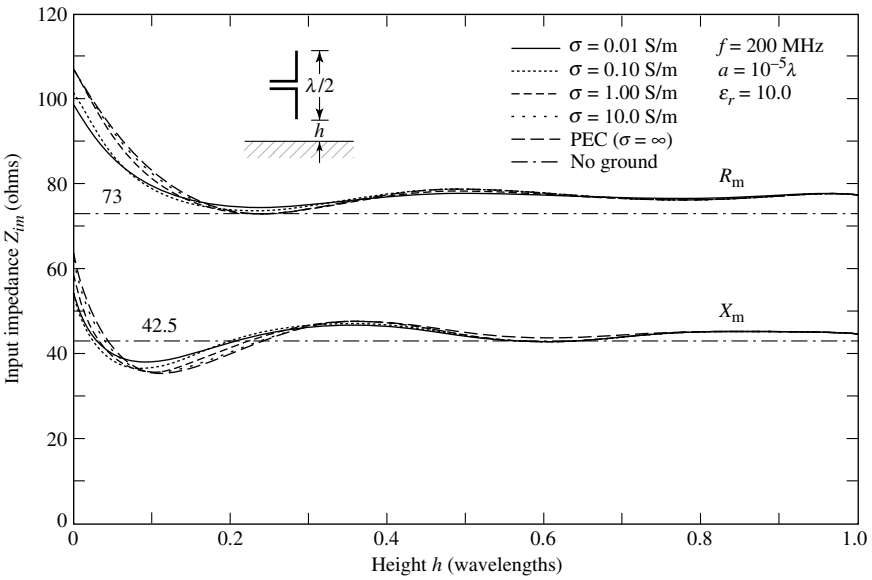

Figure 4.20 Input impedance of a vertical $\lambda/2$ dipole above a flat lossy electric conducting surface.

can be obtained using simpler but approximate expressions. Defining G as

$$G = kl/2 \text{ for dipole} \tag{4-107a}$$

$$G = kl \text{ for monopole} \tag{4-107b}$$

where l is the total length of each respective element, it has been shown that the input resistance of the dipole and monopole can be computed approximately using [13]

$$0 < G < \pi/4$$

(*maximum input resistance of dipole is less than 12.337 ohms*)

$$R_{in} \text{ (dipole)} = 20G^2 \qquad 0 < l < \lambda/4 \tag{4-108a}$$

$$R_{in} \text{ (monopole)} = 10G^2 \quad 0 < l < \lambda/8 \tag{4-108b}$$

$$\pi/4 \leq G < \pi/2$$

(*maximum input resistance of dipole is less than 76.383 ohms*)

$$R_{in} \text{ (dipole)} = 24.7G^{2.5} \qquad \lambda/4 \leq l < \lambda/2 \tag{4-109a}$$

$$R_{in} \text{ (monopole)} = 12.35G^{2.5} \quad \lambda/8 \leq l < \lambda/4 \tag{4-109b}$$

$$\pi/2 \leq G < 2$$

(*maximum input resistance of dipole is less than 200.53 ohms*)

$$R_{in} \text{ (dipole)} = 11.14G^{4.17} \qquad \lambda/2 \leq l < 0.6366\lambda \tag{4-110a}$$

$$R_{in} \text{ (monopole)} = 5.57G^{4.17} \quad \lambda/4 \leq l < 0.3183\lambda \tag{4-110b}$$

Besides being much simpler in form, these formulas are much more convenient in design (synthesis) problems where the input resistance is given and it is desired to determine the length of the element. These formulas can be verified by plotting the actual resistance versus length on a log–log scale and observe the slope of the line [13]. For example, the slope of the line for values of G up to about $\pi/4 \simeq 0.75$ is 2.

Example 4.4

Determine the length of the dipole whose input resistance is 50 ohms. Verify the answer.

Solution: Using (4-109a)

$$50 = 24.7G^{2.5}$$

or

$$G = 1.3259 = kl/2$$

Therefore

$$l = 0.422\lambda$$

Using (4-70) and (4-79) R_{in} for 0.422λ is 45.816 ohms, which closely agrees with the desired value of 50 ohms. To obtain 50 ohms using (4-70) and (4-79), $l = 0.4363\lambda$.

4.7.4 Antennas for Mobile Communication Systems

The dipole and monopole are two of the most widely used antennas for wireless mobile communication systems [14]–[18]. An array of dipole elements is extensively used as an antenna at the base station of a land mobile system while the monopole, because of its broadband characteristics and simple construction, is perhaps to most common antenna element for portable equipment, such as cellular telephones, cordless telephones, automobiles, trains, etc. The radiation efficiency and gain characteristics of both of these elements are strongly influenced by their electrical length which is related to the frequency of operation. In a handheld unit, such as a cellular telephone, the position of the monopole element on the unit influences the pattern while it does not strongly affect the input impedance and resonant frequency. In addition to its use in mobile communication systems, the quarter-wavelength monopole is very popular in many other applications. An alternative to the monopole for the handheld unit is the loop, which is discussed in Chapter 5. Other elements include the inverted F, planar inverted F antenna (PIFA), microstrip (patch), spiral, and others [14]–[18].

The variation of the input impedance, real and imaginary parts, of a vertical monopole antenna mounted on an experimental unit, simulating a cellular telephone, are shown in Figure 4.21(a,b) [17]. It is apparent that the first resonance, around 1,000 MHz, is of the *series type* with slowly varying values of impedance versus frequency, and of desirable magnitude, for practical implementation. For frequencies below the first resonance, the impedance is capacitive (imaginary part is negative), as is typical of linear elements of small lengths (see Figure 8.17); above the first resonance, the impedance is inductive (positive imaginary part). The second resonance, around 1,500 MHz, is of the *parallel type* (*antiresonance*) with large and rapid changes in the values of the impedance. These values and variation of impedance are usually undesirable for practical implementation. The order of the types of resonance (*series* vs. *parallel*) can be interchanged by choosing another element, such as a loop, as illustrated in Chapter 5, Section 5.8, Figure 5.20 [18]. The radiation amplitude patterns are those of a typical dipole with intensity in the lower hemisphere.

Examples of monopole type antennas used in cellular and cordless telephones, walkie-talkies, and CB radios are shown in Figure 4.22. The monopoles used in these units are either stationary or retractable/telescopic. The length of the retractable/telescopic monopole, such as the one used in the Motorola StarTAC and in others, is varied during operation to improve the radiation characteristics, such as the amplitude pattern and input impedance. During nonusage, the element is usually retracted within the body of the device to prevent it from damage. Units that do not utilize a visible monopole type of antenna, such as the one of the cellular telephones in Figure 4.22, use embedded/hidden type of antenna element. One such embedded/hidden element that is often used is a planar inverted F antenna (PIFA) [16]; there are others. Many of the stationary monopoles are often covered with a dielectric cover. Within the cover, there is typically a straight wire. *However, another design that is often used is a helix antenna* (see Chapter 10, Section 10.3.1) *with a very small circumference and overall length so that the helix operates in the normal mode, whose relative pattern is exhibited in Figure 10.14(a) and which resembles that of a straight-wire monopole. The helix is used, in lieu of a straight wire, because it can be designed to have larger input impedance, which is more attractive for matching to typical feed lines, such as a coaxial line* (see Problem 10.18).

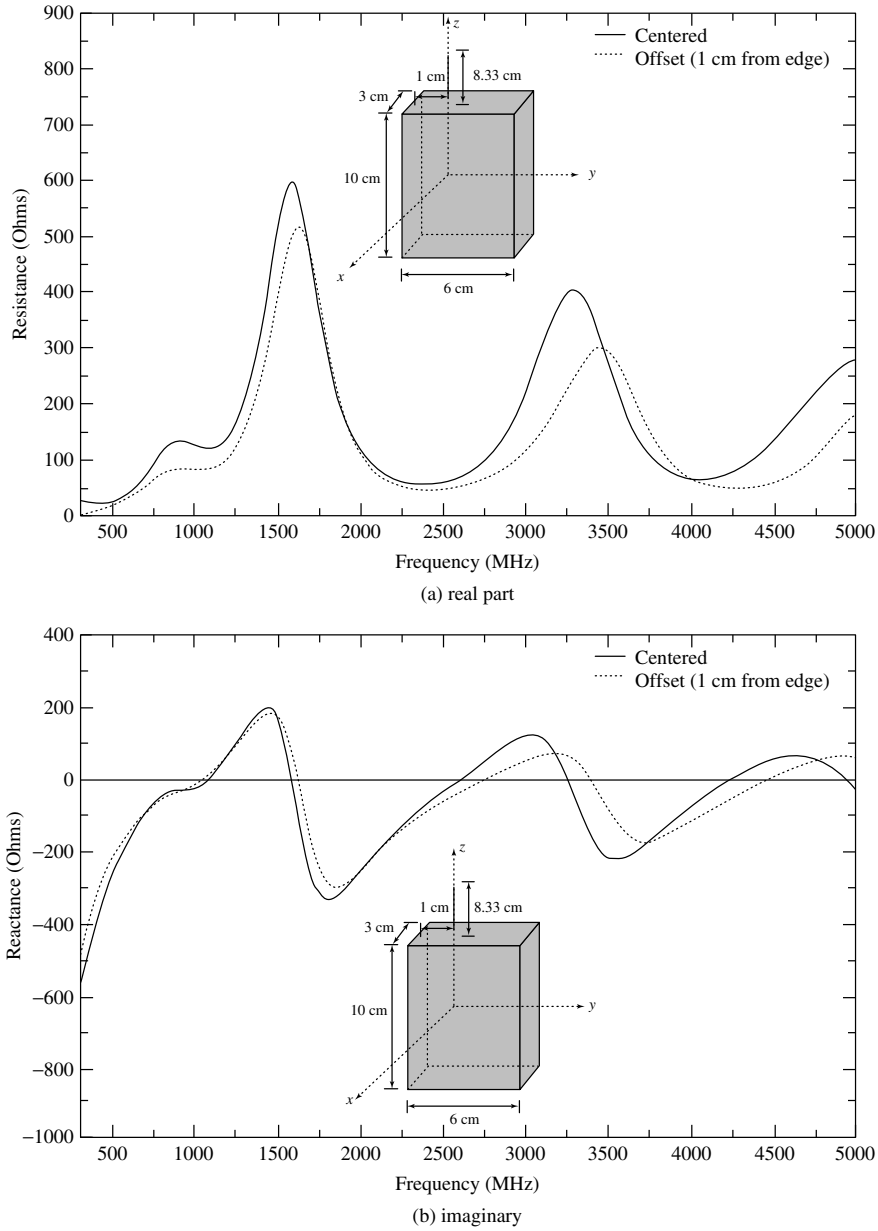

Figure 4.21 Input impedance, real and imaginary parts, of a vertical monopole mounted on an experimental cellular telephone device.

An antenna configuration that is widely used as a base-station antenna for mobile communication and is seen almost everywhere is shown in Figure 4.23. It is a triangular array configuration consisting of twelve dipoles, with four dipoles on each side of the triangle. Each four-element array, on each side of the triangle, is used to cover an angular sector of 120°, forming what is usually referred to as a sectoral array [see Section 16.3.1(B) and Figure 16.6(a)].

Figure 4.22 Examples of stationary, retractable/telescopic and embedded/hidden antennas used in commercial cellular and cordless telephones, walkie-talkies, and CB radios. (SOURCE: Reproduced with permissions from Motorola, Inc. © Motorola, Inc.; Samsung © Samsung; Midland Radio Corporation © Midland Radio Corporation).

4.7.5 Horizontal Electric Dipole

Another dipole configuration is when the linear element is placed horizontally relative to the infinite electric ground plane, as shown in Figure 4.24. The analysis procedure of this is identical to the one of the vertical dipole. Introducing an image and assuming far-field observations, as shown in Figure 4.25(a,b), the direct component can be written as

$$E_{\psi}^{d} = j\eta \frac{kI_0 l e^{-jkr_1}}{4\pi r_1} \sin\psi \tag{4-111}$$

and the reflected one by

$$E_{\psi}^{r} = jR_h \eta \frac{kI_0 l e^{-jkr_2}}{4\pi r_2} \sin\psi \tag{4-112}$$

or

$$E_{\psi}^{r} = -j\eta \frac{kI_0 l e^{-jkr_2}}{4\pi r_2} \sin\psi \tag{4-112a}$$

since the reflection coefficient is equal to $R_h = -1$.

To find the angle ψ, which is measured from the y-axis toward the observation point, we first form

$$\cos\psi = \hat{\mathbf{a}}_y \cdot \hat{\mathbf{a}}_r = \hat{\mathbf{a}}_y \cdot (\hat{\mathbf{a}}_x \sin\theta\cos\phi + \hat{\mathbf{a}}_y \sin\theta\sin\phi + \hat{\mathbf{a}}_z \cos\theta) = \sin\theta\sin\phi \tag{4-113}$$

Figure 4.23 Triangular array of dipoles used as a sectoral base-station antenna for mobile communication.

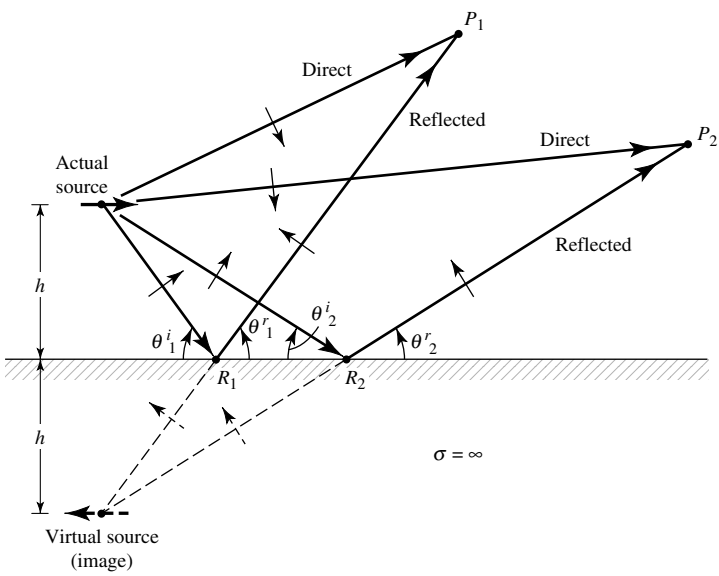

Figure 4.24 Horizontal electric dipole, and its associated image, above an infinite, flat, perfect electric conductor.

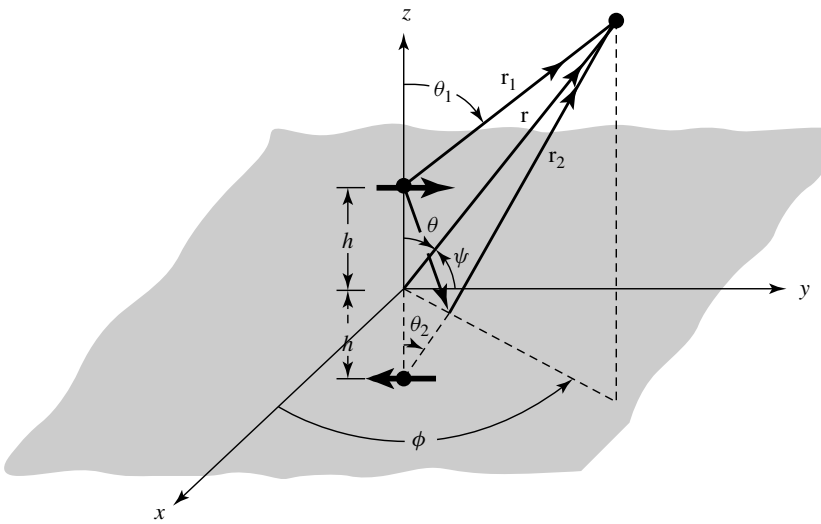

(a) Horizontal electric dipole above ground plane

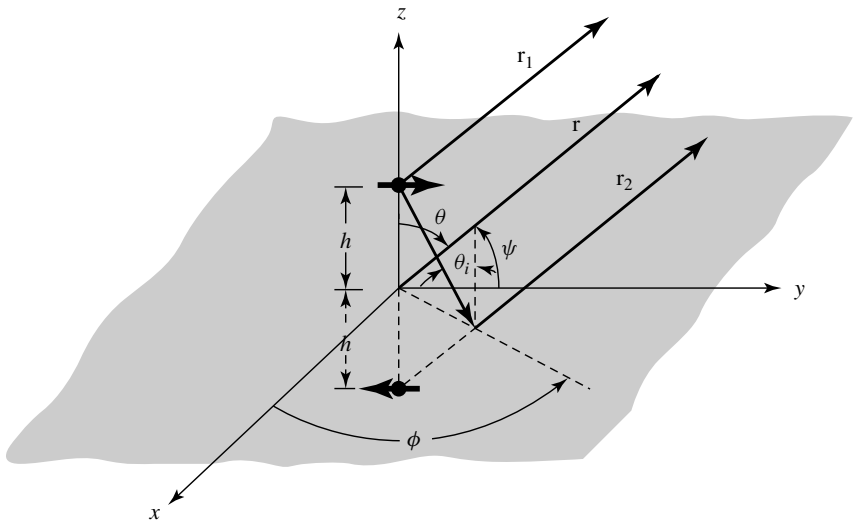

(b) Far-field observations

Figure 4.25 Horizontal electric dipole above an infinite perfect electric conductor.

from which we find

$$\sin\psi = \sqrt{1-\cos^2\psi} = \sqrt{1-\sin^2\theta\sin^2\phi} \tag{4-114}$$

Since for far-field observations

$$\left.\begin{aligned} r_1 &\simeq r - h\cos\theta \\ r_2 &\simeq r + h\cos\theta \end{aligned}\right\} \quad \text{for phase variations} \tag{4-115a}$$

$$r_1 \simeq r_2 \simeq r \qquad \text{for amplitude variations} \tag{4-115b}$$

the total field, which is valid only above the ground plane ($z \geq h; 0 \leq \theta \leq \pi/2, 0 \leq \phi \leq 2\pi$), can be written as

$$E_\psi = E_\psi^d + E_\psi^r = j\eta \frac{kI_0 l e^{-jkr}}{4\pi r} \sqrt{1 - \sin^2\theta \sin^2\phi}\ [2j \sin(kh\cos\theta)] \tag{4-116}$$

Equation (4-116) again consists of the product of the field of a single isolated element placed symmetrically at the origin and a factor (within the brackets) known as the *array factor*. This again is the pattern multiplication rule of (6-5) which is discussed in more detail in Chapter 6.

Example 4.5

Using the vector potential **A** and the procedure outlined in Section 3.6 of Chapter 3, derive the far-zone spherical electric and magnetic field components of a horizontal infinitesimal dipole placed at the origin of the coordinate system of Figure 4.1.

Solution: Using (4-4), but for a horizontal infinitesimal dipole of uniform current directed along the y-axis, the corresponding vector potential can be written as

$$\underline{A} = \hat{a}_y \frac{\mu I_0 \ell e^{-jkr}}{4\pi r}$$

with the corresponding spherical components, using the rectangular to spherical components transformation of (4-5), expressed as

$$A_\theta = A_y \cos\theta \sin\phi = \frac{\mu I_0 \ell e^{-jkr}}{4\pi r} \cos\theta \sin\phi$$

$$A_\phi = A_y \cos\phi = \frac{\mu I_0 \ell e^{-jkr}}{4\pi r} \cos\phi$$

Using (3-58a) and (3-58b), we can write the corresponding far-zone electric and magnetic field components as

$$E_\theta \cong -j\omega A_\theta = -j \frac{\omega\mu I_0 \ell e^{-jkr}}{4\pi r} \cos\theta \sin\phi$$

$$E_\phi \cong -j\omega A_\phi = -j \frac{\omega\mu I_0 \ell e^{-jkr}}{4\pi r} \cos\phi$$

$$H_\theta \cong -\frac{E_\phi}{\eta} = j \frac{\omega\mu I_0 \ell e^{-jkr}}{4\pi\eta r} \cos\phi$$

$$H_\phi \cong +\frac{E_\theta}{\eta} = +j \frac{\omega\mu I_0 \ell e^{-jkr}}{4\pi\eta r} \cos\theta \sin\phi$$

Although the electric-field components, and thus the magnetic field components, take a different analytical form than (4-111), the patterns are the same.

To examine the variations of the total field as a function of the element height above the ground plane, the two-dimensional elevation plane patterns (normalized to 0 dB) for $\phi = 90^\circ$ (y-z plane) when $h = 0, \lambda/8, \lambda/4, 3\lambda/8, \lambda/2$, and λ are plotted

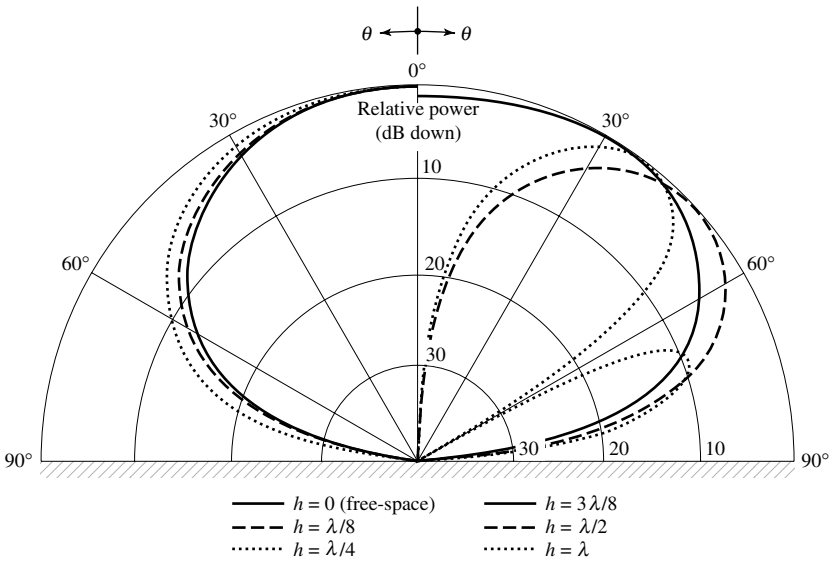

Figure 4.26 Elevation plane ($\phi = 90°$) amplitude patterns of a horizontal infinitesimal electric dipole for different heights above an infinite perfect electric conductor.

in Figure 4.26. Since this antenna system is not symmetric with respect to the z axis, the azimuthal plane (x-y plane) pattern is not isotropic.

To obtain a better visualization of the radiation intensity in all directions above the interface, the three-dimensional pattern for $h = \lambda$ is shown plotted in Figure 4.27. The radial distance on the x-y plane represents the elevation angle θ from 0° to 90°, and the z-axis represents the normalized amplitude of the radiation field intensity from 0 to 1. The azimuthal angle ϕ ($0 \leq \phi \leq 2\pi$) is measured from the x- toward the y-axis on the x-y plane.

As the height increases beyond one wavelength ($h > \lambda$), a larger number of lobes is again formed. This is illustrated in Figure 4.28 for $h = 2\lambda$ and 5λ. The scalloping effect is evident here, as in Figure 4-16 for the vertical dipole. The total number of lobes is equal to the integer that most closely is equal to

$$\boxed{\text{number of lobes} \simeq 2\left(\frac{h}{\lambda}\right)} \tag{4-117}$$

with unity being the smallest number.

Following a procedure similar to the one performed for the vertical dipole, the radiated power can be written as

$$P_{\text{rad}} = \eta\frac{\pi}{2}\left|\frac{I_0 l}{\lambda}\right|^2\left[\frac{2}{3} - \frac{\sin(2kh)}{2kh} - \frac{\cos(2kh)}{(2kh)^2} + \frac{\sin(2kh)}{(2kh)^3}\right] \tag{4-118}$$

and the radiation resistance as

$$R_r = \eta\pi\left(\frac{l}{\lambda}\right)^2\left[\frac{2}{3} - \frac{\sin(2kh)}{2kh} - \frac{\cos(2kh)}{(2kh)^2} + \frac{\sin(2kh)}{(2kh)^3}\right] \tag{4-119}$$

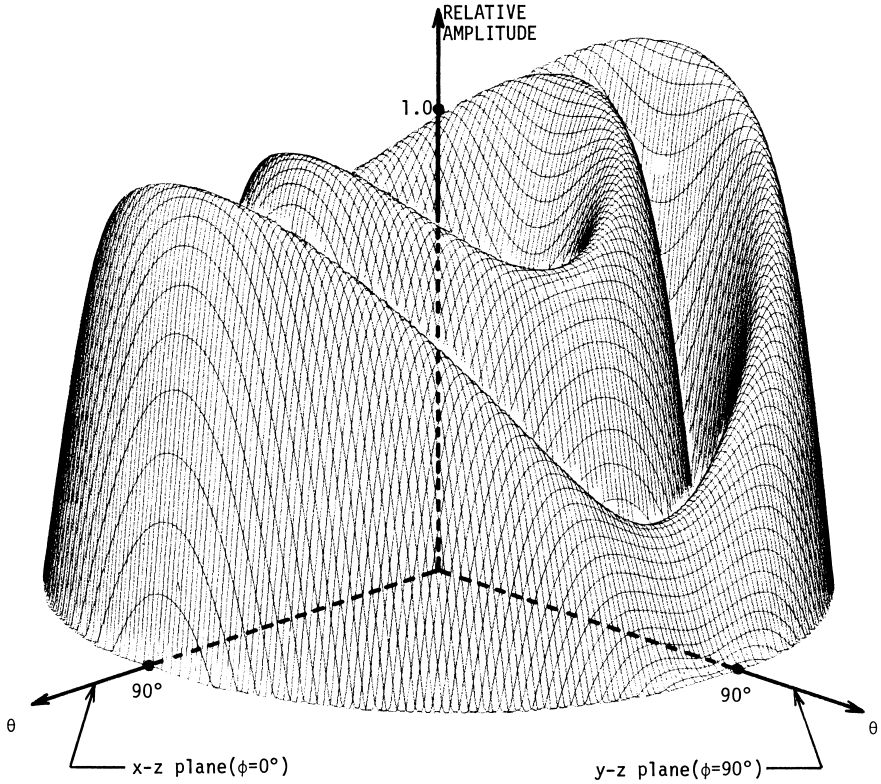

Figure 4.27 Three-dimensional amplitude pattern of an infinitesimal horizontal dipole a distance $h = \lambda$ above an infinite perfect electric conductor.

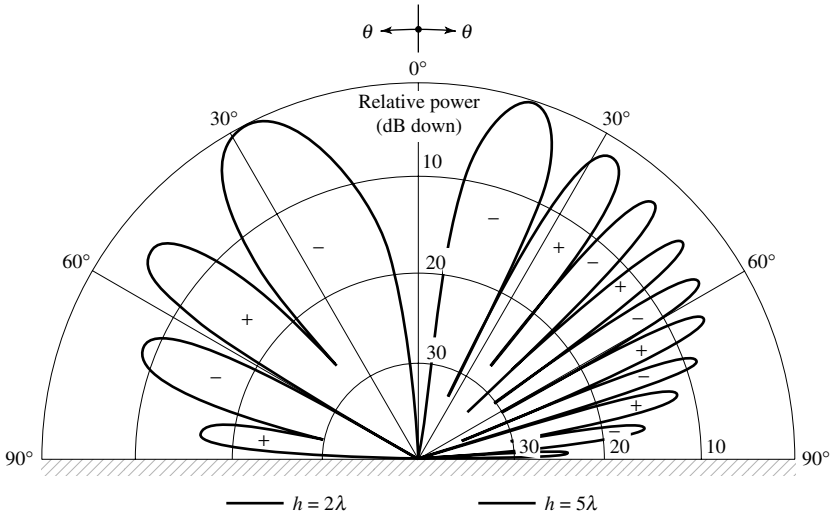

Figure 4.28 Elevation plane ($\phi = 90°$) amplitude patterns of a horizontal infinitesimal electric dipole for heights 2λ and 5λ above an infinite perfect electric conductor.

By expanding the sine and cosine functions into series, it can be shown that (4-119) reduces for small values of kh to

$$R_r \overset{kh\to 0}{=} \eta\pi\left(\frac{l}{\lambda}\right)^2\left[\frac{2}{3}-\frac{2}{3}+\frac{8}{15}\left(\frac{2\pi h}{\lambda}\right)^2\right]=\eta\frac{32\pi^3}{15}\left(\frac{l}{\lambda}\right)^2\left(\frac{h}{\lambda}\right)^2 \tag{4-120}$$

For $kh \to \infty$, (4-119) reduces to that of an isolated element. The radiation resistance, as given by (4-119), is plotted in Figure 4.29 for $0 \le h \le 5\lambda$ when $l = \lambda/50$ and the antenna is radiating into free-space ($\eta \simeq 120\pi$).

The radiation intensity is given by

$$U \simeq \frac{r^2}{2\eta}|E_\psi|^2=\frac{\eta}{2}\left|\frac{I_0 l}{\lambda}\right|^2(1-\sin^2\theta\sin^2\phi)\sin^2(kh\cos\theta) \tag{4-121}$$

The maximum value of (4-121) depends on the value of kh (whether $kh \le \pi/2, h \le \lambda/4$ or $kh > \pi/2, h > \lambda/4$). It can be shown that the maximum of (4-121) is:

$$U_{\max}=\begin{cases}\dfrac{\eta}{2}\left|\dfrac{I_0 l}{\lambda}\right|^2\sin^2(kh) & kh \le \pi/2\ (h \le \lambda/4)\ (\theta = 0^\circ) \quad \text{(4-122a)}\\[2ex] \dfrac{\eta}{2}\left|\dfrac{I_0 l}{\lambda}\right|^2 & kh > \pi/2\ (h > \lambda/4)\ [\phi = 0^\circ \text{ and } \sin(kh\cos\theta_{\max}) = 1 \text{ or } \theta_{\max} = \cos^{-1}(\pi/2kh)] \quad \text{(4-122b)}\end{cases}$$

Using (4-118) and (4-122a), (4-122b), the directivity can be written as

$$D_0=\frac{4\pi U_{\max}}{P_{\text{rad}}}=\begin{cases}\dfrac{4\sin^2(kh)}{R(kh)} & kh \le \pi/2\ (h \le \lambda/4) \quad \text{(4-123a)}\\[2ex] \dfrac{4}{R(kh)} & kh > \pi/2\ (h > \lambda/4) \quad \text{(4-123b)}\end{cases}$$

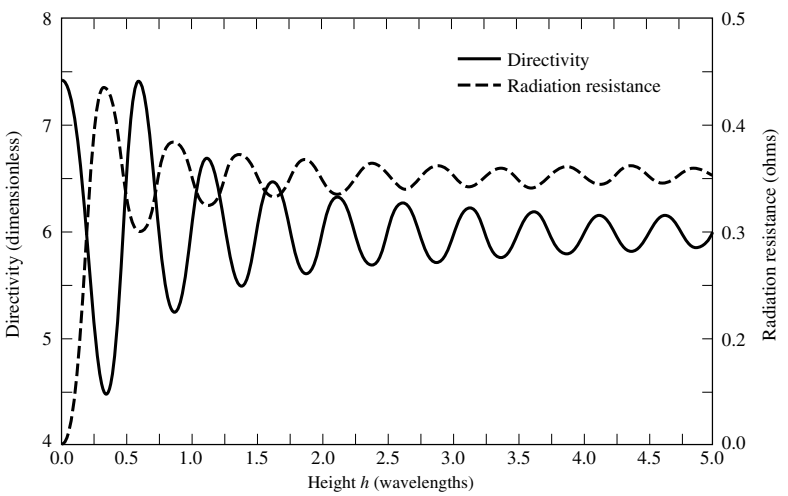

Figure 4.29 Radiation resistance and maximum directivity of a horizontal infinitesimal electric dipole as a function of its height above an infinite perfect electric conductor.

where

$$R(kh) = \left[\frac{2}{3} - \frac{\sin(2kh)}{2kh} - \frac{\cos(2kh)}{(2kh)^2} + \frac{\sin(2kh)}{(2kh)^3}\right] \tag{4-123c}$$

For small values of kh ($kh \to 0$), (4-123a) reduces to

$$D_0 \overset{kh\to 0}{=} \frac{4\sin^2(kh)}{\left[\frac{2}{3} - \frac{2}{3} + \frac{8}{15}(kh)^2\right]} = 7.5\left(\frac{\sin\ kh}{kh}\right)^2 \tag{4-124}$$

For $h = 0$ the element is shorted and it does not radiate. The directivity, as given by (4-123a)–(4-123b) is plotted for $0 \le h \le 5\lambda$ in Figure 4.29. It exhibits a maximum value of 7.5 for small values of h. Maximum values of slightly greater than 6 occur when $h \simeq (0.615 + n/2)\lambda$, $n = 1, 2, 3, \ldots$.

The input impedance $Z_{im} = R_{im} + jX_{im}$ (referred to the current maximum) of a horizontal $\lambda/2$ dipole above a flat lossy electric conductor is shown plotted in Figure 4.30 for $0 \le h \le \lambda$. Conductivities of 10^{-2}, 10^{-1}, 1, 10 S/m, and infinity (PEC) were considered. It is apparent that the conductivity does have a more pronounced effect on the impedance values, compared to those of the vertical dipole shown in Figure 4.20. The conductivity values used are representative of those of the dry to wet earth. The values of the resistance and reactance approach, as the height increases, the corresponding values of the isolated element (73 ohms for the resistance and 42.5 ohms for the reactance).

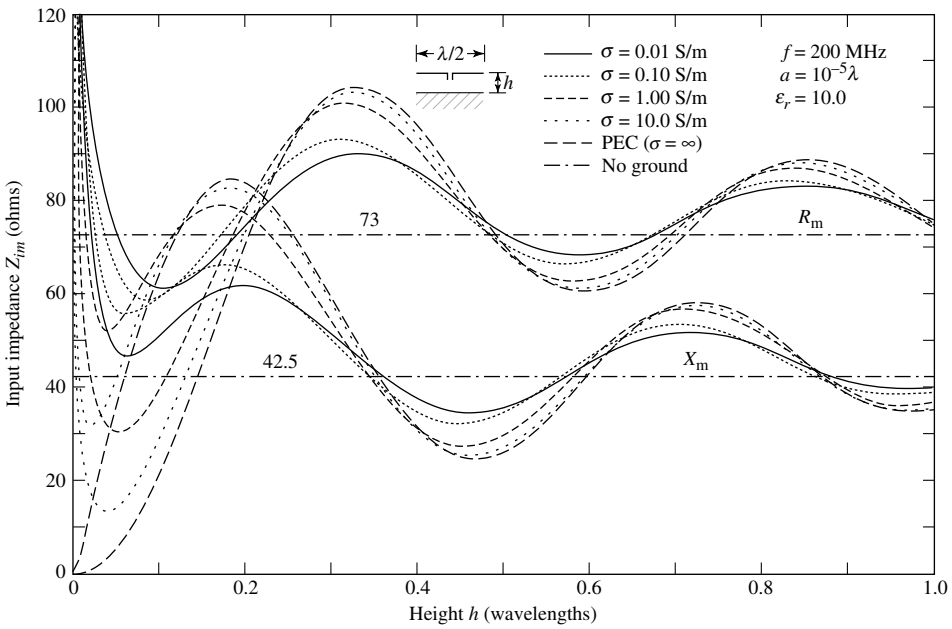

Figure 4.30 Input impedance of a horizontal $\lambda/2$ above a flat lossy electric conducting surface.

4.8 GROUND EFFECTS

In the previous two sections the variations of the radiation characteristics (pattern, radiation resistance, directivity) of infinitesimal vertical and horizontal linear elements were examined when they were placed above plane perfect electric conductors. Although ideal electric conductors ($\sigma = \infty$) are not realizable, their effects can be used as guidelines for good conductors ($\sigma \gg \omega\epsilon$, where ϵ is the permittivity of the medium).

One obstacle that is not an ideal conductor, and it is always present in any antenna system, is the ground (earth). In addition, the earth is not a plane surface. To simplify the analysis, however, the earth will initially be assumed to be flat. For pattern analysis, this is a very good engineering approximation provided the radius of the earth is large compared to the wavelength and the observation angles are greater than about $57.3/(ka)^{1/3}$ degrees from grazing (a is the earth radius) [19]. Usually these angles are greater than about 3°.

In general, the characteristics of an antenna at low (LF) and medium (MF) frequencies are profoundly influenced by the lossy earth. This is particularly evident in the input resistance. When the antenna is located at a height that is small compared to the skin depth of the conducting earth, the input resistance may even be greater than its free-space values [19]. This leads to antennas with very low efficiencies. Improvements in the efficiency can be obtained by placing radial wires or metallic disks on the ground.

The analytical procedures that are introduced to examine the ground effects are based on the geometrical optics models of the previous sections. The image (virtual) source is again placed a distance h below the interface to account for the reflection. However, for each polarization nonunity reflection coefficients are introduced which, in general, will be a function of the angles of incidence and the constitutive parameters of the two media. Although plane wave reflection coefficients are used, even though spherical waves are radiated by the source, the error is small for conducting media [20]. The spherical nature of the wavefront begins to dominate the reflection phenomenon at grazing angles (i.e., as the point of reflection approaches the horizon) [21]. If the height (h) of the antenna above the interface is much less than the skin depth $\delta[\delta = \sqrt{2/(\omega\mu\sigma)}]$ of the ground, the image depth h below the interface should be increased [20] by a complex distance $\delta(1 - j)$.

The geometrical optics formulations are valid provided the sources are located inside the lossless medium. When the sources are placed within the ground, the formulations should include possible surface-wave contributions. Exact boundary-value solutions, based on Sommerfeld integral formulations, are available [19]. However they are too complex to be included in an introductory chapter.

4.8.1 Vertical Electric Dipole

The field radiated by an electric infinitesimal dipole when placed above the ground can be obtained by referring to the geometry of Figures 4.14(a) and (b). Assuming the earth is flat and the observations are made in the far field, the direct component of the field is given by (4-94) and the reflected component by (4-95) where the reflection coefficient R_v is given by

$$R_v = \frac{\eta_0 \cos\theta_i - \eta_1 \cos\theta_t}{\eta_0 \cos\theta_i + \eta_1 \cos\theta_t} = -R_{\parallel} \tag{4-125}$$

where $R_{\parallel}$ is the reflection coefficient for parallel polarization [7] and

$\eta_0 = \sqrt{\dfrac{\mu_0}{\epsilon_0}}$ = intrinsic impedance of free-space (air)

$\eta_1 = \sqrt{\dfrac{j\omega\mu_1}{\sigma_1 + j\omega\epsilon_1}}$ = intrinsic impedance of the ground

θ_i = angle of incidence (relative to the normal)

θ_t = angle of refraction (relative to the normal)

The angles θ_i and θ_t are related by Snell's law of refraction

$$\gamma_0 \sin\theta_i = \gamma_1 \sin\theta_t \tag{4-126}$$

where

$\gamma_0 = jk_0$ = propagation constant for free-space (air)

k_0 = phase constant for free-space (air)

$\gamma_1 = (\alpha_1 + jk_1)$ = propagation constant for the ground

α_1 = attenuation constant for the ground

k_1 = phase constant for the ground

Using the far-field approximations of (4-97a)–(4-98), the total electric field above the ground ($z \geq 0$) can be written as

$$E_\theta = j\eta \frac{kI_0 l e^{-jkr}}{4\pi r} \sin\theta [e^{jkh\cos\theta} + R_v e^{-jkh\cos\theta}] \quad z \geq 0 \tag{4-127}$$

where R_v is given by (4-125).

The permittivity and conductivity of the earth are strong functions of the ground's geological constituents, especially its moisture. Typical values for the relative permittivity ϵ_r (dielectric constant) are in the range of 5–100 and for the conductivity σ in the range of $10^{-4} - 1$ S/m.

A normalized (to 0 dB) pattern for an infinitesimal dipole above the ground with $h = \lambda/4$, $\epsilon_{r1} = 5$, $f = 1$ GHz, $\sigma_1 = 10^{-2}$ S/m is shown plotted in Figure 4.31 (dashed curves) where it is compared with that (solid curve) of a perfect conductor ($\sigma_1 = \infty$). In the presence of the ground, the radiation toward the vertical direction ($60^\circ > \theta > 0^\circ$) is more intense than that for the perfect electric conductor, but it vanishes for grazing angles ($\theta = 90^\circ$). The null field toward the horizon ($\theta = 90^\circ$) is formed because the reflection coefficient R_v approaches -1 as $\theta_i \to 90^\circ$. Thus the ground effects on the pattern of a vertically polarized antenna are significantly different from those of a perfect conductor.

Significant changes also occur in the impedance. Because the formulation for the impedance is much more complex [19], it will not be presented here. Graphical illustrations for the impedance change of a vertical dipole placed a height h above a homogeneous lossy half-space, as compared to those in free-space, can be found in [22].

4.8.2 Horizontal Electric Dipole

The analytical formulation of the horizontal dipole above the ground can also be obtained in a similar manner as for the vertical electric dipole. Referring to

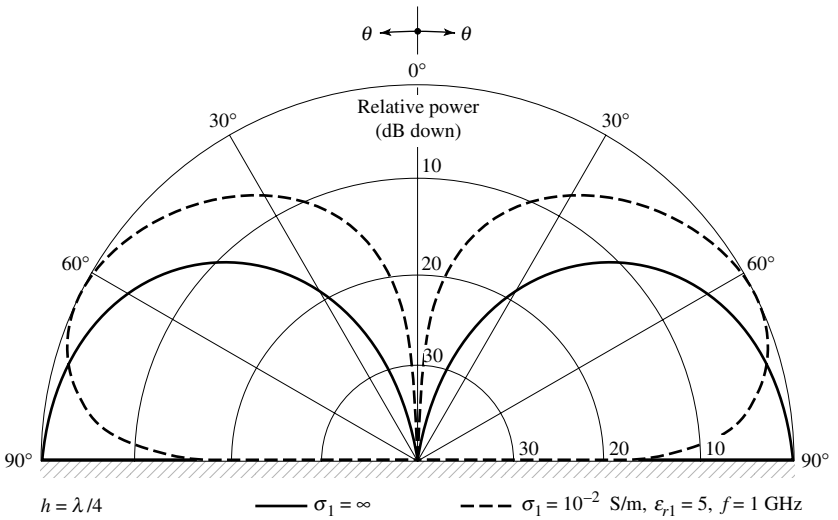

Figure 4.31 Elevation plane amplitude patterns of an infinitesimal vertical dipole above a perfect electric conductor ($\sigma_1 = \infty$) and a flat earth ($\sigma_1 = 0.01$ S/m, $\epsilon_{r1} = 5$, $f = 1$ GHz).

Figure 4.25(a) and (b), the direct component is given by (4-111) and the reflected by (4-112) where the reflection coefficient R_h is given by

$$R_h = \begin{cases} R_\perp \text{ for } \phi = 0^\circ, 180^\circ \text{ plane} \\ R_\parallel \text{ for } \phi = 90^\circ, 270^\circ \text{ plane} \end{cases} \tag{4-128}$$

where $R_\parallel$ is the reflection coefficient for parallel polarization, as given by (4-125), and $R_\perp$ is the reflection coefficient for perpendicular polarization given by [7]

$$R_\perp = \frac{\eta_1 \cos\theta_i - \eta_0 \cos\theta_t}{\eta_1 \cos\theta_i + \eta_0 \cos\theta_t} \tag{4-128a}$$

The angles θ_i and θ_t are again related by Snell's law of refraction as given by (4-126).

Using the far-field approximations of (4-115a) and (4-115b), the total field above the ground ($z \geq h$) can be written as

$$E_\psi = j\eta \frac{kI_0 e^{-jkr}}{4\pi r} \sqrt{1 - \sin^2\theta \sin^2\phi}\ [e^{jkh\cos\theta} + R_h e^{-jkh\cos\theta}], \quad z \geq h \tag{4-129}$$

where R_h is given by (4-128).

The normalized (to 0 dB) pattern in the y-z plane ($\phi = 90^\circ$) for $h = \lambda/4$ is shown plotted in Figure 4.32 (dashed curve) where it is compared with that (solid curve) of a perfect conductor ($\sigma_1 = \infty$). In the space above the interface, the relative pattern in the presence of the ground is not significantly different from that of a perfect conductor. This becomes more evident by examining R_h as given by (4-128). For a ground medium, the values of R_h for most observation angles are not much different from -1 (the value of R_h for a perfect conductor). For grazing angles ($\theta_i \to 90^\circ$), the values of R_h for the lossy ground approach -1 very rapidly. Thus the relative pattern

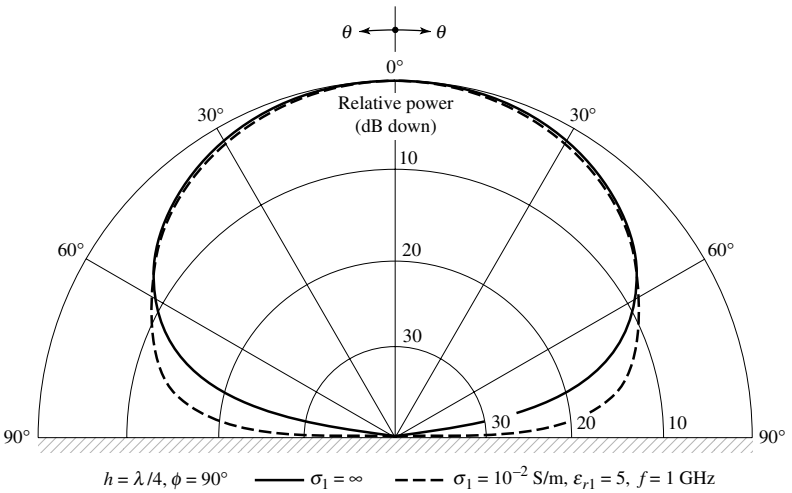

Figure 4.32 Elevation plane ($\phi = 90°$) amplitude patterns of an infinitesimal horizontal dipole above a perfect electric conductor ($\sigma_1 = \infty$) and a flat earth ($\sigma_1 = 0.01$ S/m, $\epsilon_{r1} = 5$, $f = 1$ GHz).

of a horizontal dipole above a lossy surface is not significantly different from that above a perfect conductor.

4.8.3 Earth Curvature

Antenna pattern measurements on aircraft can be made using either scale models or full scale in-flight. Scale model measurements usually are made indoors using electromagnetic anechoic chambers, as described in Chapter 17. The indoor facilities provide a controlled environment, and all-weather capability, security, and minimize electromagnetic interference. However, scale model measurements may not always simulate real-life outdoor conditions, such as the reflecting surface of seawater. Therefore full-scale model measurements may be necessary. For in-flight measurements, reflecting surfaces, such as seawater, introduce reflections, which usually interfere with the direct signal. These unwanted signals are usually referred to as *multipath*. Therefore the total measured signal in an outdoor system configuration is the combination of the direct signal and that due to multipath, and usually it cannot be easily separated in its parts using measuring techniques. Since the desired signal is that due to the direct path, it is necessary to be able to subtract from the total response the contributions due to multipath. This can be accomplished by developing analytical models to predict the contributions due to multipath, which can then be subtracted from the total signal in order to be left with the desired direct path signal. In this section we will briefly describe techniques that have been used to accomplish this [23], [24].

The analytical formulations of Sections 4.8.1 and 4.8.2 for the patterns of vertical and horizontal dipoles assume that the earth is flat. This is a good approximation provided the curvature of the earth is large compared to the wavelength and the angle of observation is greater than about 3° from grazing [or more accurately greater than about $57.3/(ka)^{1/3}$ degrees, where a is the radius of the earth] from grazing [25]. The curvature of the earth has a tendency to spread out (weaken, diffuse, diverge) the

reflected energy more than a corresponding flat surface. The spreading of the reflected energy from a curved surface as compared to that from a flat surface is taken into account by introducing a divergence factor D [21], [23], [24], defined as

$$D = \text{divergence factor} = \frac{\text{reflected field from curved surface}}{\text{reflected field from flat surface}} \tag{4-130}$$

The formula for D can be derived using purely geometrical considerations. It is accomplished by comparing the ray energy density in a small cone reflected from a sphere near the principal point of reflection with the energy density the rays (within the same cone) would have if they were reflected from a plane surface. Based on the geometrical optics energy conservation law for a bundle of rays within a cone, the reflected rays within the cone will subtend a circle on a perpendicular plane for reflections from a flat surface, as shown in Figure 4.33(a). However, according to the geometry of Figure 4.33(b), it will subtend an ellipse for a spherical reflecting surface. Therefore the divergence factor of (4-130) can also be defined as

$$D = \frac{E_s^r}{E_f^r} = \left[\frac{\text{area contained in circle}}{\text{area contained in ellipse}}\right]^{1/2} \tag{4-131}$$

where

E_s^r = reflected field from spherical surface
E_f^r = reflected field from flat surface

Using the geometry of Figure 4.34, the divergence factor can be written as [7] and [24]

$$D = \frac{\sqrt{\dfrac{\rho_1^r \rho_2^r}{(\rho_1^r + s)(\rho_2^r + s)}}}{\dfrac{s'}{s' + s}} \tag{4-132}$$

where ρ_1^r and ρ_2^r are the principal radii of curvature of the reflected wavefront at the point of reflection and are given, according to the geometry of Figure 4.34, by

$$\frac{1}{\rho_1^r} = \frac{1}{s'} + \frac{1}{\rho \sin\psi} + \sqrt{\frac{1}{(\rho \sin\psi)^2} - \frac{4}{a^2}} \tag{4-132a}$$

$$\frac{1}{\rho_2^r} = \frac{1}{s'} + \frac{1}{\rho \sin\psi} - \sqrt{\frac{1}{(\rho \sin\psi)^2} - \frac{4}{a^2}} \tag{4-132b}$$

$$\rho = \frac{a}{1 + \sin^2\psi} \tag{4-132c}$$

A simplified form of the divergence factor is that of [26]

$$D \cong \left[1 + \frac{2s's}{a(s' + s)\sin\psi}\right]^{-1/2} \cdot \left[1 + \frac{2s's}{a(s' + s)}\right]^{-1/2} \tag{4-133}$$

Both (4-132) and (4-133) take into account the earth curvature in two orthogonal planes.

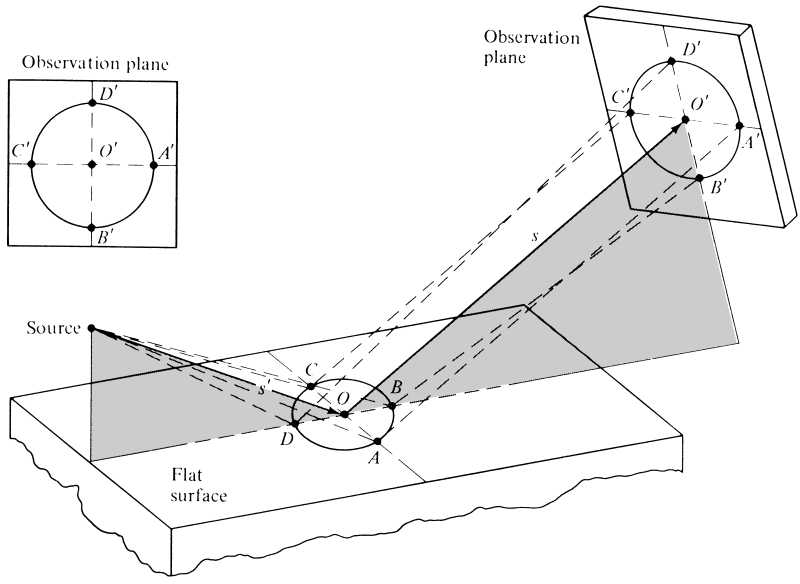

(a) Reflection from a flat surface

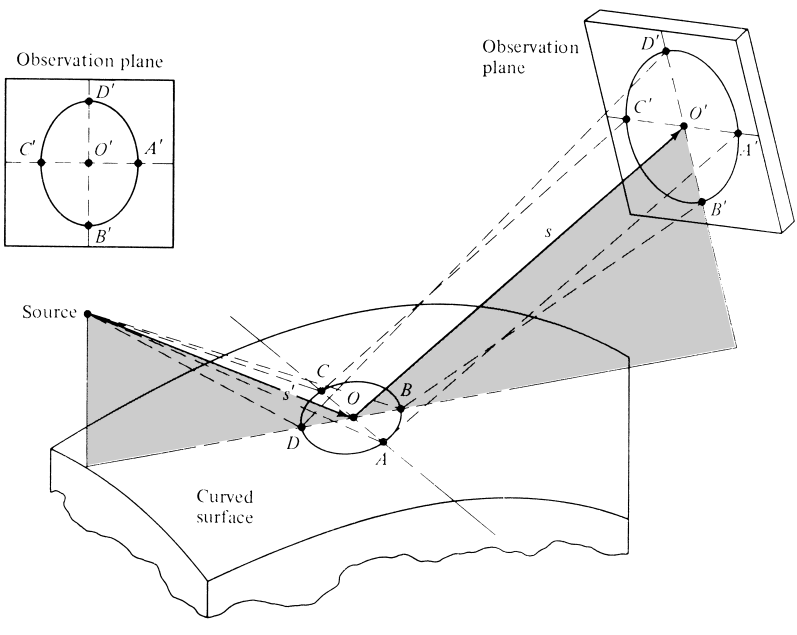

(b) Reflection from a spherical surface

Figure 4.33 Reflection from flat and spherical surfaces.

Assuming that the divergence of rays in the azimuthal plane (plane vertical to the page) is negligible (two-dimensional case), the divergence factor can be written as

$$D \simeq \left[1 + 2\frac{ss'}{ad\tan\psi}\right]^{-1/2} \tag{4-134}$$

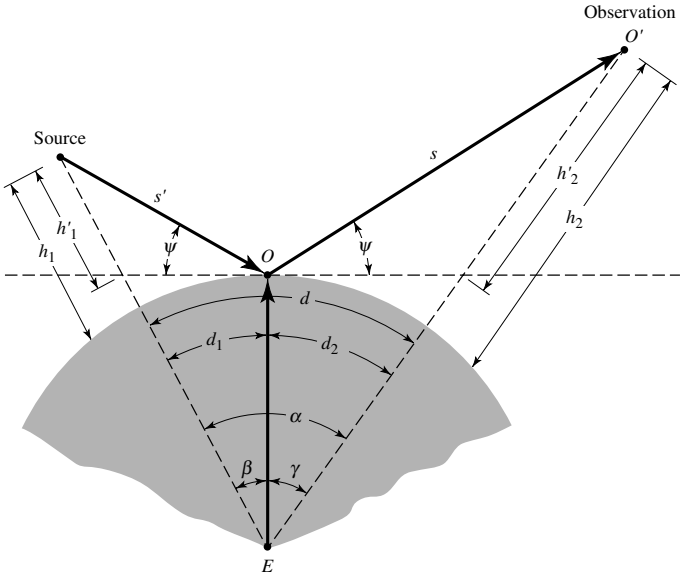

Figure 4.34 Geometry for reflections from a spherical surface.

where ψ is the grazing angle. Thus the divergence factor of (4-134) takes into account energy spreading primarily in the elevation plane. According to Figure 4.34

h_1' = height of the source above the earth (with respect to the tangent at the point of reflection)

h_2' = height of the observation point above the earth (with respect to the tangent at the point of reflection)

d = range (along the surface of the earth) between the source and the observation point

a = radius of the earth (3,959 mi). Usually a $\frac{4}{3}$ radius ($\simeq$ 5,280 mi) is used.

ψ = reflection angle (with respect to the tangent at the point of reflection).

d_1 = distance (along the surface of the earth) from the source to the reflection point

d_2 = distance (along the surface of the earth) from the observation point to the reflection point

The divergence factor can be included in the formulation of the fields radiated by a vertical or a horizontal dipole, in the presence of the earth, by modifying (4-127) and (4-129) and writing them, respectively, as

$$E_\theta = j\eta \frac{kI_0 l e^{-jkr}}{4\pi r} \sin\theta [e^{jkh\cos\theta} + DR_v e^{-jkh\cos\theta}] \tag{4-135a}$$

$$E_\psi = j\eta \frac{kI_0 l e^{-jkr}}{4\pi r} \sqrt{1 - \sin^2\theta \sin^2\phi} [e^{jkh\cos\theta} + DR_h e^{-jkh\cos\theta}] \tag{4-135b}$$

While the previous formulations are valid for smooth surfaces, they can still be used with rough surfaces, provided the surface geometry satisfies the Rayleigh criterion [21] and [26]

$$h_m < \frac{\lambda}{8\sin\psi} \tag{4-136}$$

where h_m is the maximum height of the surface roughness. Since the dividing line between a smooth and a rough surface is not that well defined, (4-136) should only be used as a guideline.

The *coherent* contributions due to scattering by a surface with Gaussian rough surface statistics can be approximately accounted for by modifying the vertical and horizontal polarization smooth surface reflection coefficients of (4-125) and (4-128) and express them as

$$R_{v,h}^{s} = R_{v,h}^{0} e^{-2(k_0 h_0 \cos\theta_i)^2} \tag{4-137}$$

where

$R_{v,h}^{s}$ = reflection coefficient of a rough surface for either vertical or horizontal polarization
$R_{v,h}^{0}$ = reflection coefficient of a smooth surface for either vertical (4-125) or horizontal (4-128) polarization
h_0^2 = mean-square roughness height

A *slightly rough surface* is defined as one whose rms height is much smaller than the wavelength, while a *very rough surface* is defined as one whose rms height is much greater than the wavelength.

Plots of the divergence factor as a function of the grazing angle ψ (or as a function of the observation point h_2') for different source heights are shown in Figure 4.35. It is observed that the divergence factor is somewhat different and smaller than unity for small grazing angles, and it approaches unity as the grazing angle becomes larger. The variations of D displayed in Figure 4.35 are typical but not unique. For different positions of the source and observation point, the variations will be somewhat different. More detailed information on the variation of the divergence factor and its effect on the overall field pattern is available [24].

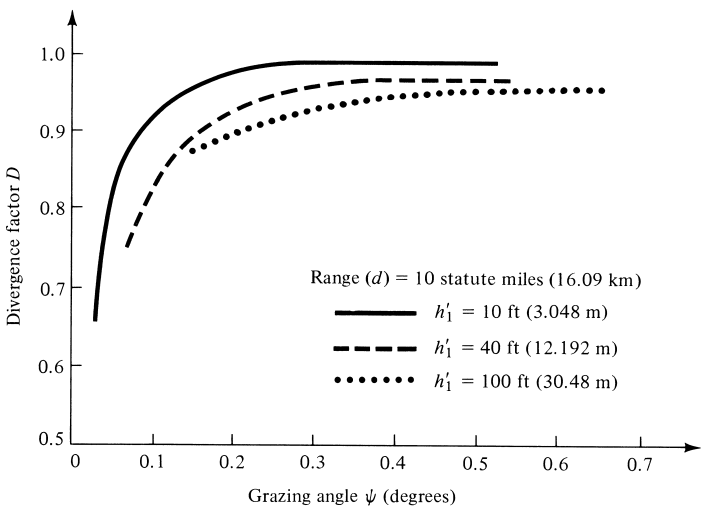

Figure 4.35 Divergence factor for a 4/3 radius earth (a_e = 5,280 mi = 8,497.3 km) as a function of grazing angle ψ.

The most difficult task usually involves the determination of the reflection point from a knowledge of the heights of the source and observation points, and the range d between them. Procedures to do this have been developed [21], [23]–[27].

However, the one presented here is more accurate and does not require either iterative or graphical solutions. To find d_1 and d_2 (given d, h_1, and h_2), the cubic equation of [21] is utilized

$$2d_1^3 - 3dd_1^2 + [d^2 - 2a(h_1 + h_2)]d_1 + 2ah_1d = 0 \tag{4-138}$$

with solution given by

$$d_1 = \frac{d}{2} + p\cos\left(\frac{\Omega + \pi}{3}\right) \tag{4-138a}$$

$$d_2 = d - d_1 \tag{4-138b}$$

$$p = \frac{2}{\sqrt{3}}\sqrt{a(h_1 + h_2) + \left(\frac{d}{2}\right)^2} \tag{4-138c}$$

$$\Omega = \cos^{-1}\left[\frac{2a(h_1 - h_2)\,d}{p^3}\right] \tag{4-138d}$$

Equation (4-138) is valid provided that $\alpha - \beta$ is small, such that $\sin(\alpha - \beta) \simeq \alpha - \beta$, $\cos(\alpha - \beta) \simeq 1 - (\alpha - \beta)^2/2$, $\sin\beta \simeq \beta$, and $\cos\beta \simeq 1 - (\beta)^2/2$. Once d_1 and d_2 are found, then successively β, γ, s', s, ψ, r_1, r_2, α_1^r, α_1^d, α_2^r, and α_2^d can be determined using the geometry of Figure 4.34.

Using the analytical model developed here, computations were made to see how well the predictions compared with measurements. For the computations it was assumed that the reflecting surface is seawater possessing a dielectric constant of 81 and a conductivity of 4.64 S/m [23], [24]. To account for atmospheric refraction, a 4/3 earth was assumed [21], [23], [28] so the atmosphere above the earth can be considered homogeneous with propagation occurring along straight lines.

For computations using the earth as the reflecting surface, all three divergence factors of (4-132)–(4-134) gave the same results. However, for nonspherical reflecting surfaces and for those with smaller radii of curvature, the divergence factor of (4-132) is slightly superior followed by (4-133) and then by (4-134). In Figure 4.36 we display and compare the predicted and measured *height gain* versus range d ($4 < d < 14$ nautical miles) for a vertical-vertical polarization system configuration at a frequency of 167.5 MHz. The *height gain* is defined as the ratio of the total field in the presence of the earth divided by the total field in the absence of the earth. A good agreement is noted between the two. The peaks and nulls are formed by constructive and destructive interferences between the direct and reflected components. If the reflecting surface were perfectly conducting, the maximum height gain would be 2 (6 dB). Because the modeled reflecting surface of Figure 4.36 was seawater with a dielectric constant of 81 and a conductivity of 4.64 S/m, the maximum height gain is less than 6 dB. The measurements were taken by aircraft and facilities of the Naval Air Warfare Center, Patuxent River, MD. Additional measurements were made but are not included here; they can be found in [29] and [30].

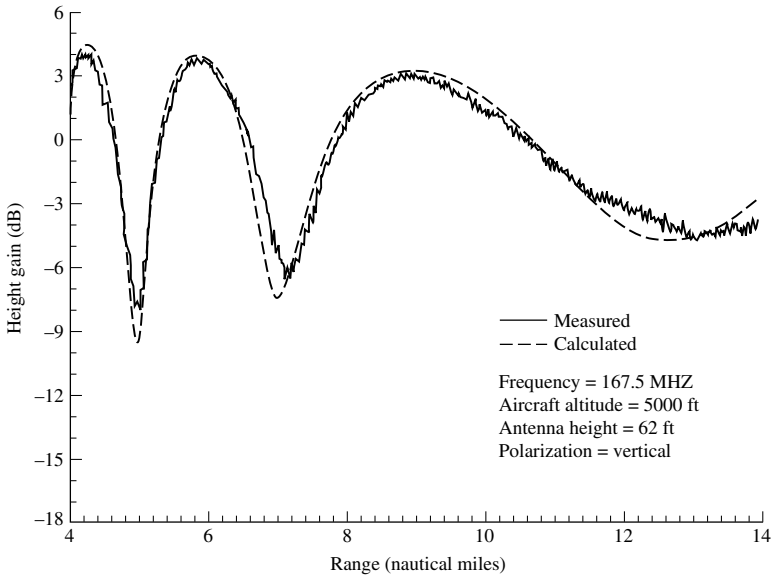

Figure 4.36 Measured and calculated height gain over the ocean ($\epsilon_r = 81, \sigma = 4.64$ S/m) for vertical polarization.

A summary of the pertinent parameters, and associated formulas and equation numbers for this chapter are listed in Table 4.2.

4.9 COMPUTER CODES

There are many computer codes that have been developed to analyze wire-type linear antennas, such as the dipole, and they are too numerous to mention here. One simple program to characterize the radiation characteristics of a dipole, designated as *Dipole* (both in FORTRAN and MATLAB), is included in the attached CD. Another much more advanced program, designated as the **Numerical Electromagnetics Code (NEC)**, is a user-oriented software developed by Lawrence Livermore National Laboratory [31]. It is a Method of Moments (MoM) code for analyzing the interaction of electromagnetic waves with arbitrary structures consisting of conducting wires and surfaces. It is probably the most widely distributed and used electromagnetics code. Included with the distribution are graphics programs for generating plots of the structure, antenna patterns, and impedance. There are also other commercial software that are based on the NEC. A compact version of the NEC is the **MININEC (Mini-Numerical Electromagnetics Code)** [31]–[33]. The MININEC is more convenient for the analysis of wire-type antennas. More information can be obtained by contacting:

G. J. Burke, L-156
Lawrence Livermore National Laboratory
P. O. Box 5504
Livermore, CA 94550

TABLE 4.2 Summary of Important Parameters and Associated Formulas and Equation Numbers for a Dipole in the Far Field

Parameter	Formula	Equation Number
	Infinitesimal Dipole $(l \le \lambda/50)$	
Normalized power pattern	$U = (E_{\theta n})^2 = C_0 \sin^2\theta$	(4-29)
Radiation resistance R_r	$R_r = \eta\left(\frac{2\pi}{3}\right)\left(\frac{l}{\lambda}\right)^2 = 80\pi^2\left(\frac{l}{\lambda}\right)^2$	(4-19)
Input resistance R_{in}	$R_{in} = R_r = \eta\left(\frac{2\pi}{3}\right)\left(\frac{l}{\lambda}\right)^2 = 80\pi^2\left(\frac{l}{\lambda}\right)^2$	(4-19)
Wave impedance Z_w	$Z_w = \frac{E_\theta}{H_\phi} \simeq \eta = 377 \text{ ohms}$	
Directivity D_0	$D_0 = \frac{3}{2} = 1.761 \text{ dB}$	(4-31)
Maximum effective area A_{em}	$A_{em} = \frac{3\lambda^2}{8\pi}$	(4-32)
Vector effective length $\boldsymbol{\ell}_e$	$\boldsymbol{\ell}_e = -\hat{\mathbf{a}}_\theta l \sin\theta$ $\lvert\boldsymbol{\ell}_e\rvert_{\max} = \lambda$	(2-91), Example 4.2
Half-power beamwidth	$\text{HPBW} = 90^\circ$	(4-65)
Loss resistance R_L	$R_L = \frac{l}{P}\sqrt{\frac{\omega\mu_0}{2\sigma}} = \frac{l}{2\pi b}\sqrt{\frac{\omega\mu_0}{2\sigma}}$	(2-90b)
	Small Dipole $(\lambda/50 < \ell \le \lambda/10)$	
Normalized power pattern	$U = (E_{\theta n})^2 = C_1 \sin^2\theta$	(4-36a)
Radiation resistance R_r	$R_r = 20\pi^2\left(\frac{l}{\lambda}\right)^2$	(4-37)
Input resistance R_{in}	$R_{in} = R_r = 20\pi^2\left(\frac{l}{\lambda}\right)^2$	(4-37)

(*continued overleaf*)

TABLE 4.2 (*continued*)

Parameter	Formula	Equation Number
Wave impedance Z_w	$Z_w = \dfrac{E_\theta}{H_\phi} \simeq \eta = 377 \text{ ohms}$	(4-36a), (4-36c)
Directivity D_0	$D_0 = \dfrac{3}{2} = 1.761 \text{ dB}$	
Maximum effective area A_{em}	$A_{em} = \dfrac{3\lambda^2}{8\pi}$	
Vector effective length $\boldsymbol{\ell}_e$	$\boldsymbol{\ell}_e = -\hat{\mathbf{a}}_\theta \dfrac{l}{2} \sin\theta$ $\lvert\boldsymbol{\ell}_e\rvert_{\max} = \dfrac{l}{2}$	(2-91), (4-36a)
Half-power beamwidth	$\text{HPBW} = 90^\circ$	(4-65)
	Half Wavelength Dipole $(l = \lambda/2)$	
Normalized power pattern	$U = (E_{\theta n})^2 = C_2 \left[\dfrac{\cos\left(\dfrac{\pi}{2}\cos\theta\right)}{\sin\theta} \right]^2 \simeq C_2 \sin^3\theta$	(4-87)
Radiation resistance R_r	$R_r = \dfrac{\eta}{4\pi} C_{in}(2\pi) \simeq 73 \text{ ohms}$	(4-93)
Input resistance R_{in}	$R_{in} = R_r = \dfrac{\eta}{4\pi} C_{in}(2\pi) \simeq 73 \text{ ohms}$	(4-79), (4-93)
Input impedance Z_{in}	$Z_{in} = 73 + j42.5$	(4-93a)
Wave impedance Z_w	$Z_w = \dfrac{E_\theta}{H_\phi} \simeq \eta = 377 \text{ ohms}$	
Directivity D_0	$D_0 = \dfrac{4}{C_{in}(2\pi)} \simeq 1.643 = 2.156 \text{ dB}$	(4-91)
Vector effective length $\boldsymbol{\ell}_e$	$\boldsymbol{\ell}_e = -\hat{\mathbf{a}}_\theta \dfrac{\lambda}{\pi} \dfrac{\cos\left(\dfrac{\pi}{2}\cos\theta\right)}{\sin\theta}$ $\lvert\boldsymbol{\ell}_e\rvert_{\max} = \dfrac{\lambda}{\pi} = 0.3183\lambda$	(2-91), (4-84)
Half-power beamwidth	$\text{HPBW} = 78^\circ$	(4-65)

TABLE 4.2 (*continued*)

Parameter	Formula	Equation Number
Loss resistance R_L	$R_L = \dfrac{l}{2P}\sqrt{\dfrac{\omega\mu_0}{2\sigma}} = \dfrac{l}{4\pi b}\sqrt{\dfrac{\omega\mu_0}{2\sigma}}$	Example (2-13)
	Quarter-Wavelength Monopole $(l = \lambda/4)$	
Normalized power pattern	$U = (E_{\theta n})^2 = C_2\left[\dfrac{\cos\left(\dfrac{\pi}{2}\cos\theta\right)}{\sin\theta}\right]^2 \simeq C_2\sin^3\theta$	(4-87)
Radiation resistance R_r	$R_r = \dfrac{\eta}{8\pi}C_{in}(2\pi) \simeq 36.5$ ohms	(4-106)
Input resistance R_{in}	$R_{in} = R_r = \dfrac{\eta}{8\pi}C_{in}(2\pi) \simeq 36.5$ ohms	(4-106)
Input impedance Z_{in}	$Z_{in} = 36.5 + j21.25$	(4-106)
Wave impedance Z_w	$Z_w = \dfrac{E_\theta}{H_\phi} \simeq \eta = 377$ ohms	
Directivity D_0	$D_0 = 3.286 = 5.167$ dB	
Vector effective length $\boldsymbol{\ell}_e$	$\boldsymbol{\ell}_e = -\hat{\mathbf{a}}_\theta\dfrac{\lambda}{\pi}\cos\left(\dfrac{\pi}{2}\cos\theta\right)$	(2-91)
	$\lvert\boldsymbol{\ell}_e\rvert_{\max} = \dfrac{\lambda}{\pi} = 0.3183\lambda$	(4-84)

4.10 MULTIMEDIA

In the CD that is part of the book, the following multimedia resources are included for the review, understanding, and visualization of the material of this chapter.

a. **Java**-based **interactive questionnaire**, with answers.
b. **Java**-based **applet** for computing and displaying the radiation characteristics of a dipole.
c. **Java**-based **visualization/animation** for displaying the radiation characteristics of a dipole of different lengths.
d. **Matlab** and **Fortran** computer program, designated ***Dipole***, for computing the radiation characteristics of a dipole. The description of the program is found in the corresponding READ ME file of the attached CD.
e. **Power Point (PPT)** viewgraphs, in multicolor.

REFERENCES

1. W. A. Wheeler, "The Spherical Coil as an Inductor, Shield, or Antenna," *Proc. IRE*, Vol. 46, pp. 1595–1602, September 1958 (correction, Vol. 48, p. 328, March 1960).
2. W. A. Wheeler, "The Radiansphere Around a Small Antenna," *Proc. IRE*, Vol. 47, pp. 1325–1331, August 1959.
3. W. A. Wheeler, "Small Antennas," *IEEE Trans. Antennas Propagat.*, Vol. AP-23, No. 4, pp. 462–469, July 1975.
4. C. H. Walter, *Traveling Wave Antennas*, McGraw-Hill, 1965, pp. 32–44.
5. W. R. Scott, Jr., "A General Program for Plotting Three-Dimensional Antenna Patterns," *IEEE Antennas Propagat. Soc. Newsletter*, pp. 6–11, December 1989.
6. S. K. Schelkunoff and H. T. Friis, *Antennas: Theory and Practice*, Wiley, New York, 1952, pp. 229–244, 351–353.
7. C. A. Balanis, *Advanced Engineering Electromagnetics*, John Wiley & Sons, Inc., New York, 1989.
8. R. F. Harrington, "Matrix Methods for Field Problems," *Proc. IEEE*, Vol. 55, No. 2, pp. 136–149, February 1967.
9. R. F. Harrington, *Field Computation by Moment Methods*, Macmillan, New York, 1968.
10. R. Mittra (Ed.), *Computer Techniques for Electromagnetics*, Pergamon, New York, 1973.
11. J. Moore and P. Pizer (Eds.), *Moment Methods in Electromagnetics: Techniques and Applications*, Research Studies Press, Letchworth, UK, 1984.
12. J. J. Wang, *Generalized Moment Methods in Electromagnetics*, John Wiley & Sons, Inc., New York, 1991.
13. R. F. Schwartz, "Input Impedance of a Dipole or Monopole," *Microwave J.*, Vol. 15, No. 12, p. 22, December 1972.
14. K. Fujimoto and J. R. James, *Mobile Antenna Systems Handbook*, Artech House, Norwood, MA, 1994.
15. M. A. Jensen and Y. Rahmat-Samii, "Performance Analysis of Antennas for Hand-Held Transceivers Using FDTD," *IEEE Trans. Antennas Propagat.*, Vol. 42, No. 8, pp. 1106–1113, August 1994.
16. M. A. Jensen and Y. Rahmat-Samii, "EM Interaction of Handset Antennas and a Human in Personal Communications," *Proc. IEEE*, Vol. 83, No. 1, pp. 7–17, January 1995.
17. K. D. Katsibas, "Analysis and Design of Mobile Antennas for Handheld Units," Master's Thesis, Arizona State University, Tempe, AZ, August 1996.
18. K. D. Katsibas, C. A. Balanis, P. A. Tirkas, and C. R. Birtcher, "Folded Loop Antenna for Mobile Handheld Units," *IEEE Trans. Antennas Propagat.*, Vol. 46, No. 2, pp. 260–266, February 1998.
19. R. E. Collin and F. J. Zucker (Eds.), *Antenna Theory Part 2*, Chapters 23 and 24 (by J. R. Wait), McGraw-Hill, New York, 1969.
20. P. R. Bannister, "Image Theory Results for the Mutual Impedance of Crossing Earth Return Circuits," *IEEE Trans. Electromagn. Compat.*, Vol. 15, No. 4, pp. 158–160, 1973.
21. D. E. Kerr, *Propagation of Short Radio Waves*, MIT Radiation Laboratory Series, McGraw-Hill, New York, 1951, Vol. 13, pp. 98–109, 112–122, 396–444.
22. L. E. Vogler and J. L. Noble, "Curves of Input Impedance Change due to Ground for Dipole Antennas," U.S. National Bureau of Standards, Monograph 72, January 31, 1964.
23. H. R. Reed and C. M. Russell, *Ultra High Frequency Propagation*, Boston Technical Publishers, Inc., Lexington, Mass., 1964, Chapter 4, pp. 102–116.

24. C. A. Balanis, R. Hartenstein, and D. DeCarlo, "Multipath Interference for In-Flight Antenna Measurements," *IEEE Trans. Antennas Propagat.*, Vol. AP-32, No. 1, pp. 100–104, January 1984.
25. J. R. Wait and A. M. Conda, "Pattern of an Antenna on a Curved Lossy Surface," *IRE Trans. Antennas Propagat.*, Vol. AP-6, No. 4, pp. 348–359, October 1958.
26. P. Bechmann and A. Spizzichino, *The Scattering of Electromagnetic Waves from Rough Surfaces*, Macmillan, New York, 1963.
27. G. May, "Determining the Point of Reflection on MW Radio Links," *Microwave J.*, Vol. 20, No. 9, pp. 74, 76, September 1977.
28. D. T. Paris and F. K. Hurd, *Basic Electromagnetic Theory*, McGraw-Hill Book Co., pp. 385–386, 1969.
29. C. A. Balanis, "Multipath Interference in Airborne Antenna Measurements," Final Report, prepared for Naval Air Station, Patuxent River, MD, May 28, 1982.
30. D. DeCarlo, "Automation of In-Flight Antenna Measurements," MSEE Problem Report, Dept. of Electrical Engineering, West Virginia University, July 1980.
31. G. J. Burke and A. J. Poggio, "Numerical Electromagnetics Code (NEC)-Method of Moments," Technical Document 116, Naval Ocean Systems Center, San Diego, CA, January 1981.
32. A. J. Julian, J. M. Logan, and J. W. Rockway, "MININEC: A Mini-Numerical Electromagnetics Code," Technical Document 516, Naval Ocean Systems Center, San Diego, CA, September 6, 1982.
33. J. Rockway, J. Logan, D. Tam, and S. Li, *The MININEC SYSTEM: Microcomputer Analysis of Wire Antennas*, Artech House, Inc., Norwood, MA, 1988.

PROBLEMS

4.1. A horizontal infinitesimal electric dipole of constant current I_0 is placed symmetrically about the origin and directed along the x-axis. Derive the
(a) far-zone fields radiated by the dipole
(b) directivity of the antenna

4.2. Repeat Problem 4.1 for a horizontal infinitesimal electric dipole directed along the y-axis.

4.3. Repeat Problem 4.1 using the procedure of Example 4.5.

4.4. For Example 4.5,
(a) formulate an expression for the directivity.
(b) determine the radiated power.
(c) determine the maximum directivity by integrating the radiated power. Compare with that of Problem 4.2 or any other infinitesimal dipole.
(d) determine the maximum directivity using the computer program **Dipole**; compare with that of part (c).

4.5. For Problem 4.1 determine the polarization of the radiated far-zone electric fields (E_θ, E_ϕ) and normalized amplitude pattern in the following planes:
(a) $\phi = 0^\circ$ (b) $\phi = 90^\circ$ (c) $\theta = 90^\circ$

4.6. Repeat Problem 4.5 for the horizontal infinitesimal electric dipole of Problem 4.2, which is directed along the y-axis.

4.7. For Problem 4.3, determine the polarization of the radiated far-zone fields (E_θ, E_ϕ) in the following planes:
(a) $\phi = 0^\circ$ (b) $\phi = 90^\circ$ (c) $\theta = 90^\circ$
Compare with those of Problem 4.5.

4.8. For Example 4.5, determine the polarization of the radiated far-zone fields (E_θ, E_ϕ) in the following planes:
(a) $\phi = 0^\circ$ (b) $\phi = 90^\circ$ (c) $\theta = 90^\circ$
Compare with those of Problem 4.6.

4.9. An infinitesimal magnetic dipole of constant current I_m and length l is symmetrically placed about the origin along the z-axis. Find the
(a) spherical **E**- and **H**-field components radiated by the dipole in all space
(b) directivity of the antenna

4.10. For the infinitesimal magnetic dipole of Problem 4.9, find the far-zone fields when the element is placed along the
(a) x-axis, (b) y-axis

4.11. An infinitesimal electric dipole is centered at the origin and lies on the x-y plane along a line which is at an angle of 45° with respect to the x-axis. Find the far-zone electric and magnetic fields radiated. The answer should be a function of spherical coordinates.

4.12. Repeat Problem 4.11 for an infinitesimal magnetic dipole.

4.13. Derive (4-10a)–(4-10c) using (4-8a)–(4-9).

4.14. Derive the radiated power of (4-16) by forming the average power density, using (4-26a)–(4-26c), and integrating it over a sphere of radius r.

4.15. Derive the far-zone fields of an infinitesimal electric dipole, of length l and constant current I_0, using (4-4) and the procedure outlined in Section 3.6. Compare the results with (4-26a)–(4-26c).

4.16. Derive the fifth term of (4-41).

4.17. For an antenna with a maximum linear dimension of D, find the inner and outer boundaries of the Fresnel region so that the maximum phase error does not exceed
(a) $\pi/16$ rad (b) $\pi/4$ rad (c) 18° (d) 15°

4.18. The boundaries of the far-field (Fraunhofer) and Fresnel regions were selected based on a maximum phase error of 22.5°, which occur, respectively, at directions of 90° and 54.74° from the axis along the largest dimension of the antenna. For an antenna of maximum length of 5λ, what do these maximum phase errors reduce to at an angle of 30° from the axis along the length of the antenna? Assume that the phase error in each case is totally contributed by the respective first higher order term that is being neglected in the infinite series expansion of the distance from the source to the observation point.

4.19. The current distribution on a terminated and matched long linear (traveling wave) antenna of length l, positioned along the z-axis and fed at its one end, is given by

$$\mathbf{I} = \hat{\mathbf{a}}_z I_0 e^{-jkz'}, \quad 0 \le z' \le l$$

where I_0 is a constant. Derive expressions for the

(a) far-zone spherical electric and magnetic field components

(b) radiation power density

4.20. A line source of infinite length and constant current I_0 is positioned along the z-axis. Find the

(a) vector potential $\mathbf{A}$

(b) cylindrical $\mathbf{E}$- and $\mathbf{H}$-field components radiated

$$\text{Hint: } \int_{-\infty}^{+\infty} \frac{e^{-j\beta\sqrt{b^2+t^2}}}{\sqrt{b^2+t^2}}\, dt = -j\pi H_0^{(2)}(\beta b)$$

where $H_0^{(2)}(\alpha x)$ is the Hankel function of the second kind of order zero.

4.21. Show that (4-67) reduces to (4-68) and (4-88) to (4-89).

4.22. A thin linear dipole of length l is placed symmetrically about the z-axis. Find the far-zone spherical electric and magnetic components radiated by the dipole whose current distribution can be approximated by

(a) $I_z(z') = \begin{cases} I_0\left(1+\dfrac{2}{l}z'\right), & -l/2 \le z' \le 0 \\ I_0\left(1-\dfrac{2}{l}z'\right), & 0 \le z' \le l/2 \end{cases}$

(b) $I_z(z') = I_0 \cos\left(\dfrac{\pi}{l}z'\right), \quad -l/2 \le z' \le l/2$

(c) $I_z(z') = I_0 \cos^2\left(\dfrac{\pi}{l}z'\right), \quad -l/2 \le z' \le l/2$

4.23. A center-fed electric dipole of length l is attached to a balanced lossless transmission line whose characteristic impedance is 50 ohms. Assuming the dipole is resonant at the given length, find the input VSWR when
(a) $l = \lambda/4$ (b) $l = \lambda/2$ (c) $l = 3\lambda/4$ (d) $l = \lambda$

4.24. Use the equations in the book or the computer program of this chapter. Find the radiation efficiency of resonant linear electric dipoles of length
(a) $l = \lambda/50$ (b) $l = \lambda/4$ (c) $l = \lambda/2$ (d) $l = \lambda$
Assume that each dipole is made out of copper [$\sigma = 5.7 \times 10^7$ S/m], has a radius of $10^{-4}\lambda$, and is operating at $f = 10$ MHz. Use the computer program of this chapter to find the radiation resistances.

4.25. Write the far-zone electric and magnetic fields radiated by a magnetic dipole of $l = \lambda/2$ aligned with the z-axis. Assume a sinusoidal magnetic current with maximum value I_{mo}.

4.26. A resonant center-fed dipole is connected to a 50-ohm line. It is desired to maintain the input VSWR = 2.

(a) What should the largest input resistance of the dipole be to maintain the VSWR = 2?

(b) What should the length (in wavelengths) of the dipole be to meet the specification?

(c) What is the radiation resistance of the dipole?

4.27. The radiation field of a particular antenna is given by:

$$\mathbf{E} = \hat{\mathbf{a}}_\theta j\omega\mu k \sin\theta \frac{I_0 A_1 e^{-jkr}}{4\pi r} + \hat{\mathbf{a}}_\phi \omega\mu \sin\theta \frac{I_0 A_2 e^{-jkr}}{2\pi r}$$

The values A_1 and A_2 depend on the antenna geometry. Obtain an expression for the radiation resistance. What is the polarization of the antenna?

4.28. For a $\lambda/2$ dipole placed symmetrical along the z-axis, determine the

(a) vector effective height

(b) maximum value (magnitude) of the vector effective height

(c) ratio (in percent) of the maximum value (magnitude) of the vector effective height to its total length

(d) maximum open-circuit output voltage when a uniform plane wave with an electric field of

$$\mathbf{E}^i|_{\theta=90^\circ} = -\hat{\mathbf{a}}_\theta 10^{-3} \text{ volts/wavelength}$$

impinges at broadside incidence on the dipole.

4.29. A base-station cellular communication system utilizes arrays of $\lambda/2$ dipoles as transmitting and receiving antennas. Assuming that each element is *lossless* and that the *input power* to each of the $\lambda/2$ dipoles is 1 watt, determine at *1,900 MHz* and a distance of *5 km* the maximum

(a) radiation intensity *Specify also the units.*

(b) radiation density (*in watts*$/m^2$)

for each $\lambda/2$ *dipole*. This determines the safe level for human exposure to EM radiation.

4.30. A $\lambda/2$ dipole situated with its center at the origin radiates a time-averaged power of 600 W at a frequency of 300 MHz. A second $\lambda/2$ dipole is placed with its center at a point $P(r, \theta, \phi)$, where $r = 200$ m, $\theta = 90^\circ$, $\phi = 40^\circ$. It is oriented so that its axis is parallel to that of the transmitting antenna. What is the available power at the terminals of the second (receiving) dipole?

4.31. A half-wave dipole is radiating into free-space. The coordinate system is defined so that the origin is at the center of the dipole and the z-axis is aligned with the dipole. Input power to the dipole is 100 W. Assuming an overall efficiency of 50%, find the power density (in W/m^2) at $r = 500$ m, $\theta = 60^\circ$, $\phi = 0^\circ$.

4.32. A small dipole of length $l = \lambda/20$ and of wire radius $a = \lambda/400$ is fed symmetrically, and it is used as a communications antenna at the lower end of the VHF band ($f = 30$ *MHz*). *The antenna is made of perfect electric conductor (PEC).* The *input reactance* of the dipole is given by

$$X_{in} = -j120 \frac{[\ln(l/2a) - 1]}{\tan\left(\dfrac{\pi l}{\lambda}\right)}$$

Determine the following:

(a) Input impedance of the antenna. *State whether it is inductive or capacitive*.

(b) Radiation efficiency (*in percent*).

(c) Capacitor (*in farads*) *or* inductor (*in henries*) that must be connected *in series* with the dipole at the feed in order to resonate the element. *Specify which element is used and its value*.

4.33. A half-wavelength ($l = \lambda/2$) dipole is connected to a transmission line with a characteristic impedance of 75 ohms. Determine the following:

(a) Reflection coefficient. Magnitude and phase (*in degrees*).

(b) VSWR.

It is now desired to resonate the dipole using, *in series*, an inductor or capacitor. At a frequency of 100 MHz, determine:

(c) What kind of an element, inductor or capacitor, is needed to resonate the dipole?

(d) What is the inductance or capacitance?

(e) The new VSWR of the resonant dipole.

4.34. A $\lambda/2$ dipole is used as a radiating element while it is connected to a 50-ohm lossless transmission line. It is desired to resonate the element at *1.9 GHz* by placing *in series capacitor(s) or inductor(s)* (whichever are appropriate) at its input terminals. Determine the following:

(a) VSWR inside the transmission line *before the dipole is resonated [before the capacitor(s) or inductor(s) are placed in series]*.

(b) Total single capacitance C_T (in farads) or inductance L_T (in henries) that must be placed *in series* with the element at its input terminals in order to resonate it. (*See diagram a*).

(c) Individual two capacitances C_o (in farads) or inductances L_o (in henries) that must be placed *in series* with the element at its input terminals in order to resonate it. We need to use two capacitors or two inductors to keep the system balanced by placing in series one with each arm of the dipole (*see diagram b*).

(d) VSWR after the element is resonated with capacitor(s) or inductor(s).

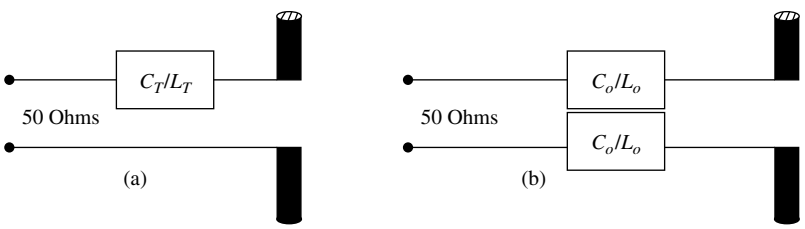

4.35. The input impedance of a $\lambda/2$ dipole, assuming the input (feed) terminals are at the center of the dipole, is equal to $73 + j42.5$. Assuming the dipole is lossless, find the

(a) input impedance (real and imaginary parts) assuming the input (feed) terminals have been shifted to a point on the dipole which is $\lambda/8$ from either end point of the dipole length

(b) capacitive or inductive reactance that must be placed across the new input terminals of part (a) so that the dipole is self-resonant

(c) VSWR at the new input terminals when the self-resonant dipole of part (b) is connected to a "twin-lead" 300-ohm line

4.36. A linear half-wavelength dipole is operating at a frequency of 1 GHz; determine the capacitance *or* inductance that must be placed *across* (in parallel) the input terminals of the dipole so that the antenna becomes resonant (make the total input impedance real). What is then the VSWR of the resonant half-wavelength dipole when it is connected to a 50-ohm line?

4.37. The field radiated by an infinitesimal electric dipole, placed along the z-axis a distance s along the x-axis, is incident upon a waveguide aperture antenna of dimensions a and b, mounted on an infinite ground plane, as shown in the figure. The normalized electric field radiated by the aperture in the E-plane (x-z plane; $\phi = 0^\circ$) is given by

$$\mathbf{E} = -\hat{\mathbf{a}}_\theta j \frac{\omega \mu b I_0 e^{-jkr}}{4\pi r} \frac{\sin\left(\frac{kb}{2}\cos\theta\right)}{\frac{kb}{2}\cos\theta}$$

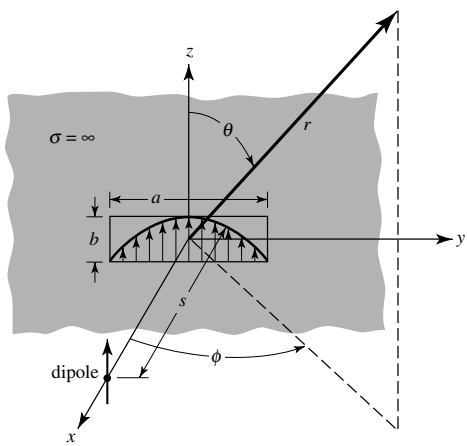

Assuming the dipole and aperture antennas are in the far field of each other, determine the polarization loss (in dB) between the two antennas.

4.38. We are given the following information about antenna A:

(a) When A is transmitting, its radiated far-field expression for the E field is given by:

$$\mathbf{E}_a(z) = E_0 \frac{e^{-jkz}}{4\pi z}\left(\frac{\hat{\mathbf{a}}_x + j\hat{\mathbf{a}}_y}{\sqrt{2}}\right) \quad V/m$$

(b) When A is receiving an incident plane wave given by:

$$\mathbf{E}_1(z) = \hat{\mathbf{a}}_y e^{jkz} \quad V/m$$

its open-circuit voltage is $V_1 = 4e^{j20^\circ}\,V$.

If we use the same antenna to receive a second incident plane given by:

$$\mathbf{E}_2(z) = 10(2\hat{\mathbf{a}}_x + \hat{\mathbf{a}}_y E^{j30^\circ})e^{jkz} \quad V/m$$

find its received open-circuit voltage V_2.

4.39. A 3-cm long dipole carries a phasor current $I_0 = 10e^{j60}$A. Assuming that $\lambda = 5$ cm, determine the E- and H-fields at 10 cm away from the dipole and at $\theta = 45^\circ$.

4.40. The radiation resistance of a thin, lossless linear electric dipole of length $l = 0.6\lambda$ is 120 ohms. What is the input resistance?

4.41. A lossless, resonant, center-fed $3\lambda/4$ linear dipole, radiating in free-space is attached to a balanced, lossless transmission line whose characteristic impedance is 300 ohms. Calculate the

(a) radiation resistance (referred to the current maximum)

(b) input impedance (referred to the input terminals)

(c) VSWR on the transmission line

For parts (a) and (b) use the computer program at the end of the chapter.

4.42. Repeat Problem 4.41 for a center-fed $5\lambda/8$ dipole.

4.43. A dipole antenna, with a triangular current distribution, is used for communication with submarines at a frequency of 150 kHz. The overall length of the dipole is 200 m, and its radius is 1 m. Assume a loss resistance of 2 ohms in series with the radiation resistance of the antenna.

(a) Evaluate the input impedance of the antenna including the loss resistance. The input reactance can be approximated by

$$X_{in} = -120\frac{[\ln(l/2a) - 1]}{\tan(\pi l/\lambda)}$$

(b) Evaluate the radiation efficiency of the antenna.

(c) Evaluate the radiation power factor of the antenna.

(d) Design a conjugate-matching network to provide a perfect match between the antenna and a 50-ohm transmission line. Give the value of the series reactance X and the turns ratio n of the ideal transformer.

(e) Assuming a conjugate match, evaluate the instantaneous 2:1 VSWR bandwidth of the antenna.

4.44. A uniform plane wave traveling along the negative z-axis given by

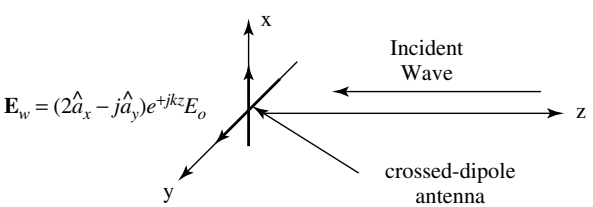

impinges upon an crossed-dipole antenna consisting of *two identical dipoles*, one directed along the x-axis and the other directed along the y-axis, *both fed with the same amplitude*. The *y-directed dipole is fed with a* 90° *phase lead* compared to the x-directed dipole.

(a) Write an expression for the polarization unit vector of the incident wave.

(b) Write an expression for the polarization unit vector of the receiving antenna *along the* $+$ *z-axis*.

(c) For the incident wave, state the following:

1. Polarization (linear, circular, elliptical) and axial ratio.
2. Rotation of the polarization vector (CW, CCW).

(d) For the receiving antenna, state the following:

1. Polarization (linear, circular, elliptical) and axial ratio.
2. Rotation of the polarization vector (CW, CCW).

(e) Determine the polarization loss factor (*dimensionless* and *in dB*) between the incident wave and the receiving antenna.

4.45. A half-wavelength ($l = \lambda/2$) dipole, positioned symmetrically about the origin along the z-axis, is used as a receiving antenna. A 300 MHz uniform plane wave, traveling along the x-axis in the negative x direction, impinges upon the $\lambda/2$ dipole. The incident plane wave has a power density of 2μ watts/m^2, and its electric field is given by

$$\mathbf{E}^{\mathbf{i}}{}_w = (3\hat{a}_z + j\hat{a}_y)E_0 e^{+\mathrm{jkx}}$$

where E_0 is a constant. Determine the following:

(a) Polarization of the incident wave (*including its axial ratio and sense of rotation*, if applicable).

(b) Polarization of the antenna toward the x-axis (*including its axial ratio and sense of direction*, if applicable).

(c) Polarization losses (*in dB*) between the antenna and the incoming wave (assume far-zone fields for the antenna).

(d) Maximum power (*in watts*) that can be delivered to a matched load connected to the $\lambda/2$ dipole (assume no other losses).

4.46. Derive (4-102) using (4-99).

4.47. Determine the smallest height that an infinitesimal vertical electric dipole of $l = \lambda/50$ must be placed above an electric ground plane so that its pattern has only one null (aside from the null toward the vertical), and it occurs at 30° from the vertical. For that height, find the directivity and radiation resistance.

4.48. A $\lambda/50$ linear dipole is placed vertically at a height $h = 2\lambda$ above an infinite electric ground plane. Determine the angles (in degrees) where all the nulls of its pattern occur.

4.49. A linear infinitesimal dipole of length l and constant current is placed vertically a distance h above an infinite electric ground plane. Find the first five smallest heights (in ascending order) so that a null is formed (for each height) in the far-field pattern at an angle of 60° from the vertical.

4.50. A vertical infinitesimal linear dipole is placed a distance $h = 3\lambda/2$ above an infinite perfectly conducting flat ground plane. Determine the

(a) angle (*in degrees* from the vertical) where the *array factor* of the system will achieve its *maximum* value

(b) angle (*in degrees* from the vertical) where the maximum of the *total field* will occur

(c) relative (compared to its maximum) field strength (*in dB*) of the total field at the angles where the array factor of the system achieves its maximum value (as obtained in part a).

4.51. An infinitesimal dipole of length ℓ is placed a distance s from an air-conductor interface and at an angle of $\theta = 60^\circ$ from the vertical axis, as shown in the figure. Determine the location and direction of the image source which can be used to account for reflections. Be very clear in indicating the location and direction of the image. Your answer can be in the form of a very clear sketch.

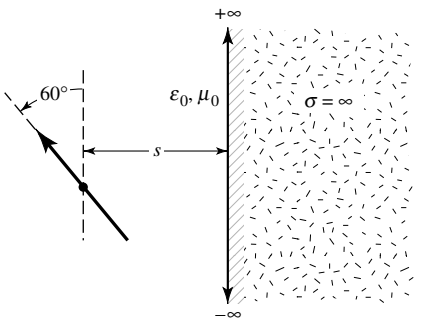

4.52. It is desired to design an antenna system, which utilizes a vertical infinitesimal dipole of length ℓ placed a height h above a flat, perfect electric conductor of infinite extent. The design specifications require that the pattern of the array factor of the source and its image has only one maximum, and that maximum is pointed at an angle of 60° from the vertical. Determine (in wavelengths) the height of the source to achieve this desired design specification.

4.53. A very short ($l \leq \lambda/50$) vertical electric dipole is mounted on a pole a height h above the ground, which is assumed to be flat, perfectly conducting, and of infinite extent. The dipole is used as a transmitting antenna in a VHF ($f =$ 50 MHz) ground-to-air communication system. In order for the communication system transmitting antenna signal not to interfere with a nearby radio station, it is necessary to place a null in the vertical dipole system pattern at an angle of 80° from the vertical. What should the shortest height (in meters) of the dipole be to achieve the desired specifications?

4.54. A half-wavelength dipole is placed vertically on an infinite electric ground plane. Assuming that the dipole is fed at its base, find the

(a) radiation impedance (referred to the current maximum)

(b) input impedance (referred to the input terminals)

(c) VSWR when the antenna is connected to a lossless 50-ohm transmission line.

4.55. A vertical $\lambda/2$ *dipole* is the radiating element in a circular array used for over-the-horizon communication system operating at *1 GHz*. The circular array (*center of the dipoles*) is placed at a *height h* above the ground that is assumed to be flat, perfect electric conducting, and infinite in extent.

(a) In order for the array not to be interfered with by another communication system that is operating in the same frequency, it is desired to place *only one null* in the *elevation pattern of the array factor* of a single vertical $\lambda/2$ dipole at an angle of $\theta = 30^\circ$ from zenith (axis of the dipole). Determine the *smallest nonzero height h* (*in meters*) above the ground at which the center of the dipole must be placed to accomplish this.

(b) If the height (*at its center*) of the vertical dipole is *0.3 m* above ground, determine *all the angles* θ from zenith (*in degrees*) where *all* the

1. null(s) of the *array factor* of a single dipole in the elevation plane will be directed toward.
2. main maximum (maxima) of the *array factor* of a single dipole in the elevation plane will be directed toward.

4.56. A vertical $\lambda/2$ dipole antenna is used as a ground-to-air, over-the-horizon communication antenna at the VHF band ($f = 200$ *MHz*). The antenna is elevated at a height *h* (*measured from its center/feed point*) above ground (*assume the ground is flat, smooth, and perfect electric conductor extending to infinity*). In order to avoid interference with other simultaneously operating communication systems, it is desired to place a null in the far-field amplitude pattern of the antenna system at an angle of 60° *from the vertical*.
Determine the *three smallest physical/nontrivial heights* (*in meters at 200 MHz*) above the ground at which the antenna can be placed to meet the desired pattern specifications.

4.57. A base-station cellular communication systems lossless antenna, which is placed in a residential area of a city, has a maximum gain of *16 dB* (above isotropic) *toward the residential area* at *1,900 MHz*. Assuming the *input* power to the antenna is 8 watts, what is the

(a) maximum radiated power density (*in watts*$/cm^2$) at a distance of 100 m (*line of sight*) from the base station to the residential area? This will determine the safe level for human exposure to electromagnetic radiation.

(b) power (*in watts*) received at that point of the residential area by a cellular telephone whose antenna is a *lossless* $\lambda/4$ vertical monopole and whose maximum value of the amplitude pattern is directed toward the maximum incident power density. *Assume the* $\lambda/4$ *monopole is mounted on an infinite ground plane*.

4.58. A vertical $\lambda/4$ monopole is used as the antenna on a cellular telephone operating at 1.9 GHz. Even though the monopole is mounted on a box-type cellular telephone, for simplicity purposes, assume here that it is mounted on a perfectly electric conducting (PEC) ground plane. Assuming an incident maximum power density of 10^{-6} watts/m^2, *state or determine*, for the monopole's omnidirectional pattern, the

(a) maximum directivity (*dimensionless and in dB*). *You must state the rationale or method you are using to find the directivity*.

(b) maximum power that can be delivered to the cellular telephone receiver. *Assume no losses*.

4.59. A homeowner uses a CB antenna mounted on the top of his house. Let us assume that the operating frequency is 900 MHz and the radiated power is *1,000 watts*. In order not to be exposed to a long-term microwave radiation, there have been some standards, although controversial, developed that set the maximum safe power density that humans can be exposed to and not be subject to any harmful effects. Let us assume that the maximum safe power density of long-term human RF exposure is 10^{-3} *watts*$/cm^2$ or *10 watts*$/m^2$. Assuming no losses, determine the *shortest distance* (*in meters*) from the CB antenna you must be in order not to exceed the safe level of power density exposure. Assume that the CB antenna is radiating into free-space and it is

(a) an isotropic radiator.

(b) a $\lambda/4$ monopole mounted on an infinite PEC and radiating towards its maximum.

4.60. Derive (4-118) using (4-116).

4.61. An infinitesimal horizontal electric dipole of length $l = \lambda/50$ is placed parallel to the y-axis a height h above an infinite electric ground plane.

(a) Find the smallest height h (excluding $h = 0$) that the antenna must be elevated so that a null in the $\phi = 90^\circ$ plane will be formed at an angle of $\theta = 45^\circ$ from the vertical axis.

(b) For the height of part (a), determine the (1) radiation resistance and (2) directivity (for $\theta = 0^\circ$) of the antenna system.

4.62. A horizontal $\lambda/50$ infinitesimal dipole of constant current and length l is placed parallel to the y-axis a distance $h = 0.707\lambda$ above an infinite electric ground plane. Find *all* the nulls formed by the antenna system in the $\phi = 90^\circ$ plane.

4.63. An infinitesimal electric dipole of length $l = \lambda/50$ is placed horizontally at a height of $h = 2\lambda$ above a flat, smooth, perfect electric conducting plane which extends to infinity. It is desired to measure its far-field radiation characteristics (e.g. amplitude pattern, phase pattern, polarization pattern, etc.). The system is operating at 300 MHz. What should the minimum radius (*in meters*) of the circle be where the measurements should be carried out? The radius should be measured from the origin of the coordinate system, which is taken at the interface between the actual source and image.

4.64. An infinitesimal magnetic dipole is placed vertically a distance h above an infinite, perfectly conducting electric ground plane. Derive the far-zone fields radiated by the element above the ground plane.

4.65. Repeat Problem 4.64 for an electric dipole above an infinite, perfectly conducting magnetic ground plane.

4.66. Repeat Problem 4.64 for a magnetic dipole above an infinite, perfectly conducting magnetic ground plane.

4.67. An infinitesimal vertical electric dipole is placed at height h above an infinite PMC (perfect magnetic conductor) ground plane.

(a) Find the smallest height h (excluding $h = 0$) to which the antenna must be elevated so that a null is formed at an angle $\theta = 60^\circ$ from the vertical axis

(b) For the value of h found in part (a), determine

1. the directive gain of the antenna in the $\theta = 45^\circ$ direction
2. the radiation resistance of the antenna normalized to the intrinsic impedance of the medium above the ground plane

Assume that the length of the antenna is $l = \lambda/100$.

4.68. A vertical $\lambda/2$ dipole, operating at 1 GHz, is placed a distance of 5 m (with respect to the tangent at the point of reflections) above the earth. Find the total field at a point 20 km from the source ($d = 20 \times 10^3$ m), at a height of 1,000 m (with respect to the tangent) above the ground. Use a 4/3 radius earth and assume that the electrical parameters of the earth are $\epsilon_r = 5, \sigma = 10^{-2}$ S/m.

4.69. Two astronauts equipped with handheld radios land on different parts of a large asteroid. The radios are identical and transmit 5 W average power at 300 MHz. Assume the asteroid is a smooth sphere with physical radius of 1,000 km, has no atmosphere, and consists of a lossless dielectric material with relative permittivity $\epsilon_r = 9$. Assume that the radios' antennas can be modeled as vertical infinitesimal electric dipoles. Determine the signal power (in microwatts) received by each radio from the other, if the astronauts are separated by a range (distance along the asteroid's surface) of 2 km, and hold their radios vertically at heights of 1.5 m above the asteroid's surface.

Additional Information Required to Answer this Question: Prior to landing on the asteroid the astronauts calibrated their radios. Separating themselves in outer space by 10 km, the astronauts found the received signal power at each radio from the other was 10 microwatts, when both antennas were oriented in the same direction.

4.70. A satellite S transmits an electromagnetic wave, at 10 GHz, via its transmitting antenna. The characteristics of the satellite-based transmitter are:

(a) The power radiated from the satellite antenna is 10 W.

(b) The distance between the satellite antenna and a point A on the earth's surface is 3.7×10^7 m, and

(c) The satellite transmitting antenna directivity in the direction SA is 50 dB Ignoring ground effects,

1. Determine the magnitude of the E-field at A.
2. If the receiver at point A is a $\lambda/2$ dipole, what would be the voltage reading at the terminals of the antenna?

4.71. Derive (4-133) based on geometrical optics as presented in section 13.2 of [7].

Copyrighted Materials
Copyright © 2005 John Wiley & Sons Retrieved from www.knovel.com

CHAPTER 5

Loop Antennas

5.1 INTRODUCTION

Another simple, inexpensive, and very versatile antenna type is the loop antenna. Loop antennas take many different forms such as a rectangle, square, triangle, ellipse, circle, and many other configurations. Because of the simplicity in analysis and construction, the circular loop is the most popular and has received the widest attention. It will be shown that a small loop (circular or square) is equivalent to an infinitesimal magnetic dipole whose axis is perpendicular to the plane of the loop. That is, the fields radiated by an electrically small circular or square loop are of the same mathematical form as those radiated by an infinitesimal magnetic dipole.

Loop antennas are usually classified into two categories, electrically small and electrically large. Electrically small antennas are those whose overall length (circumference) is usually less than about one-tenth of a wavelength ($C < \lambda/10$). However, electrically large loops are those whose circumference is about a free-space wavelength ($C \sim \lambda$). Most of the applications of loop antennas are in the HF (3–30 MHz), VHF (30–300 MHz), and UHF (300–3,000 MHz) bands. When used as field probes, they find applications even in the microwave frequency range.

Loop antennas with electrically small circumferences or perimeters have small radiation resistances that are usually smaller than their loss resistances. Thus they are very poor radiators, and they are seldom employed for transmission in radio communication. When they are used in any such application, it is usually in the receiving mode, such as in portable radios and pagers, where antenna efficiency is not as important as the signal-to-noise ratio. They are also used as probes for field measurements and as directional antennas for radiowave navigation. The field pattern of electrically small antennas of any shape (circular, elliptical, rectangular, square, etc.) is similar to that of an infinitesimal dipole with a null perpendicular to the plane of the loop and with its maximum along the plane of the loop. As the overall length of the loop increases and its circumference approaches one free-space wavelength, the maximum of the pattern shifts from the plane of the loop to the axis of the loop which is perpendicular to its plane.

The radiation resistance of the loop can be increased, and made comparable to the characteristic impedance of practical transmission lines, by increasing (electrically) its perimeter and/or the number of turns. Another way to increase the radiation resistance

Antenna Theory: Analysis Design, Third Edition, by Constantine A. Balanis
ISBN 0-471-66782-X Copyright © 2005 John Wiley & Sons, Inc.

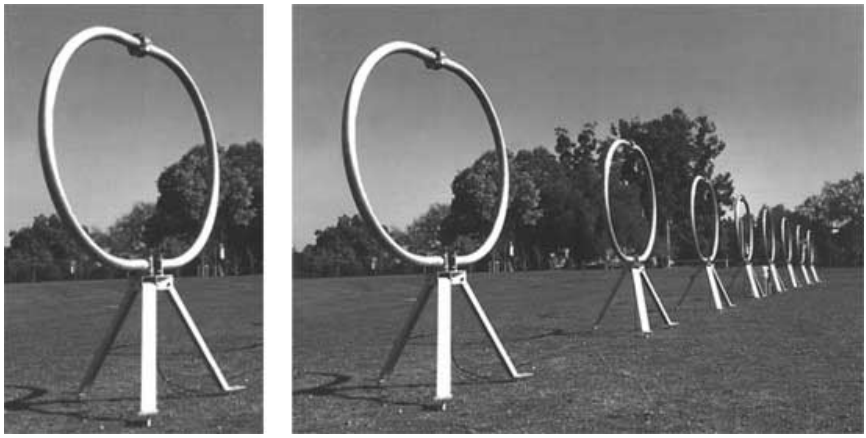

(a) single element (b) array of eight elements

Figure 5.1 Commercial loop antenna as a single vertical element and in the form of an eight-element linear array. (Courtesy: TCI, A Dielectric Company).

of the loop is to insert, within its circumference or perimeter, a ferrite core of very high permeability which will raise the magnetic field intensity and hence the radiation resistance. This forms the so-called ferrite loop.

Electrically large loops are used primarily in directional arrays, such as in helical antennas (see Section 10.3.1), Yagi-Uda arrays (see Section 10.3.3), quad arrays (see Section 10.3.4), and so on. For these and other similar applications, the maximum radiation is directed toward the axis of the loop forming an end-fire antenna. To achieve such directional pattern characteristics, the circumference (perimeter) of the loop should be about one free-space wavelength. The proper phasing between turns enhances the overall directional properties.

Loop antennas can be used as single elements, as shown in Figure 5.1(a), whose plane of its area is perpendicular to the ground. The relative orientation of the loop can be in other directions, including its plane being parallel relative to the ground. Thus, its mounting orientation will determine its radiation characteristics relative to the ground. Loops are also used in arrays of various forms. The particular array configuration will determine its overall pattern and radiation characteristics. One form of arraying is shown in Figure 5.1(b), where eight loops of Figure 5.1(a) are placed to form a linear array of eight vertical elements.

5.2 SMALL CIRCULAR LOOP

The most convenient geometrical arrangement for the field analysis of a loop antenna is to position the antenna symmetrically on the x-y plane, at $z = 0$, as shown in Figure 5.2(a). The wire is assumed to be very thin and the current spatial distribution is given by

$$I_\phi = I_0 \tag{5-1}$$

where I_0 is a constant. Although this type of current distribution is accurate only for a loop antenna with a very small circumference, a more complex distribution makes the mathematical formulation quite cumbersome.

5.2.1 Radiated Fields

To find the fields radiated by the loop, the same procedure is followed as for the linear dipole. The potential function **A** given by (3-53) as

$$\mathbf{A}(x, y, z) = \frac{\mu}{4\pi} \int_C \mathbf{I}_e(x', y', z') \frac{e^{-jkR}}{R} dl' \tag{5-2}$$

is first evaluated. Referring to Figure 5.2(a), R is the distance from any point on the loop to the observation point and dl' is an infinitesimal section of the loop antenna. In general, the current spatial distribution $\mathbf{I}_e(x', y', z')$ can be written as

$$\mathbf{I}_e(x', y', z') = \hat{\mathbf{a}}_x I_x(x', y', z') + \hat{\mathbf{a}}_y I_y(x', y', z') + \hat{\mathbf{a}}_z I_z(x', y', z') \tag{5-3}$$

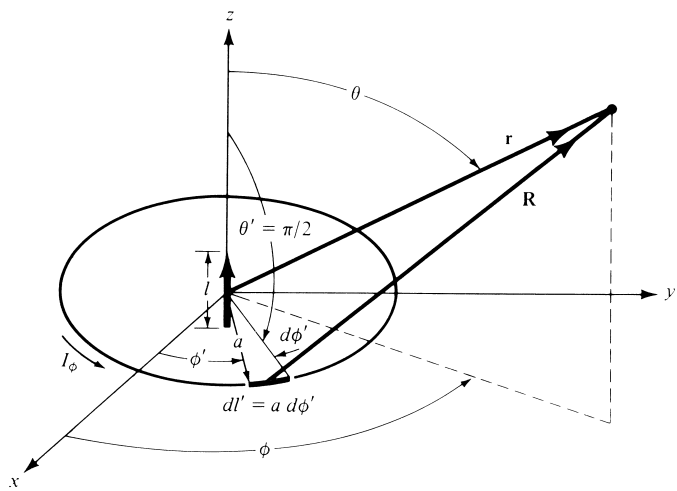

(a) Geometry for circular loop

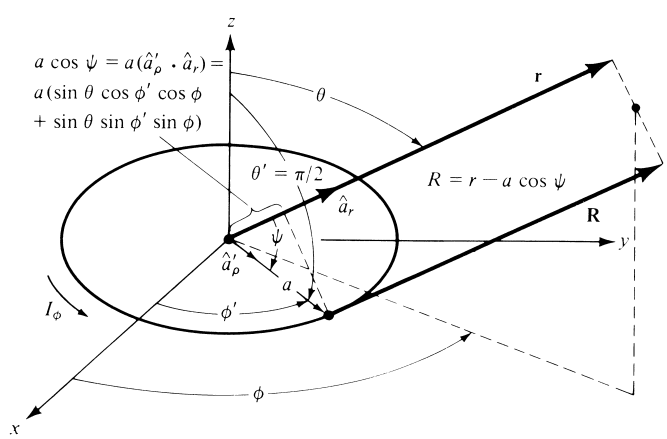

(b) Geometry for far-field observations

Figure 5.2 Geometrical arrangement for loop antenna analysis.

whose form is more convenient for linear geometries. For the circular-loop antenna of Figure 5.2(a), whose current is directed along a circular path, it would be more convenient to write the rectangular current components of (5-3) in terms of the cylindrical components using the transformation (see Appendix VII)

$$\begin{bmatrix} I_x \\ I_y \\ I_z \end{bmatrix} = \begin{bmatrix} \cos\phi' & -\sin\phi' & 0 \\ \sin\phi' & \cos\phi' & 0 \\ 0 & 0 & 1 \end{bmatrix} \begin{bmatrix} I_\rho \\ I_\phi \\ I_z \end{bmatrix} \tag{5-4}$$

which when expanded can be written as

$$\left.\begin{aligned} I_x &= I_\rho \cos\phi' - I_\phi \sin\phi' \\ I_y &= I_\rho \sin\phi' + I_\phi \cos\phi' \\ I_z &= I_z \end{aligned}\right\} \tag{5-5}$$

Since the radiated fields are usually determined in spherical components, the rectangular unit vectors of (5-3) are transformed to spherical unit vectors using the transformation matrix given by (4-5). That is,

$$\left.\begin{aligned} \hat{\mathbf{a}}_x &= \hat{\mathbf{a}}_r \sin\theta\cos\phi + \hat{\mathbf{a}}_\theta \cos\theta\cos\phi - \hat{\mathbf{a}}_\phi \sin\phi \\ \hat{\mathbf{a}}_y &= \hat{\mathbf{a}}_r \sin\theta\sin\phi + \hat{\mathbf{a}}_\theta \cos\theta\sin\phi + \hat{\mathbf{a}}_\phi \cos\phi \\ \hat{\mathbf{a}}_z &= \hat{\mathbf{a}}_r \cos\theta - \hat{\mathbf{a}}_\theta \sin\theta \end{aligned}\right\} \tag{5-6}$$

Substituting (5-5) and (5-6) in (5-3) reduces it to

$$\begin{aligned} \mathbf{I}_e = {} & \hat{\mathbf{a}}_r [I_\rho \sin\theta\cos(\phi - \phi') + I_\phi \sin\theta \sin(\phi - \phi') + I_z \cos\theta] \\ & + \hat{\mathbf{a}}_\theta [I_\rho \cos\theta\cos(\phi - \phi') + I_\phi \cos\theta \sin(\phi - \phi') - I_z \sin\theta] \\ & + \hat{\mathbf{a}}_\phi [-I_\rho \sin(\phi - \phi') + I_\phi \cos(\phi - \phi')] \end{aligned} \tag{5-7}$$

It should be emphasized that the source coordinates are designated as primed (ρ', ϕ', z') and the observation coordinates as unprimed (r, θ, ϕ). For the circular loop, the current is flowing in the ϕ direction (I_ϕ) so that (5-7) reduces to

$$\mathbf{I}_e = \hat{\mathbf{a}}_r I_\phi \sin\theta \sin(\phi - \phi') + \hat{\mathbf{a}}_\theta I_\phi \cos\theta \sin(\phi - \phi') + \hat{\mathbf{a}}_\phi I_\phi \cos(\phi - \phi') \tag{5-8}$$

The distance R, from any point on the loop to the observation point, can be written as

$$R = \sqrt{(x - x')^2 + (y - y')^2 + (z - z')^2} \tag{5-9}$$

Since

$$\begin{aligned} x &= r\sin\theta\cos\phi \\ y &= r\sin\theta\sin\phi \\ z &= r\cos\theta \\ x^2 + y^2 + z^2 &= r^2 \\ x' &= a\cos\phi' \end{aligned} \tag{5-10}$$

$$y' = a\sin\phi'$$
$$z' = 0$$
$$x'^2 + y'^2 + z'^2 = a^2$$

(5-9) reduces to

$$R = \sqrt{r^2 + a^2 - 2ar\sin\theta\cos(\phi - \phi')} \tag{5-11}$$

By referring to Figure 5.2(a), the differential element length is given by

$$dl' = a\,d\phi' \tag{5-12}$$

Using (5-8), (5-11), and (5-12), the ϕ-component of (5-2) can be written as

$$A_\phi = \frac{a\mu}{4\pi}\int_0^{2\pi} I_\phi\cos(\phi - \phi')\frac{e^{-jk\sqrt{r^2+a^2-2ar\sin\theta\cos(\phi-\phi')}}}{\sqrt{r^2 + a^2 - 2ar\sin\theta\cos(\phi - \phi')}}\,d\phi' \tag{5-13}$$

Since the spatial current I_ϕ as given by (5-1) is constant, the field radiated by the loop will not be a function of the observation angle ϕ. Thus any observation angle ϕ can be chosen; for simplicity $\phi = 0$. Therefore (5-13) reduces to

$$A_\phi = \frac{a\mu I_0}{4\pi}\int_0^{2\pi} \cos\phi'\frac{e^{-jk\sqrt{r^2+a^2-2ar\sin\theta\cos\phi'}}}{\sqrt{r^2 + a^2 - 2ar\sin\theta\cos\phi'}}\,d\phi' \tag{5-14}$$

The integration of (5-14), for very thin circular loop of any radius, can be carried out and is represented by a complex infinite series whose real part contains complete elliptic integrals of the first and second kind while the imaginary part consists of elementary functions [1]. This treatment is only valid provided the observation distance is greater than the radius of the loop ($r > a$). Another very detailed and systematic treatment is that of [2], [3] which is valid for any observation distance ($r < a, r > a$) except when the observation point is on the loop itself ($r = a, \theta = \pi/2$). The development in [2], [3] has been applied to circular loops whose current distribution is uniform, cosinusoidal, and Fourier cosine series. Asymptotic expansions have been presented in [2], [3] to find simplified and approximate forms for far-field observations.

Both treatments, [1]–[3], are too complex to be presented here. The reader is referred to the literature. In this chapter a method will be presented that approximates the integration of (5-14). For small loops, the function

$$f = \frac{e^{-jk\sqrt{r^2+a^2-2ar\sin\theta\cos\phi'}}}{\sqrt{r^2 + a^2 - 2ar\sin\theta\cos\phi'}} \tag{5-15}$$

which is part of the integrand of (5-14), can be expanded in a Maclaurin series in a using

$$f = f(0) + f'(0)a + \frac{1}{2!}f''(0)a^2 + \cdots + \frac{1}{(n-1)!}f^{(n-1)}(0)a^{n-1} + \cdots \tag{5-15a}$$

where $f'(0) = \partial f/\partial a|_{a=0}$, $f''(0) = \partial^2 f/\partial a^2|_{a=0}$, and so forth. Taking into account only the first two terms of (5-15a), or

$$f(0) = \frac{e^{-jkr}}{r} \tag{5-15b}$$

$$f'(0) = \left(\frac{jk}{r} + \frac{1}{r^2}\right) e^{-jkr} \sin\theta \cos\phi' \tag{5-15c}$$

$$f \simeq \left[\frac{1}{r} + a\left(\frac{jk}{r} + \frac{1}{r^2}\right) \sin\theta \cos\phi'\right] e^{-jkr} \tag{5-15d}$$

reduces (5-14) to

$$A_\phi \simeq \frac{a\mu I_0}{4\pi} \int_0^{2\pi} \cos\phi' \left[\frac{1}{r} + a\left(\frac{jk}{r} + \frac{1}{r^2}\right) \sin\theta \cos\phi'\right] e^{-jkr}\, d\phi'$$

$$A_\phi \simeq \frac{a^2\mu I_0}{4} e^{-jkr} \left(\frac{jk}{r} + \frac{1}{r^2}\right) \sin\theta \tag{5-16}$$

In a similar manner, the r- and θ-components of (5-2) can be written as

$$A_r \simeq \frac{a\mu I_0}{4\pi} \sin\theta \int_0^{2\pi} \sin\phi' \left[\frac{1}{r} + a\left(\frac{jk}{r} + \frac{1}{r^2}\right) \sin\theta \cos\phi'\right] e^{-jkr}\, d\phi' \tag{5-16a}$$

$$A_\theta \simeq -\frac{a\mu I_0}{4\pi} \cos\theta \int_0^{2\pi} \sin\phi' \left[\frac{1}{r} + a\left(\frac{jk}{r} + \frac{1}{r^2}\right) \sin\theta \cos\phi'\right] e^{-jkr}\, d\phi' \tag{5-16b}$$

which when integrated reduce to zero. Thus

$$\mathbf{A} \simeq \hat{\mathbf{a}}_\phi A_\phi = \hat{\mathbf{a}}_\phi \frac{a^2\mu I_0}{4} e^{-jkr} \left[\frac{jk}{r} + \frac{1}{r^2}\right] \sin\theta$$

$$= \hat{\mathbf{a}}_\phi j \frac{k\mu a^2 I_0 \sin\theta}{4r} \left[1 + \frac{1}{jkr}\right] e^{-jkr} \tag{5-17}$$

Substituting (5-17) into (3-2a) reduces the magnetic field components to

$$H_r = j\frac{ka^2 I_0 \cos\theta}{2r^2} \left[1 + \frac{1}{jkr}\right] e^{-jkr} \tag{5-18a}$$

$$H_\theta = -\frac{(ka)^2 I_0 \sin\theta}{4r} \left[1 + \frac{1}{jkr} - \frac{1}{(kr)^2}\right] e^{-jkr} \tag{5-18b}$$

$$H_\phi = 0 \tag{5-18c}$$

Using (3-15) or (3-10) with $\mathbf{J} = 0$, the corresponding electric-field components can be written as

$$\boxed{E_r = E_\theta = 0} \tag{5-19a}$$

$$\boxed{E_\phi = \eta \frac{(ka)^2 I_0 \sin\theta}{4r}\left[1 + \frac{1}{jkr}\right]e^{-jkr}} \tag{5-19b}$$

5.2.2 Small Loop and Infinitesimal Magnetic Dipole

A comparison of (5-18a)–(5-19b) with those of the infinitesimal magnetic dipole indicates that they have similar forms. In fact, the electric and magnetic field components of an infinitesimal magnetic dipole of length l and constant "magnetic" spatial current I_m are given by

$$E_r = E_\theta = H_\phi = 0 \tag{5-20a}$$

$$E_\phi = -j\frac{kI_m l \sin\theta}{4\pi r}\left[1 + \frac{1}{jkr}\right]e^{-jkr} \tag{5-20b}$$

$$H_r = \frac{I_m l \cos\theta}{2\pi\eta r^2}\left[1 + \frac{1}{jkr}\right]e^{-jkr} \tag{5-20c}$$

$$H_\theta = j\frac{kI_m l \sin\theta}{4\pi\eta r}\left[1 + \frac{1}{jkr} - \frac{1}{(kr)^2}\right]e^{-jkr} \tag{5-20d}$$

These can be obtained, using duality, from the fields of an infinitesimal electric dipole, (4-8a)–(4-10c). When (5-20a)–(5-20d) are compared with (5-18a)–(5-19b), they indicate that *a magnetic dipole of magnetic moment $I_m l$ is equivalent to a small electric loop of radius a and constant electric current I_0 provided that*

$$\boxed{I_m l = jS\omega\mu I_0} \tag{5-21}$$

where $S = \pi a^2$ (area of the loop). Thus, for analysis purposes, the small electric loop can be replaced by a small linear magnetic dipole of constant current. The geometrical equivalence is illustrated in Figure 5.2(a) where the magnetic dipole is directed along the z-axis which is also perpendicular to the plane of the loop.

5.2.3 Power Density and Radiation Resistance

The fields radiated by a small loop, as given by (5-18a)–(5-19b), are valid everywhere except at the origin. As was discussed in Section 4.1 for the infinitesimal dipole, the power in the region very close to the antenna (near field, $kr \ll 1$) is predominantly reactive and in the far field ($kr \gg 1$) is predominantly real. To illustrate this for the loop, the complex power density

$$\begin{aligned}\mathbf{W} &= \tfrac{1}{2}(\mathbf{E} \times \mathbf{H}^*) = \tfrac{1}{2}[(\hat{\mathbf{a}}_\phi E_\phi) \times (\hat{\mathbf{a}}_r H_r^* + \hat{\mathbf{a}}_\theta H_\theta^*)] \\ &= \tfrac{1}{2}(-\hat{\mathbf{a}}_r E_\phi H_\theta^* + \hat{\mathbf{a}}_\theta E_\phi H_r^*)\end{aligned} \tag{5-22}$$

is first formed. When (5-22) is integrated over a closed sphere, only its radial component given by

$$W_r = \eta \frac{(ka)^4}{32} |I_0|^2 \frac{\sin^2\ \theta}{r^2} \left[1 + j \frac{1}{(kr)^3}\right] \tag{5-22a}$$

contributes to the complex power P_r. Thus

$$P_r = \oiint_S \mathbf{W} \cdot d\mathbf{s} = \eta \frac{(ka)^4}{32} |I_0|^2 \int_0^{2\pi} \int_0^{\pi} \left[1 + j \frac{1}{(kr)^3}\right] \sin^3\ \theta\, d\theta\, d\phi \tag{5-23}$$

which reduces to

$$P_r = \eta \left(\frac{\pi}{12}\right) (ka)^4 |I_0|^2 \left[1 + j \frac{1}{(kr)^3}\right] \tag{5-23a}$$

and whose real part is equal to

$$P_{\text{rad}} = \eta \left(\frac{\pi}{12}\right) (ka)^4 |I_0|^2 \tag{5-23b}$$

For small values of $kr (kr \ll 1)$, the second term within the brackets of (5-23a) is dominant which makes the power mainly reactive. In the far field ($kr \gg 1$), the second term within the brackets diminishes, which makes the power real. *A comparison between (5-23a) with (4-14) indicates a difference in sign between the terms within the brackets. Whereas for the infinitesimal dipole the radial power density in the near field is capacitive, for the small loop it is inductive. This is illustrated in Figure 4.21 for the dipole and in Figures 5.13 and 5.20 for the loop.*

The radiation resistance of the loop is found by equating (5-23b) to $|I_0|^2 R_r/2$. Doing this, the radiation resistance can be written as

$$\boxed{R_r = \eta \left(\frac{\pi}{6}\right) (k^2a^2)^2 = \eta \frac{2\pi}{3} \left(\frac{kS}{\lambda}\right)^2 = 20\pi^2 \left(\frac{C}{\lambda}\right)^4 \simeq 31{,}171 \left(\frac{S^2}{\lambda^4}\right)} \tag{5-24}$$

where $S = \pi a^2$ is the area and $C = 2\pi a$ is the circumference of the loop. The last form of (5-24) holds for loops of other configurations, such as rectangular, elliptical, etc. (See Problem 5.30).

The radiation resistance as given by (5-24) is only for a single-turn loop. If the loop antenna has N turns wound so that the magnetic field passes through all the loops, the radiation resistance is equal to that of single turn multiplied by N^2. That is,

$$\boxed{R_r = \eta \left(\frac{2\pi}{3}\right) \left(\frac{kS}{\lambda}\right)^2 N^2 = 20\pi^2 \left(\frac{C}{\lambda}\right)^4 N^2 \simeq 31{,}171\, N^2 \left(\frac{S^2}{\lambda^4}\right)} \tag{5-24a}$$

Even though the radiation resistance of a single-turn loop may be small, the overall value can be increased by including many turns. This is a very desirable and practical mechanism that is not available for the infinitesimal dipole.

Example 5.1

Find the radiation resistance of a single-turn and an eight-turn small circular loop. The radius of the loop is $\lambda/25$ and the medium is free-space.

Solution:

$$S = \pi a^2 = \pi \left(\frac{\lambda}{25}\right)^2 = \frac{\pi\lambda^2}{625}$$

$$R_r \text{ (single turn)} = 120\pi \left(\frac{2\pi}{3}\right)\left(\frac{2\pi^2}{625}\right)^2 = 0.788 \text{ ohms}$$

$$R_r \text{ (8 turns)} = 0.788(8)^2 = 50.43 \text{ ohms}$$

The radiation and loss resistances of an antenna determine the radiation efficiency, as defined by (2-90). The loss resistance of a single-turn small loop is, in general, much larger than its radiation resistance; thus the corresponding radiation efficiencies are very low and depend on the loss resistance. To increase the radiation efficiency, multiturn loops are often employed. However, because the current distribution in a multiturn loop is quite complex, great confidence has not yet been placed in analytical methods for determining the radiation efficiency. Therefore greater reliance has been placed on experimental procedures. Two experimental techniques that can be used to measure the radiation efficiency of a small multiturn loop are those that are usually referred to as the *Wheeler method* and the *Q method* [4].

Usually it is assumed that the loss resistance of a small loop is the same as that of a straight wire whose length is equal to the circumference of the loop, and it is computed using (2-90b). Although this assumption is adequate for single-turn loops, it is not valid for multiturn loops. In a multiturn loop, the current is not uniformly distributed around the wire but depends on the skin and proximity effects [5]. In fact, for close spacings between turns, the contribution to the loss resistance due to the proximity effect can be larger than that due to the skin effect.

The total ohmic resistance for an N-turn circular-loop antenna with loop radius a, wire radius b, and loop separation $2c$, shown in Figure 5.3(a) is given by [6]

$$R_{\text{ohmic}} = \frac{Na}{b} R_s \left(\frac{R_p}{R_0} + 1\right) \tag{5-25}$$

where

$$R_s = \sqrt{\frac{\omega\mu_0}{2\sigma}} = \text{surface impedance of conductor}$$

$$R_p = \text{ohmic resistance per unit length due to proximity effect}$$

$$R_0 = \frac{NR_s}{2\pi b} = \text{ohmic skin effect resistance per unit length (ohms/m)}$$

The ratio of R_p/R_0 has been computed [6] as a function of the spacing c/b for loops with $2 \le N \le 8$ and it is shown plotted in Figure 5.3(b). It is evident that for close spacing the ohmic resistance is twice as large as that in the absence of the proximity effect ($R_p/R_0 = 0$).

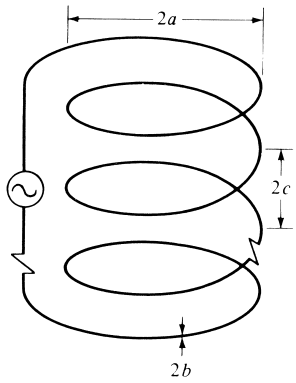

(a) N-turn circular loop

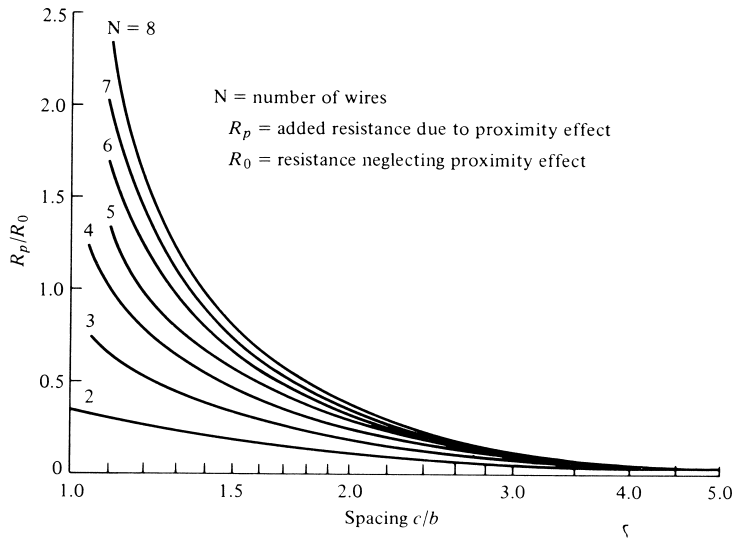

(b) Ohmic resistance due to proximity (after G. N. Smith)

Figure 5.3 N-turn circular loop and ohmic resistance due to proximity effect. (SOURCE: G. S. Smith, "Radiation Efficiency of Electrically Small Multiturn Loop Antennas," *IEEE Trans. Antennas Propagat.*, Vol. AP-20, No. 5, September, pp. 656–657. 1972 © 1972 IEEE).

Example 5.2

Find the radiation efficiency of a single-turn and an eight-turn small circular loop at $f =$ 100 MHz. The radius of the loop is $\lambda/25$, the radius of the wire is $10^{-4}\lambda$, and the turns are spaced $4 \times 10^{-4}\lambda$ apart. Assume the wire is copper with a conductivity of 5.7×10^7(S/m) and the antenna is radiating into free-space.

Solution: From Example 5.1

$$R_r \text{ (single turn)} = 0.788 \text{ ohms}$$

$$R_r \text{ (8 turns)} = 50.43 \text{ ohms}$$

The loss resistance for a single turn is given, according to (2-90b), by

$$R_L = R_{hf} = \frac{a}{b}\sqrt{\frac{\omega\mu_0}{2\sigma}} = \frac{1}{25(10^{-4})}\sqrt{\frac{\pi(10^8)(4\pi \times 10^{-7})}{5.7 \times 10^7}}$$
$$= 1.053 \text{ ohms}$$

and the radiation efficiency, according to (2-90), by

$$e_{cd} = \frac{0.788}{0.788 + 1.053} = 0.428 = 42.8\%$$

From Figure 5.3(b)

$$\frac{R_p}{R_0} = 0.38$$

and from (5-25)

$$R_L = R_{\text{ohmic}} = \frac{8}{25(10^{-4})}\sqrt{\frac{\pi(10^8)(4\pi \times 10^{-7})}{5.7 \times 10^7}}(1.38) = 11.62$$

Thus

$$e_{cd} = \frac{50.43}{50.43 + 11.62} = 0.813 = 81.3\%$$

5.2.4 Near-Field ($kr \ll 1$) Region

The expressions for the fields, as given by (5-18a)–(5-19b), can be simplified if the observations are made in the near field ($kr \ll 1$). As for the infinitesimal dipole, the predominant term in each expression for the field in the near-zone region is the last one within the parentheses of (5-18a)–(5-19b). Thus for $kr \ll 1$

$$\left.\begin{aligned} H_r &\simeq \frac{a^2 I_0 e^{-jkr}}{2r^3}\cos\theta \\ H_\theta &\simeq \frac{a^2 I_0 e^{-jkr}}{4r^3}\sin\theta \\ H_\phi &= E_r = E_\theta = 0 \\ E_\phi &\simeq -j\frac{a^2 k I_0 e^{-jkr}}{4r^2}\sin\theta \end{aligned}\right\} \quad kr \ll 1$$

(5-26a)
(5-26b)
(5-26c)
(5-26d)

The two **H**-field components are in time-phase. However, they are in time quadrature with those of the electric field. This indicates that the average power (real power) is zero, as is for the infinitesimal electric dipole. The condition of $kr \ll 1$ can be satisfied at moderate distances away from the antenna provided the frequency of operation is very low. The fields of (5-26a)–(5-26d) are usually referred to as *quasi-stationary*.

5.2.5 Far-Field ($kr \gg 1$) Region

The other space of interest where the fields can be approximated is the far-field ($kr \gg 1$) region. In contrast to the near field, the dominant term in (5-18a)–(5-19b) for $kr \gg 1$ is the first one within the parentheses. Since for $kr > 1$ the H_r component will be inversely proportional to r^2 whereas H_θ will be inversely proportional to r. For large values of $kr (kr \gg 1)$, the H_r component will be small compared to H_θ. Thus it can be assumed that it is approximately equal to zero. Therefore for $kr \gg 1$,

$$\left.\begin{aligned} H_\theta &\simeq -\frac{k^2 a^2 I_0 e^{-jkr}}{4r}\sin\theta = -\frac{\pi S I_0 e^{-jkr}}{\lambda^2 r}\sin\theta \\ E_\phi &\simeq \eta\frac{k^2 a^2 I_0 e^{-jkr}}{4r}\sin\theta = \eta\frac{\pi S I_0 e^{-jkr}}{\lambda^2 r}\sin\theta \end{aligned}\right\} \quad kr \gg 1 \tag{5-27a}$$

$$E_\phi \simeq \eta\frac{k^2 a^2 I_0 e^{-jkr}}{4r}\sin\theta = \eta\frac{\pi S I_0 e^{-jkr}}{\lambda^2 r}\sin\theta \tag{5-27b}$$

$$H_r \simeq H_\phi = E_r = E_\theta = 0 \tag{5-27c}$$

where $S = \pi a^2$ is the geometrical area of the loop.

Forming the ratio of $-E_\phi/H_\theta$, the wave impedance can be written as

$$Z_w = -\frac{E_\phi}{H_\theta} \simeq \eta \tag{5-28}$$

where

Z_w = wave impedance
η = intrinsic impedance

As for the infinitesimal dipole, the **E**- and **H**-field components of the loop in the far-field ($kr \gg 1$) region are perpendicular to each other and transverse to the direction of propagation. They form a *T*ransverse *E*lectro *M*agnetic (TEM) field whose wave impedance is equal to the intrinsic impedance of the medium. Equations (5-27a)– (5-27c) can also be derived using the procedure outlined and relationships developed in Section 3.6. This is left as an exercise to the reader (Problem 5.9).

5.2.6 Radiation Intensity and Directivity

The real power P_{rad} radiated by the loop was found in Section 5.2.3 and is given by (5-23b). The same expression can be obtained by forming the average power density, using (5-27a)–(5-27c), and integrating it over a closed sphere of radius r. This is left as an exercise to the reader (Problem 5.8). Associated with the radiated power P_{rad} is an average power density $\mathbf{W}_{\text{av}}$. It has only a radial component W_r which is related to the radiation intensity U by

$$U = r^2 W_r = \frac{\eta}{2}\left(\frac{k^2 a^2}{4}\right)^2 |I_0|^2 \sin^2\theta = \frac{r^2}{2\eta}|E_\phi(r,\theta,\phi)|^2 \tag{5-29}$$

and it conforms to (2-12a). The normalized pattern of the loop, as given by (5-29), is identical to that of the infinitesimal dipole shown in Figure 4.3. The maximum value

occurs at $\theta = \pi/2$, and it is given by

$$U_{\max} = U|_{\theta=\pi/2} = \frac{\eta}{2}\left(\frac{k^2a^2}{4}\right)^2 |I_0|^2 \tag{5-30}$$

Using (5-30) and (5-23b), the directivity of the loop can be written as

$$\boxed{D_0 = 4\pi \frac{U_{\max}}{P_{\text{rad}}} = \frac{3}{2}} \tag{5-31}$$

and its maximum effective area as

$$\boxed{A_{em} = \left(\frac{\lambda^2}{4\pi}\right) D_0 = \frac{3\lambda^2}{8\pi}} \tag{5-32}$$

It is observed that the directivity, and as a result the maximum effective area, of a small loop is the same as that of an infinitesimal electric dipole. This should be expected since their patterns are identical.

The far-field expressions for a small loop, as given by (5-27a)–(5-27c), will be obtained by another procedure in the next section. In that section a loop of any radius but of constant current will be analyzed. The small loop far-field expressions will then be obtained as a special case of that problem.

Example 5.3

The radius of a small loop of constant current is $\lambda/25$. Find the physical area of the loop and compare it with its maximum effective aperture.

Solution:

$$S \text{ (physical)} = \pi a^2 = \pi\left(\frac{\lambda}{25}\right)^2 = \frac{\pi\lambda^2}{625} = 5.03 \times 10^{-3}\lambda^2$$

$$A_{em} = \frac{3\lambda^2}{8\pi} = 0.119\lambda^2$$

$$\frac{A_{em}}{S} = \frac{0.119\lambda^2}{5.03 \times 10^{-3}\lambda^2} = 23.66$$

Electrically the loop is about 24 times larger than its physical size, which should not be surprising. To be effective, a small loop must be larger electrically than its physical size.

5.2.7 Equivalent Circuit

A small loop is primarily inductive, and it can be represented by a lumped element equivalent circuit similar to those of Figure 2.28.

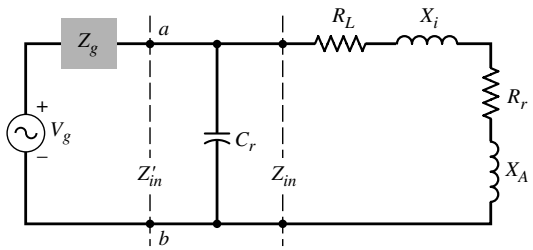

Figure 5.4 Equivalent circuit of loop antenna in transmitting mode.

A. Transmitting Mode

The equivalent circuit for its input impedance when the loop is used as a transmitting antenna is that shown in Figure 5.4. This is similar to the equivalent circuit of Figure 2.28(b). Therefore its input impedance Z_{in} is represented by

$$Z_{in} = R_{in} + jX_{in} = (R_r + R_L) + j(X_A + X_i) \tag{5-33}$$

where

R_r = radiation resistance as given by (5-24)
R_L = loss resistance of loop conductor
X_A = external inductive reactance of loop antenna = ωL_A
X_i = internal high-frequency reactance of loop conductor = ωL_i

In Figure 5.4 the capacitor C_r is used in parallel to (5-33) to resonate the antenna; it can also be used to represent distributed stray capacitances. In order to determine the capacitance of C_r at resonance, it is easier to represent (5-33) by its equivalent admittance Y_{in} of

$$Y_{in} = G_{in} + jB_{in} = \frac{1}{Z_{in}} = \frac{1}{R_{in} + jX_{in}} \tag{5-34}$$

where

$$G_{in} = \frac{R_{in}}{R_{in}^2 + X_{in}^2} \tag{5-34a}$$

$$B_{in} = -\frac{X_{in}}{R_{in}^2 + X_{in}^2} \tag{5-34b}$$

At resonance, the susceptance B_r of the capacitor C_r must be chosen to eliminate the imaginary part B_{in} of (5-34) given by (5-34b). This is accomplished by choosing C_r according to

$$C_r = \frac{B_r}{2\pi f} = -\frac{B_{in}}{2\pi f} = \frac{1}{2\pi f}\frac{X_{in}}{R_{in}^2 + X_{in}^2} \tag{5-35}$$

Under resonance the input impedance Z'_{in} is then equal to

$$Z'_{in} = R'_{in} = \frac{1}{G_{in}} = \frac{R_{in}^2 + X_{in}^2}{R_{in}} = R_{in} + \frac{X_{in}^2}{R_{in}} \tag{5-36}$$

The loss resistance R_L of the loop conductor can be computed using techniques illustrated in Example 5.2. The inductive reactance X_A of the loop is computed using the inductance L_A [7] of:

Circular loop of radius a and wire radius b:

$$L_A = \mu_0 a \left[\ln\left(\frac{8a}{b}\right) - 2 \right] \tag{5-37a}$$

Square loop with sides a and wire radius b:

$$L_A = 2\mu_0 \frac{a}{\pi} \left[\ln\left(\frac{a}{b}\right) - 0.774 \right] \tag{5-37b}$$

The internal reactance of the loop conductor X_i can be found using the internal inductance L_i of the loop which for a single turn can be approximated by

$$L_i = \frac{l}{\omega P}\sqrt{\frac{\omega\mu_0}{2\sigma}} = \frac{a}{\omega b}\sqrt{\frac{\omega\mu_0}{2\sigma}} \tag{5-38}$$

where l is the length and P is the perimeter (circumference) of the wire of the loop.

B. Receiving Mode

The loop antenna is often used as a receiving antenna or as a probe to measure magnetic flux density. Therefore when a plane wave impinges upon it, as shown in Figure 5.5(a), an open-circuit voltage develops across its terminals. This open-circuit voltage is related according to (2-93) to its vector effective length and incident electric field. This open-circuit voltage is proportional to the incident magnetic flux density B_z^i, which is normal

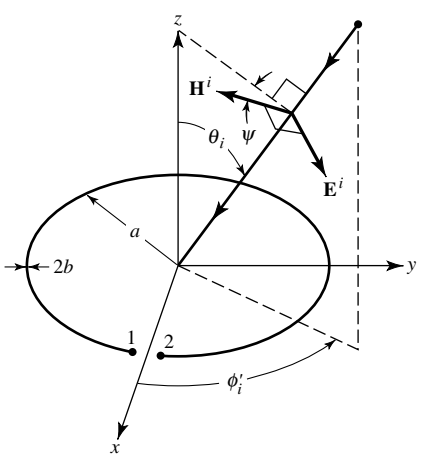

(a) Plane wave incident on a receiving loop (G.S. Smith, "Loop Antennas," Copyright © 1984, McGraw-Hill, Inc. Permission by McGraw-Hill, Inc.)

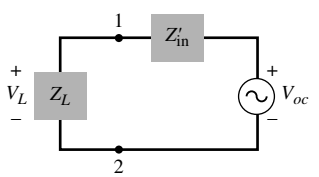

(b) Thevenin equivalent

Figure 5.5 Loop antenna and its equivalent in receiving mode.

to the plane of the loop. Assuming the incident field is uniform over the plane of the loop, the open-circuit voltage for a single-turn loop can be written as [8]

$$V_{oc} = j\omega\pi a^2 B_z^i \tag{5-39}$$

Defining in Figure 5.5(a) the plane of incidence as the plane formed by the z axis and radical vector, then the open-circuit voltage of (5-39) can be related to the magnitude of the incident magnetic and electric fields by

$$V_{oc} = j\omega\pi a^2 \mu_0 H^i \cos\psi_i \sin\theta_i = jk_0\pi a^2 E^i \cos\psi_i \sin\theta_i \tag{5-39a}$$

where ψ_i is the angle between the direction of the magnetic field of the incident plane wave and the plane of incidence, as shown in Figure 5.5(a).

Since the open-circuit voltage is also related to the vector effective length by (2-93), then the effective length for a single-turn loop can be written as

$$\boldsymbol{\ell}_e = \hat{\mathbf{a}}_\phi l_e = \hat{\mathbf{a}}_\phi jk_0\pi a^2 \cos\psi_i \sin\theta_i = \hat{\mathbf{a}}_\phi jk_0 S \cos\psi_i \sin\theta_i \tag{5-40}$$

where S is the area of the loop. The factor $\cos\psi_i \sin\theta_i$ is introduced because the open-circuit voltage is proportional to the magnetic flux density component B_z^i which is normal to the plane of the loop.

When a load impedance Z_L is connected to the output terminals of the loop as shown in Figure 5.5(b), the voltage V_L across the load impedance Z_L is related to the input impedance Z'_{in} of Figure 5.5(b) and the open-circuit voltage of (5-39a) by

$$V_L = V_{oc} \frac{Z_L}{Z'_{in} + Z_L} \tag{5-41}$$

5.3 CIRCULAR LOOP OF CONSTANT CURRENT

Let us now reconsider the loop antenna of Figure 5.2(a) but with a radius that may not necessarily be small. The current in the loop will again be assumed to be constant, as given by (5-1). For this current distribution, the vector potential is given by (5-14). The integration in (5-14) is quite complex, as is indicated right after (5-14). However, if the observation are restricted in the far-field ($r \gg a$) region, the small radius approximation is not needed to simplify the integration of (5-14).

Although the uniform current distribution along the perimeter of the loop is only valid provided the circumference is less than about 0.1λ (radius less than about 0.016λ), the procedure developed here for a constant current can be followed to find the far-zone fields of any size loop with not necessarily uniform current.

5.3.1 Radiated Fields

To find the fields in the far-field region, the distance R can be approximated by

$$R = \sqrt{r^2 + a^2 - 2ar\sin\theta\cos\phi'} \simeq \sqrt{r^2 - 2ar\sin\theta\cos\phi'} \quad \text{for} \quad r \gg a \tag{5-42}$$

which can be reduced, using the binomial expansion, to

$$\left.\begin{aligned} R &\simeq r\sqrt{1-\frac{2a}{r}\sin\theta\cos\phi'} = r - a\sin\theta\cos\phi' = r - a\cos\psi_0 \\ &\qquad\qquad\qquad\qquad\qquad\qquad\qquad\qquad\qquad\qquad \text{for phase terms} \\ R &\simeq r \qquad\qquad\qquad\qquad\qquad\qquad\qquad\qquad\qquad\qquad \text{for amplitude terms} \end{aligned}\right\} \tag{5-43}$$

since

$$\begin{aligned} \cos\psi_0 = \hat{\mathbf{a}}'_\rho \cdot \hat{\mathbf{a}}_r|_{\phi=0} &= (\hat{\mathbf{a}}_x\cos\phi' + \hat{\mathbf{a}}_y\sin\phi') \\ &\quad\cdot(\hat{\mathbf{a}}_x\sin\theta\cos\phi + \hat{\mathbf{a}}_y\sin\theta\sin\phi + \hat{\mathbf{a}}_z\cos\theta)|_{\phi=0} \\ &= \sin\theta\cos\phi' \end{aligned} \tag{5-43a}$$

The geometrical relation between R and r, for any observation angle ϕ in the far-field region, is shown in Figure 5.2(b). For observations at $\phi = 0$, it simplifies to that given by (5-43) and shown in Figure 5.6. Thus (5-14) can be simplified to

$$A_\phi \simeq \frac{a\mu I_0 e^{-jkr}}{4\pi r}\int_0^{2\pi}\cos\phi' e^{+jka\sin\theta\cos\phi'}\,d\phi' \tag{5-44}$$

and it can be separated into two terms as

$$A_\phi \simeq \frac{a\mu I_0 e^{-jkr}}{4\pi r}\left[\int_0^{\pi}\cos\phi' e^{+jka\sin\theta\cos\phi'}\,d\phi' + \int_{\pi}^{2\pi}\cos\phi' e^{+jka\sin\theta\cos\phi'}\,d\phi'\right] \tag{5-45}$$

The second term within the brackets can be rewritten by making a change of variable of the form

$$\phi' = \phi'' + \pi \tag{5-46}$$

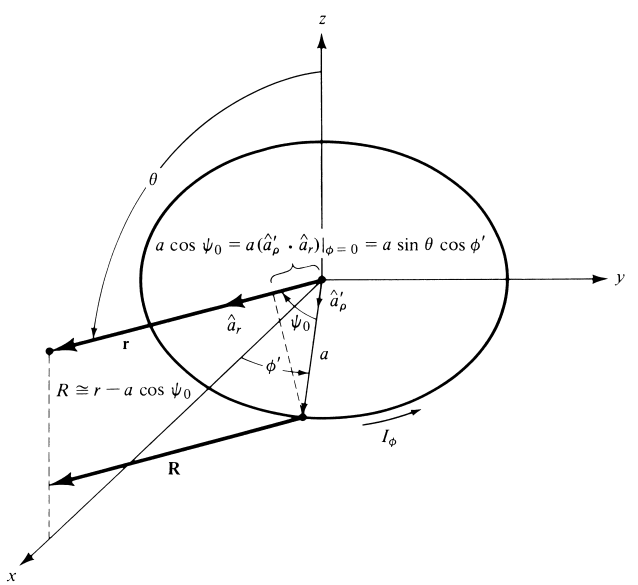

Figure 5.6 Geometry for far-field analysis of a loop antenna.

Thus (5-45) can also be written as

$$A_\phi \simeq \frac{a\mu I_0 e^{-jkr}}{4\pi r}\left[\int_0^\pi \cos\phi' e^{+jka\sin\theta\cos\phi'}\,d\phi' - \int_0^\pi \cos\phi'' e^{-jka\sin\theta\cos\phi''}\,d\phi''\right] \tag{5-47}$$

Each of the integrals in (5-47) can be integrated by the formula (see Appendix V)

$$\pi j^n J_n(z) = \int_0^\pi \cos(n\phi) e^{+jz\cos\phi}\,d\phi \tag{5-48}$$

where $J_n(z)$ is the Bessel function of the first kind of order n. Using (5-48) reduces (5-47) to

$$A_\phi \simeq \frac{a\mu I_0 e^{-jkr}}{4\pi r}[\pi j J_1(ka\sin\theta) - \pi j J_1(-ka\sin\theta)] \tag{5-49}$$

The Bessel function of the first kind and order n is defined (see Appendix V) by the infinite series

$$J_n(z) = \sum_{m=0}^{\infty} \frac{(-1)^m (z/2)^{n+2m}}{m!(m+n)!} \tag{5-50}$$

By a simple substitution into (5-50), it can be shown that

$$J_n(-z) = (-1)^n J_n(z) \tag{5-51}$$

which for $n = 1$ is equal to

$$J_1(-z) = -J_1(z) \tag{5-52}$$

Using (5-52) we can write (5-49) as

$$A_\phi \simeq j\frac{a\mu I_0 e^{-jkr}}{2r} J_1(ka\sin\theta) \tag{5-53}$$

The next step is to find the **E-** and **H-**fields associated with the vector potential of (5-53). Since (5-53) is only valid for far-field observations, the procedure outlined in Section 3.6 can be used. The vector potential **A**, as given by (5-53), is of the form suggested by (3-56). That is, the r variations are separable from those of θ and ϕ. Therefore according to (3-58a)–(3-58b) and (5-53)

$$E_r \simeq E_\theta = 0 \tag{5-54a}$$

$$E_\phi \simeq \frac{ak\eta I_0 e^{-jkr}}{2r} J_1(ka\sin\theta) \tag{5-54b}$$

$$H_r \simeq H_\phi = 0 \tag{5-54c}$$

$$H_\theta \simeq -\frac{E_\phi}{\eta} = -\frac{akI_0 e^{-jkr}}{2r} J_1(ka\sin\theta) \tag{5-54d}$$

5.3.2 Power Density, Radiation Intensity, Radiation Resistance, and Directivity

The next objective for this problem will be to find the power density, radiation intensity, radiation resistance, and directivity. To do this, the time-average power density is formed. That is,

$$\mathbf{W}_{\text{av}} = \frac{1}{2}\text{Re}[\mathbf{E} \times \mathbf{H}^*] = \frac{1}{2}\text{Re}[\hat{\mathbf{a}}_\phi E_\phi \times \hat{\mathbf{a}}_\theta H_\theta^*] = \hat{\mathbf{a}}_r \frac{1}{2\eta}|E_\phi|^2 \tag{5-55}$$

which can be written using (5-54b) as

$$\mathbf{W}_{\text{av}} = \hat{\mathbf{a}}_r W_r = \hat{\mathbf{a}}_r \frac{(a\omega\mu)^2|I_0|^2}{8\eta r^2} J_1{}^2(ka\sin\theta) \tag{5-56}$$

with the radiation intensity given by

$$U = r^2 W_r = \frac{(a\omega\mu)^2|I_0|^2}{8\eta} J_1{}^2(ka\sin\theta) \tag{5-57}$$

The radiation patterns for $a = \lambda/10, \lambda/5$, and $\lambda/2$ are shown in Figure 5.7. These patterns indicate that the field radiated by the loop along its axis ($\theta = 0^\circ$) is zero. Also the shape of these patterns is similar to that of a linear dipole with $l \leq \lambda$ (a figure-eight shape). As the radius a increases beyond 0.5λ, the field intensity along the plane of the loop ($\theta = 90^\circ$) diminishes and eventually it forms a null when $a \simeq 0.61\lambda$. This is left as an exercise to the reader for verification (Prob. 5.18). Beyond $a = 0.61\lambda$, the radiation along the plane of the loop begins to intensify and the pattern attains a multilobe form.

Three-dimensional patterns for loop circumferences of $C = 0.1\lambda$ and 5λ, assuming uniform current distribution, are shown in Figure 5.8. It is apparent that for the 0.1λ circumference the pattern is basically that of figure eight ($\sin\theta$), while for the 5λ loop it exhibits multiple lobes. The multiple lobes in a large loop begin to form when the circumference exceeds about 3.83λ (radius exceeds about 0.61λ); see Problem 5.18.

The patterns represented by (5-57) (some of them are illustrated in Figure 5.7) assume that the current distribution, no matter what the loop size, is constant. This is not a valid assumption if the loop circumference $C (C = 2\pi a)$ exceeds about 0.1λ (i.e., $a > 0.016\lambda$) [9]. For radii much greater than about 0.016λ, the current variation along the circumference of the loop begins to attain a distribution that is best represented by a Fourier series [8]. Although a most common assumption is that the current distribution is nearly cosinusoidal, it is not satisfactory particularly near the driving point of the antenna.

A uniform and nonuniform in-phase current distribution can be attained on a loop antenna even if the radius is large. To accomplish this, the loop is subdivided into sections, with each section/arc of the loop fed with a different feed line; all feed lines are typically fed from a common feed source. Such an arrangement, although more complex, can approximate either uniform or nonuniform in-phase current distribution.

It has been shown [10] that when the circumference of the loop is about one wavelength ($C \simeq \lambda$), its maximum radiation based on a nonuniform current distribution is along its axis ($\theta = 0^\circ, 180^\circ$) which is perpendicular to the plane of the loop. This

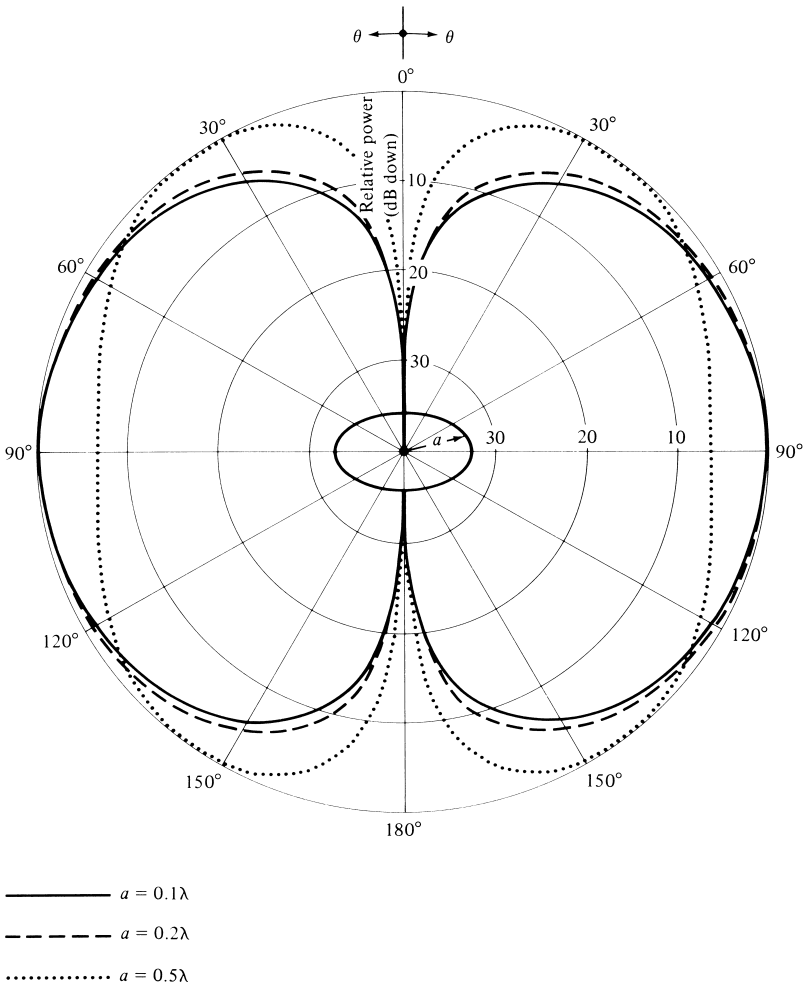

Figure 5.7 Elevation plane amplitude patterns for a circular loop of constant current ($a = 0.1\lambda$, 0.2λ, and 0.5λ).

feature of the loop antenna has been utilized to design Yagi-Uda arrays whose basic elements (feed, directors, and reflectors) are circular loops [11]–[14]. Because of its many applications, the one-wavelength circumference circular-loop antenna is considered as fundamental as a half-wavelength dipole.

The radiated power can be written using (5-56) as

$$P_{\text{rad}} = \iint_S \mathbf{W}_{\text{av}} \cdot d\mathbf{s} = \frac{\pi (a\omega\mu)^2 |I_0|^2}{4\eta} \int_0^\pi J_1{}^2(ka \sin\theta) \sin\theta \, d\theta \tag{5-58}$$

The integral in (5-58) can be rewritten [15] as

$$\int_0^\pi J_1{}^2(ka \sin\theta) \sin\theta \, d\theta = \frac{1}{ka} \int_0^{2ka} J_2(x) \, dx \tag{5-59}$$

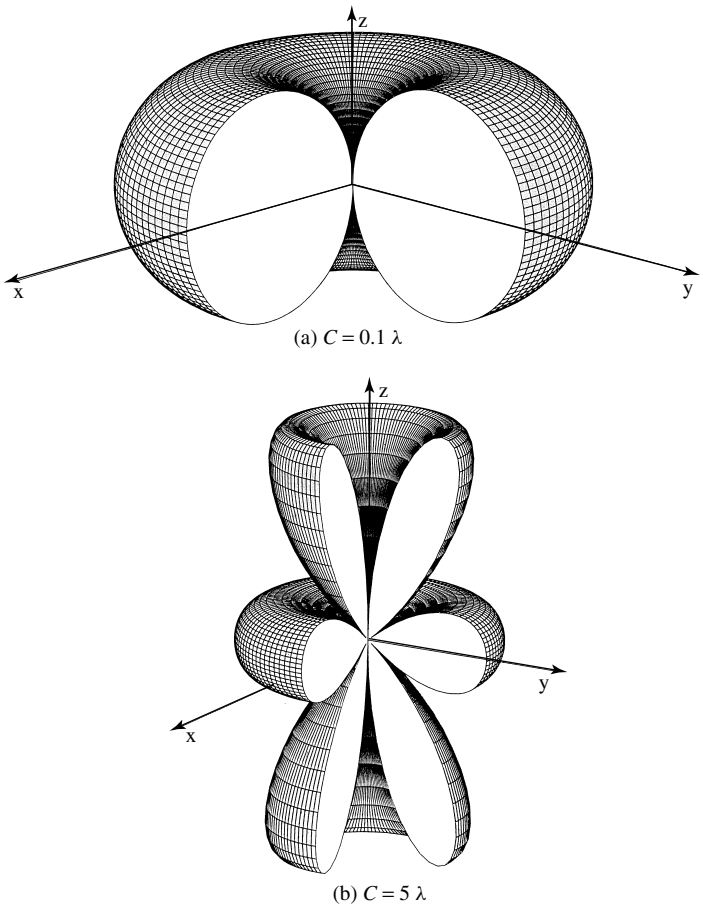

(a) $C = 0.1\ \lambda$

(b) $C = 5\ \lambda$

Figure 5.8 Three-dimensional amplitude patterns of a circular loop with constant current distribution.

The evaluation of the integral of (5-59) has been the subject of recent papers [16]–[20]. In these references, *along with some additional corrections*, the integral of (5-59)

$$Q_{11}^{(1)}(ka) = \frac{1}{2}\int_0^{\pi} J_1^2(ka\sin\theta)\sin\theta\, d\theta = \frac{1}{2ka}\int_0^{2ka} J_2(x)\, dx \tag{5-59a}$$

can be represented by a series of Bessel functions

$$Q_{11}^{(1)}(ka) = \frac{1}{ka}\sum_{m=0}^{\infty} J_{2m+3}(2ka) \tag{5-59b}$$

where $J_m(x)$ is the Bessel function of the first kind, mth order. This is a highly convergent series (typically no more than $2ka$ terms are necessary), and its numerical evaluation is very efficient. Approximations to (5-59) can be made depending upon the values of the upper limit (large or small radii of the loop).

A. Large Loop Approximation ($a \geq \lambda/2$)
To evaluate (5-59), the first approximation will be to assume that the radius of the loop is large ($a \geq \lambda/2$). For that case, the integral in (5-59) can be approximated by

$$\int_0^{\pi} J_1{}^2(ka\sin\theta)\sin\theta\, d\theta = \frac{1}{ka}\int_0^{2ka} J_2(x)\, dx \simeq \frac{1}{ka} \tag{5-60}$$

and (5-58) by

$$P_{\text{rad}} \simeq \frac{\pi(a\omega\mu)^2|I_0|^2}{4\eta(ka)} \tag{5-61}$$

The maximum radiation intensity occurs when $ka\sin\theta = 1.84$ so that

$$U|_{\max} = \frac{(a\omega\mu)^2|I_0|^2}{8\eta} J_1{}^2(ka\sin\theta)|_{ka\sin\theta=1.84} = \frac{(a\omega\mu)^2|I_0|^2}{8\eta}(0.582)^2 \tag{5-62}$$

Thus

$$R_r = \frac{2P_{\text{rad}}}{|I_0|^2} = \frac{2\pi(a\omega\mu)^2}{4\eta(ka)} = \eta\left(\frac{\pi}{2}\right)ka = 60\pi^2(ka) = 60\pi^2\left(\frac{C}{\lambda}\right) \tag{5-63a}$$

$$D_0 = 4\pi\frac{U_{\max}}{P_{\text{rad}}} = 4\pi\frac{ka(0.582)^2}{2\pi} = 2ka(0.582)^2 = 0.677\left(\frac{C}{\lambda}\right) \tag{5-63b}$$

$$A_{em} = \frac{\lambda^2}{4\pi}D_0 = \frac{\lambda^2}{4\pi}\left[0.677\left(\frac{C}{\lambda}\right)\right] = 5.39\times 10^{-2}\lambda C \tag{5-63c}$$

where C(circumference) $= 2\pi a$ and $\eta \simeq 120\pi$.

B. Intermediate Loop Approximation ($\lambda/6\pi \leq a < \lambda/2$)
If the radius of the loop is $\lambda/(6\pi) = 0.053\lambda \leq a < \lambda/2$, the integral of (5-59) for $Q_{11}^{1}(ka)$ is approximated by (5-59a) and (5-59b), and the radiation resistance and directivity can be expressed, respectively, as

$$R_r = \frac{2P_{rad}}{|I_0|^2} = \eta\pi(ka)^2 Q_{11}^{(1)}(ka) \tag{5-64a}$$

$$D_0 = \frac{4\pi U_{\max}}{P_{rad}} = \frac{F_m(ka)}{Q_{11}^{(1)}(ka)} \tag{5-64b}$$

where

$$F_m(ka) = J_1^2(ka\sin\theta)|_{\max} = \begin{cases} J_1^2(1.840) = (0.582)^2 = 0.339 & \text{(5-64c)} \\ \quad ka > 1.840\ (a > 0.293\lambda) & \\ J_1^2(ka) & \\ \quad ka < 1.840\ (a < 0.293\lambda) & \text{(5-64d)} \end{cases}$$

C. Small Loop Approximation ($a < \lambda/6\pi$)
If the radius of the loop is small ($a < \lambda/6\pi$), the expressions for the fields as given by (5-54a)–(5-54d) can be simplified. To do this, the Bessel function $J_1(ka\sin\theta)$ is expanded, by the definition of (5-50), in an infinite series of the form (see Appendix V)

$$J_1(ka\sin\theta) = \tfrac{1}{2}(ka\sin\theta) - \tfrac{1}{16}(ka\sin\theta)^3 + \cdots \tag{5-65}$$

For small values of $ka (ka < \frac{1}{3})$, (5-65) can be approximated by its first term, or

$$J_1(ka \sin\theta) \simeq \frac{ka \sin\theta}{2} \tag{5-65a}$$

Thus (5-54a)–(5-54d) can be written as

$$\left.\begin{aligned} E_r &\simeq E_\theta = 0 && \text{(5-66a)}\\ E_\phi &\simeq \frac{a^2\omega\mu k I_0 e^{-jkr}}{4r}\sin\theta = \eta\frac{a^2k^2 I_0 e^{-jkr}}{4r}\sin\theta && \text{(5-66b)}\\ H_r &\simeq H_\phi = 0 && \text{(5-66c)}\\ H_\theta &\simeq -\frac{a^2\omega\mu k I_0 e^{-jkr}}{4\eta r}\sin\theta = -\frac{a^2k^2 I_0 e^{-jkr}}{4r}\sin\theta && \text{(5-66d)} \end{aligned}\right\} \quad a < \lambda/6\pi$$

which are identical to those of (5-27a)–(5-27c). Thus the expressions for the radiation resistance, radiation intensity, directivity, and maximum effective aperture are those given by (5-24), (5-29), (5-31), and (5-32).

To demonstrate the variation of the radiation resistance as a function of the radius a of the loop, it is plotted in Figure 5.9 for $\lambda/100 \le a \le \lambda/30$, based on the approximation of (5-65a). It is evident that the values are extremely low (less than 1 ohm), and they are usually smaller than the loss resistances of the wires. These radiation resistances also lead to large mismatch losses when connected to practical transmission

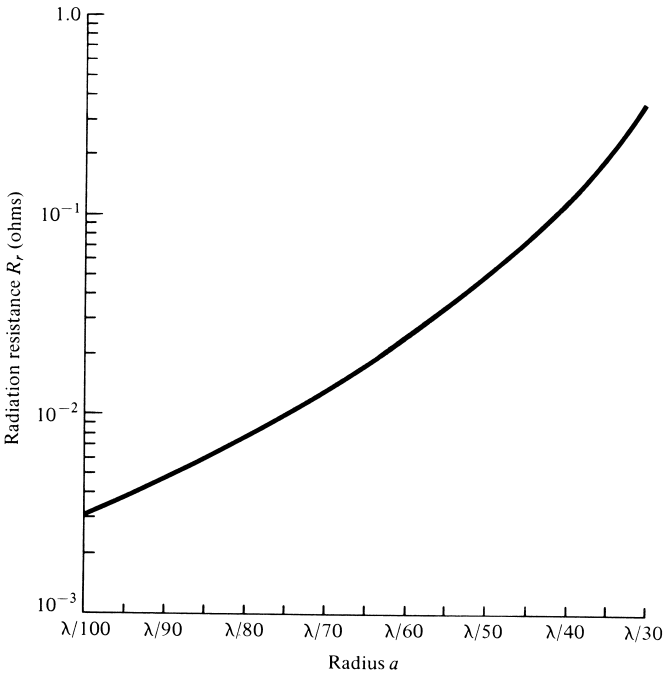

Figure 5.9 Radiation resistance for a constant current circular-loop antenna based on the approximation of (5-65a).

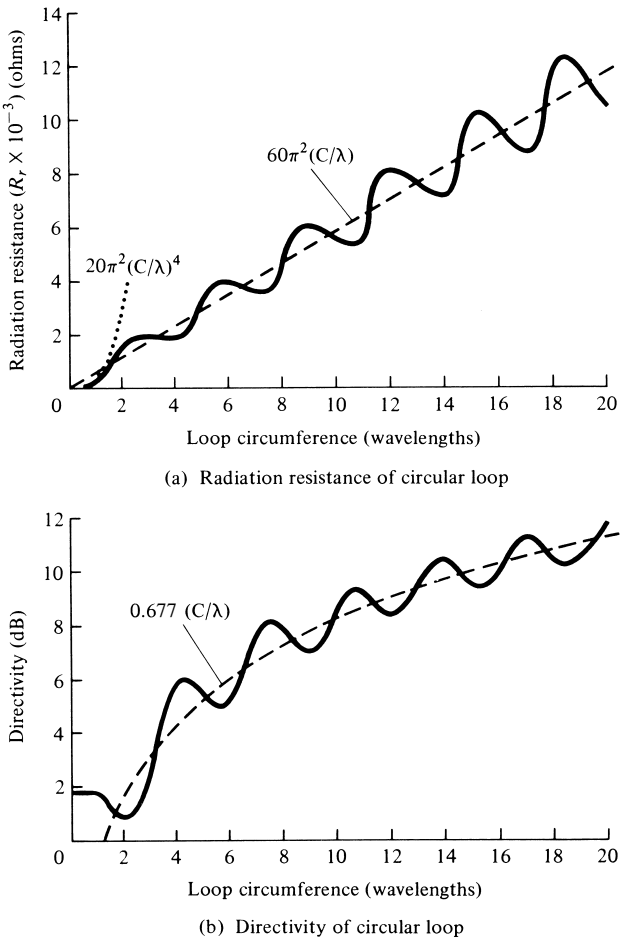

Figure 5.10 Radiation resistance and directivity for circular loop of constant current. (SOURCE: E. A. Wolff, *Antenna Analysis*, Wiley, New York, 1966).

lines of 50 or 75 ohms. To increase the radiation resistance, it would require multiple turns as suggested by (5-24a). This, however, also increases the loss resistance which contributes to the inefficiency of the antenna. A plot of the radiation resistance for $0 < ka = C/\lambda < 20$, based on the evaluation of (5-59) by numerical techniques, is shown in Figure 5.10. The dashed line represents the values based on the large loop approximation of (5-60) and the dotted ($\cdots\cdots$) represents the values based on the small loop approximation of (5-65a).

In addition to the real part of the input impedance, there is also an imaginary component which would increase the mismatch losses even if the real part is equal to the characteristic impedance of the lossless transmission line. However, the imaginary component can always, in principle at least, be eliminated by connecting a reactive element (capacitive or inductive) across the terminals of the loop to make the antenna a resonant circuit.

To facilitate the computations for the directivity and radiation resistance of a circular loop with a constant current distribution, a MATLAB and FORTRAN computer

program has been developed. The program utilizes (5-62) and (5-58) to compute the directivity [(5-58) is integrated numerically]. The program requires as an input the radius of the loop (in wavelengths). A Bessel function subroutine is contained within the FORTRAN program. A listing of the program is included in the CD attached with the book.

5.4 CIRCULAR LOOP WITH NONUNIFORM CURRENT

The analysis in the previous sections was based on a uniform current, which would be a valid approximation when the radius of the loop is small electrically (usually $a < 0.016\lambda$). As the dimensions of the loop increase, the current variations along the circumference of the loop must be taken into account. As stated previously, a very common assumption for the current distribution is a cosinusoidal variation [21], [22]. This, however, is not a satisfactory approximation particularly near the driving point of the antenna [9]. A better distribution would be to represent the current by a Fourier series [23]

$$I(\phi') = I_0 + 2\sum_{n=1}^{M} I_n \cos(n\phi') \tag{5-67}$$

where ϕ' is measured from the feed point of the loop along the circumference, as shown at the inset of Figure 5.11.

A complete analysis of the fields radiated by a loop with nonuniform current distribution is somewhat complex, laborious, and quite lengthy [2], [3]. Instead of attempting to include the analytical formulations, which are cumbersome but well documented in the cited references, a number of graphical illustrations of numerical and experimental data is presented. These curves can be used in facilitating designs.

To illustrate that the current distribution of a wire loop antenna is not uniform unless its radius is very small, the magnitude and phase of it have been plotted in Figure 5.11 as a function of ϕ' (in degrees). The loop circumference C is $ka = C/\lambda = 0.1$, 0.2, 0.3, and 0.4 and the wire size was chosen so that $\Omega = 2\ln(2\pi a/b) = 10$. It is apparent that for $ka = 0.1$ the current is nearly uniform. For $ka = 0.2$ the variations are slightly greater and become even larger as ka increases. On the basis of these results, loops much larger than $ka = 0.1$ (radius much greater than 0.016λ) cannot be considered small.

As was indicated earlier, the maximum of the pattern for a loop antenna shifts from the plane of the loop ($\theta = 90^\circ$) to its axis ($\theta = 0^\circ, 180^\circ$) as the circumference of the loop approaches one wavelength, assuming that simultaneously the current changes from uniform to nonuniform. Based on the nonuniform current distribution of (5-67), the directivity of the loop along $\theta = 0^\circ$ has been computed, and it is plotted in Figure 5.12 versus the circumference of the loop in wavelengths [8]. The maximum directivity is about 4.5 dB, and it occurs when the circumference is about 1.4λ. For a one-wavelength circumference, which is usually the optimum design for a helical antenna, the directivity is about 3.4 dB. It is also apparent that the directivity is basically independent of the radius of the wire, as long as the circumference is equal or less than about 1.3 wavelengths; there are differences in directivity as a function of the wire radius for greater circumferences.

Computed impedances, based on the Fourier series representation of the current, are shown plotted in Figure 5.13. The input resistance and reactance are plotted as

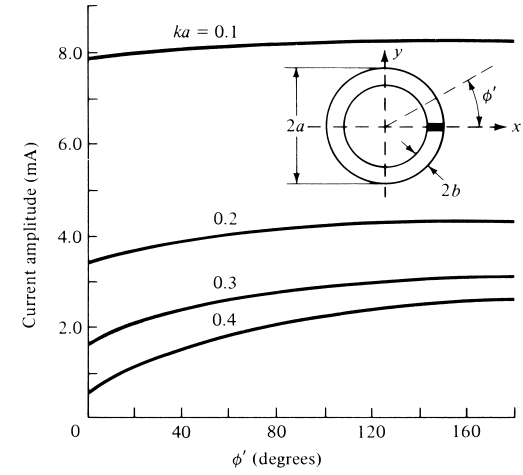

(a) Magnitude

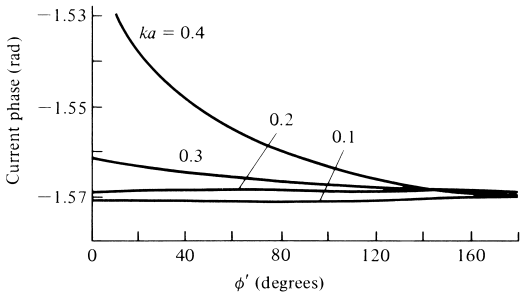

(b) Phase

Figure 5.11 Current magnitude and phase distributions on small circular loop antennas. (SOURCE: J. E. Storer, "Impedance of Thin-Wire Loop Antennas," *AIEE Trans.*, Vol. 75, November 1956. © 1956 IEEE).

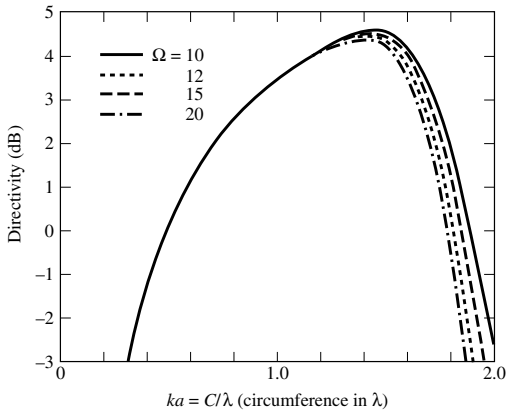

Figure 5.12 Directivity of circular-loop antenna for $\theta = 0, \pi$ versus electrical size (circumference/wavelength). (SOURCE: G. S. Smith, "Loop Antennas," Chapter 5 of *Antenna Engineering Handbook*, 1984, © 1984 McGraw-Hill, Inc. Permission by McGraw-Hill, Inc).

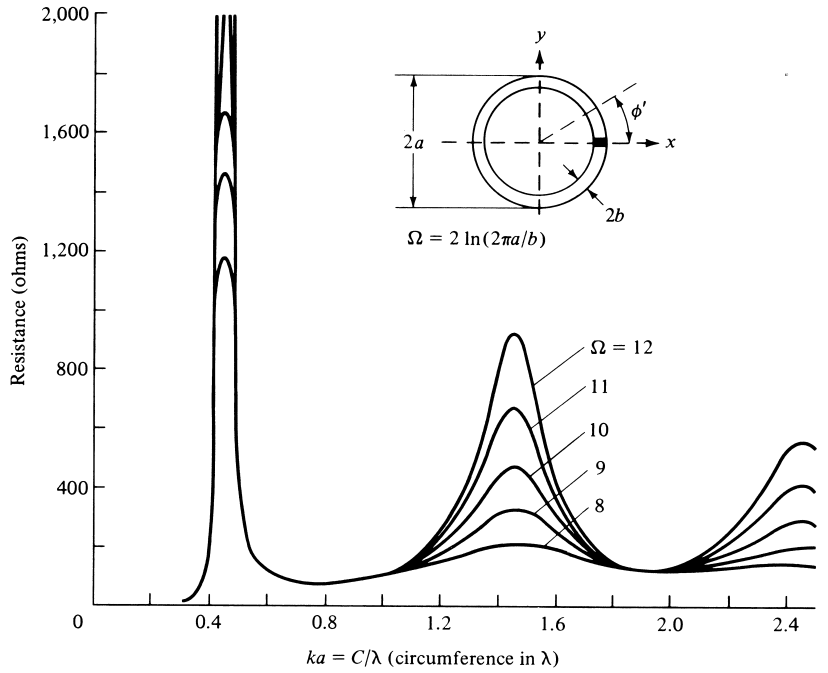

(a) Resistance

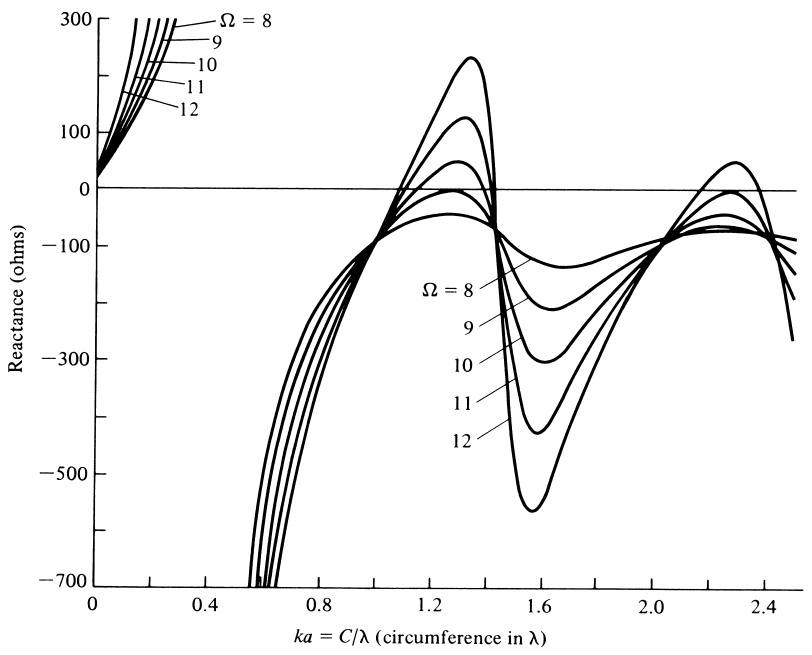

(b) Reactance

Figure 5.13 Input impedance of circular-loop antennas. (SOURCE: J. E. Storer, "Impedance of Thin-Wire Loop Antennas," *AIEE Trans.*, Vol. 75, November 1956. © 1956 IEEE).

a function of the circumference C (in wavelengths) for $0 \leq ka = C/\lambda \leq 2.5$. The diameter of the wire was chosen so that $\Omega = 2\ln(2\pi a/b) = 8$, 9, 10, 11, and 12. It is apparent that the first antiresonance occurs when the circumference of the loop is about $\lambda/2$, and it is extremely sharp. It is also noted that as the loop wire increases in thickness, there is a rapid disappearance of the resonances. As a matter of fact, for $\Omega < 9$ there is only one antiresonance point. These curves (for $C > \lambda$) are similar, both qualitatively and quantitatively, to those of a linear dipole. The major difference is that the loop is more capacitive (by about 130 ohms) than a dipole. This shift in reactance allows the dipole to have several resonances and antiresonances while moderately thick loops ($\Omega < 9$) have only one antiresonance. *Also small loops are primarily inductive while small dipoles are primarily capacitive*. The resistance curves for the loop and the dipole are very similar.

To verify the analytical formulations and the numerical computations, loop antennas were built and measurements of impedance were made [9]. The measurements were conducted using a half-loop over an image plane, and it was driven by a two-wire line. An excellent agreement between theory and experiment was indicated everywhere except near resonances where computed conductance curves were slightly higher than those measured. This is expected since ohmic losses were not taken into account in the analytical formulation. It was also noted that the measured susceptance curve was slightly displaced vertically by a constant value. This can be attributed to the "end effect" of the experimental feeding line and the "slice generator" used in the analytical modeling of the feed. For a dipole, the correction to the analytical model is usually a negative capacitance in shunt with the antenna [24]. A similar correction for the loop would result in a better agreement between the computed and measured susceptances. Computations for a half-loop above a ground plane were also performed by J. E. Jones [25] using the Moment Method.

The radiation resistance and directivity of a loop antenna with a cosinusoidal current distribution $I_\phi(\phi) = I_0 \cos\phi$ was derived in [2] and evaluated in [16] by integrating in far-zone fields and expressing the integral in terms of five $Q_{mn}^{(1)}(ka)$ integrals of similar form as (5-59a) and (5-59b). Doing this, the values are plotted, respectively, in Figures 5.14(a,b) where they are compared with those based on a uniform current distribution.

5.4.1 Arrays

In addition to being used as single elements and in arrays, as shown in Figure 5.1(a,b), there are some other classic arrays of loop configurations. Two of the most popular arrays of loop antennas are the helical antenna and the Yagi-Uda array. The loop is also widely used to form a solenoid which in conjunction with a ferrite cylindrical rod within its circumference is used as a receiving antenna and as a tuning element, especially in transistor radios. This is discussed in Section 5.7.

The helical antenna, which is discussed in more detail in Section 10.3.1, is a wire antenna, which is wound in the form of a helix, as shown in Figure 10.13. It is shown that it can be modeled approximately by a series of loops and vertical dipoles, as shown in Figure 10.15. The helical antenna possesses in general elliptical polarization, but it can be designed to achieve nearly circular polarization. There are two primary modes of operation for a helix, the normal mode and the axial mode. The helix operates in its normal mode when its overall length is small compared to the wavelength, and it has a pattern with a null along its axis and the maximum along

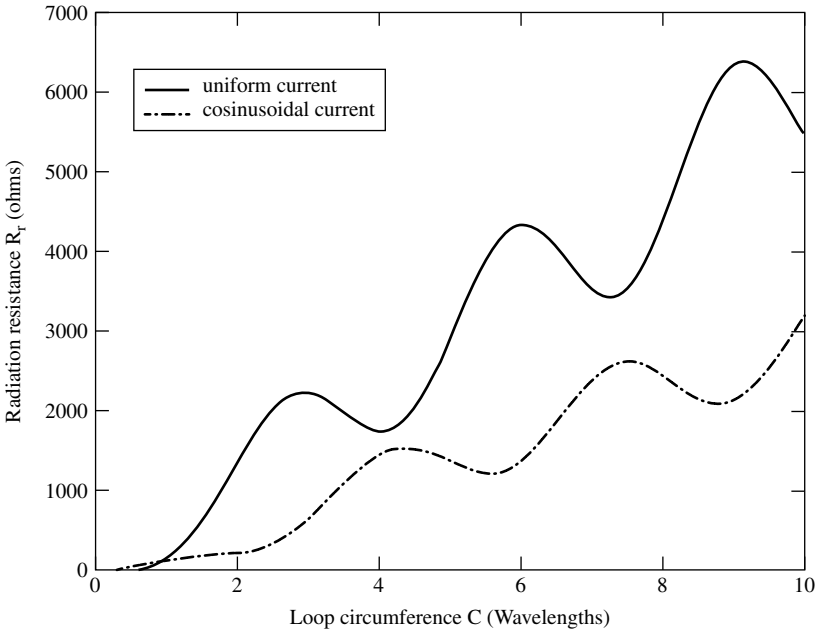

(a) Radiation resistance R_r

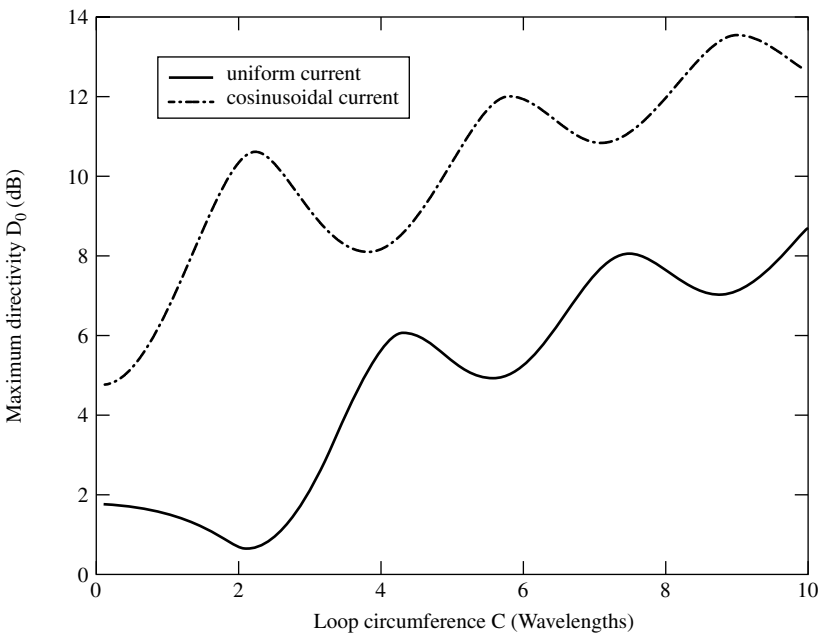

(b) Maximum directivity D_o

Figure 5.14 Radiation resistance (R_r) and maximum directivity (D_0) of a circular loop with constant current distribution. (SOURCE: S. V. Savov, "An Efficient Solution of a Class of Integrals Arising in Antenna Theory," *IEEE Antennas and Propagation Magazine*, Vol. 44, October 2002, pp. 98–101. © 2002 IEEE).

the plane of the loop. This pattern (figure-eight type in the elevation plane) is similar to that of a dipole or a small loop. *A helical antenna operating in the normal mode is sometimes used as a monopole antenna for mobile cell and cordless telephones, and it is usually covered with a plastic cover. This helix monopole is used because its input impedance is larger than that of a regular monopole and more attractive for matching to typical transmission lines used as feed lines, such as a coaxial line* (see Problem 10.18).

The helix operates in the axial mode when the circumference of the loop is between $3/4\lambda < C < 4/3\lambda$ with an optimum design when the circumference is nearly one wavelength. When the circumference of the loop approaches one wavelength, the maximum of the pattern is along its axis. In addition, the phasing among the turns is such that overall the helix forms an end-fire antenna with attractive impedance and polarization characteristics (see Example 10.1). In general, the helix is a popular communication antenna in the VHF and UHF bands.

The Yagi-Uda antenna is primarily an array of linear dipoles with one element serving as the feed while the others act as parasitic. However this arrangement has been extended to include arrays of loop antennas, as shown in Figure 10.30. As for the helical antenna, in order for this array to perform as an end-fire array, the circumference of each of the elements is near one wavelength. More details can be found in Section 10.3.4 and especially in [11]–[14]. A special case is the quad antenna which is very popular amongst ham radio operators. It consists of two square loops, one serving as the excitation while the other is acting as a reflector; there are no directors. The overall perimeter of each loop is one wavelength.

5.4.2 Design Procedure

The design of small loops is based on the equations for the radiation resistance (5-24), (5-24a), directivity (5-31), maximum effective aperture (5-32), resonance capacitance (5-35), resonance input impedance (5-36) and inductance (5-37a), (5-37b). In order to resonate the element, the capacitor C_r of Figure 5.4 is chosen based on (5-35) so as to cancel out the imaginary part of the input impedance Z_{in}.

For large loops with a nonuniform current distribution, the design is accomplished using the curves of Figure 5.12 for the axial directivity and those of Figure 5.13 for the impedance. To resonate the loop, usually a capacitor in parallel or an inductor in series is added, depending on the radius of the loop and that of the wire.

Example 5.4

Design a resonant loop antenna to operate at 100 MHz so that the pattern maximum is along the axis of the loop. Determine the radius of the loop and that of the wire (in meters), the axial directivity (in dB), and the parallel lumped element (capacitor in parallel or inductor in series) that must be used in order to resonate the antenna.

Solution: In order for the pattern maximum to be along the axis of the loop, the circumference of the loop must be large compared to the wavelength. Therefore the current distribution will be nonuniform. To accomplish this, Figure 5.13 should be used. There is not only one unique design which meets the specifications, but there are many designs that can accomplish the goal.

One design is to select a circumference where the loop is self resonant, and there is no need for a resonant capacitor. For example, referring to Figure 5.13(b) and choosing an $\Omega = 12$, the circumference of the loop is nearly 1.125λ. Since the free-space wavelength at 100 MHz is 3 meters, then the circumference is

$$\text{circumference} \simeq 1.125(3) = 3.375 \text{ meters}$$

while the radius of the loop is

$$\text{radius} = a = \frac{3.375}{2\pi} = 0.5371 \text{ meters}$$

The radius of the wire is obtained using

$$\Omega = 12 = 2 \ln\left(\frac{2\pi a}{b}\right)$$

or

$$\frac{a}{b} = 64.2077$$

Therefore the radius of the wire is

$$b = \frac{a}{64.2077} = \frac{0.5371}{64.2077} = 0.8365 \text{ cm} = 8.365 \times 10^{-3} \text{meters}$$

Using Figure 5.12, the axial directivity for this design is approximately 3.6 dB. Using Figure 5.13(a), the input impedance is approximately

$$Z_{in} = Z'_{in} \simeq 840 \text{ ohms}$$

Since the antenna chosen is self resonant, there is no need for a lumped element to resonate the radiator.

Another design will be to use another circumference where the loop is not self resonant. This will necessitate the use of a capacitor C_r to resonate the antenna. This is left as an end of the chapter exercise.

5.5 GROUND AND EARTH CURVATURE EFFECTS FOR CIRCULAR LOOPS

The presence of a lossy medium can drastically alter the performance of a circular loop. The parameters mostly affected are the pattern, directivity, input impedance, and antenna efficiency. The amount of energy dissipated as heat by the lossy medium directly affects the antenna efficiency. As for the linear elements, geometrical optics techniques can be used to analyze the radiation characteristics of loops in the presence of conducting surfaces. The reflections are taken into account by introducing appropriate image (virtual) sources. Divergence factors are introduced to take into account the effects of the ground curvature. Because the techniques are identical to the formulations of Section 4.8, they will not be repeated here. The reader is directed to that section for the details. It should be pointed out, however, that a horizontal loop has horizontal polarization in contrast to the vertical polarization of a vertical electric dipole. Exact boundary-value solutions, based on Sommerfeld integral formulations, are available [25]. However they are too complex to be included in an introductory chapter.

By placing the loop above a reflector, the pattern is made unidirectional and the directivity is increased. To simplify the problem, initially the variations of the axial directivity ($\theta = 0^\circ$) of a circular loop with a circumference of one wavelength ($ka = 1$) when placed horizontally a height h above an infinite in extent perfect electric conductor are examined as a function of the height above the ground plane. These were obtained using image theory and the array factor of two loops, and they are shown for $10 < \Omega < 20$ in Figure 5.15[8], [26]. Since only one curve is shown for $10 < \Omega < 20$, it is evident that the directivity variations as a function of the height are not strongly dependent on the radius of the wire of the loop. It is also apparent that for $0.05\lambda < h < 0.2\lambda$ and $0.65\lambda < h < 0.75\lambda$ the directivity is about 9 dB. For the same size loop, the corresponding variations of the impedance as a function of the height are shown in Figure 5.16[8], [26]. While the directivity variations are not strongly influenced by the radius of the wire, the variations of the impedance do show a dependence on the radius of the wire of the loop for $10 < \Omega < 20$.

A qualitative criterion that can be used to judge the antenna performance is the ratio of the radiation resistance in free-space to that in the presence of the homogeneous lossy medium [27]. This is a straightforward but very tedious approach. A much simpler method [28] is to find directly the self-impedance changes (real and imaginary) that result from the presence of the conducting medium.

Since a small horizontal circular loop is equivalent to a small vertical magnetic dipole (see Section 5.2.2), computations [29] were carried out for a vertical magnetic dipole placed a height h above a homogeneous lossy half-space. The changes in the self-impedance, normalized with respect to the free-space radiation resistance R_0 given by (5-24), are found in [29]. Significant changes, compared to those of a perfect conductor, are introduced by the presence of the ground.

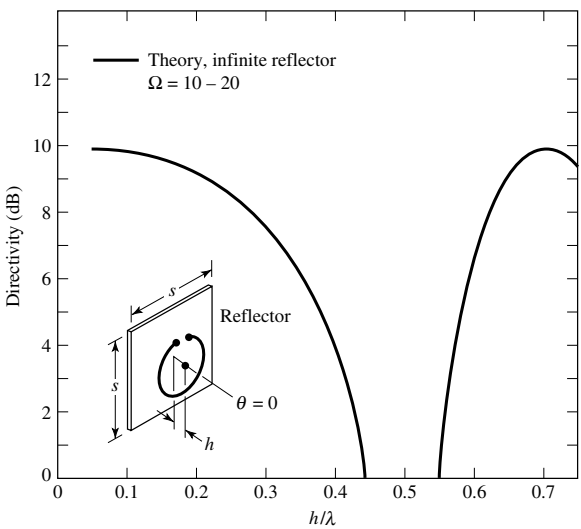

Figure 5.15 Directivity of circular-loop antenna, $C = ka = 1$, for $\theta = 0$ versus distance from reflector h/λ. Theoretical curve is for infinite planar reflector. (SOURCE: G. S. Smith, "Loop Antennas," Chapter 5 of *Antenna Engineering Handbook*, 1984, © 1984 McGraw-Hill, Inc. Permission by McGraw-Hill, Inc).

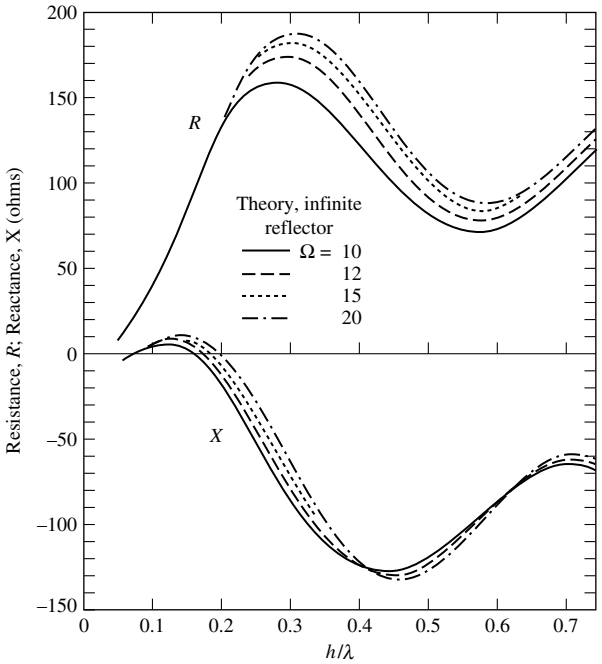

Figure 5.16 Input impedance of circular-loop antenna $C = ka = 1$ versus distance from reflector h/λ. Theoretical curves are for infinite planar reflector; measured points are for square reflector. (SOURCE: G. S. Smith, "Loop Antennas," Chapter 5 of *Antenna Engineering Handbook*, 1984, © 1984, McGraw-Hill, Inc. Permission by McGraw-Hill, Inc).

The effects that a stratified lossy half-space have on the characteristics of a horizontal small circular loop have also been investigated and documented [30]. It was found that when a resonant loop is close to the interface, the changes in the input admittance as a function of the antenna height and the electrical properties of the lossy medium were very pronounced. This suggests that a resonant loop can be used effectively to sense and to determine the electrical properties of an unknown geological structure.

5.6 POLYGONAL LOOP ANTENNAS

The most attractive polygonal loop antennas are the square, rectangular, triangular, and rhombic. These antennas can be used for practical applications such as for aircraft, missiles, and communications systems. However, because of their more complex structure, theoretical analyses seem to be unsuccessful [31]. Thus the application of these antennas has received much less attention. However design curves, computed using the Moment Method, do exist [32] and can be used to design polygonal loop antennas for practical applications. Usually the circular loop has been used in the UHF range because of its higher directivity while triangular and square loops have been applied in the HF and UHF bands because of advantages in their mechanical construction. Broadband impedance characteristics can be obtained from the different polygonal loops.

5.6.1 Square Loop

Next to the circular loop, the square loop is the simplest loop configuration. The far-field pattern for a small loop, in each of its principal planes, can be obtained by assuming that each of its sides is a small linear dipole of constant current I_0 and length a. Referring to Figure 5.17, the field in the y-z plane is given according to (4-26a) by

$$E_\phi = E_{\phi 1} + E_{\phi 2} = -j\eta \frac{kI_0 a}{4\pi}\left[\frac{e^{-jkr_1}}{r_1} - \frac{e^{-jkr_2}}{r_2}\right] \tag{5-68}$$

since the pattern of each element is omnidirectional in that plane. Using the far-field approximations of

$$\left.\begin{aligned} r_1 &\simeq r - \frac{a}{2}\sin\theta \\ r_2 &\simeq r + \frac{a}{2}\sin\theta \end{aligned}\right\} \quad \text{for phase variations} \tag{5-68a}$$

$$r_1 \simeq r_2 \simeq r \qquad \text{for amplitude variations} \tag{5-68b}$$

(5-68) can be written as

$$E_\phi = \eta \frac{kI_0 a e^{-jkr}}{2\pi r}\sin\left(\frac{ka}{2}\sin\theta\right) \tag{5-69}$$

For small values of $a (a < \lambda/50)$, (5-69) reduces to

$$\boxed{E_\phi = \eta \frac{(ka)^2 I_0 e^{-jkr}}{4\pi r}\sin\theta = \eta \frac{\pi S I_0 e^{-jkr}}{\lambda^2 r}\sin\theta} \tag{5-70}$$

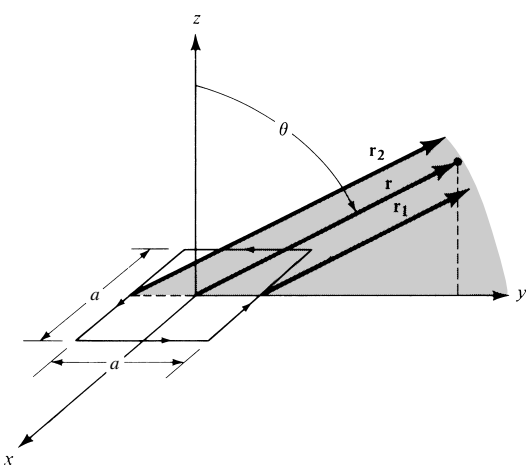

Figure 5.17 Square loop geometry for far-field observations on the y-z plane.

where $S = a^2$ is the geometrical area of the loop. The corresponding magnetic field is given by

$$H_\theta = -\frac{E_\phi}{\eta} = -\frac{\pi S I_0 e^{-jkr}}{\lambda^2 r} \sin\theta \tag{5-71}$$

Equations (5-70) and (5-71) are identical to (5-27b) and (5-27a), respectively, for the small circular loop. Thus the far-zone principal-plane fields of a small square loop are identical to those of a small circular loop. The fields in the other planes are more difficult to obtain, and they will not be attempted here. However design curves are included which can be used for practical design applications.

5.6.2 Triangular, Rectangular, and Rhombic Loops

Shown in Figure 5.18 are the polygonal loops for which design data will be presented. They consist of top- and base-driven triangular loops, a rectangular loop, and a rhombic loop. The top-driven triangular loop has its feed at the top corner of the isosceles triangle while the base-driven configuration has its terminals at the base. The rectangular loop has its feed at the center of one of its sides while the rhombic configuration has its terminals at one of its corners.

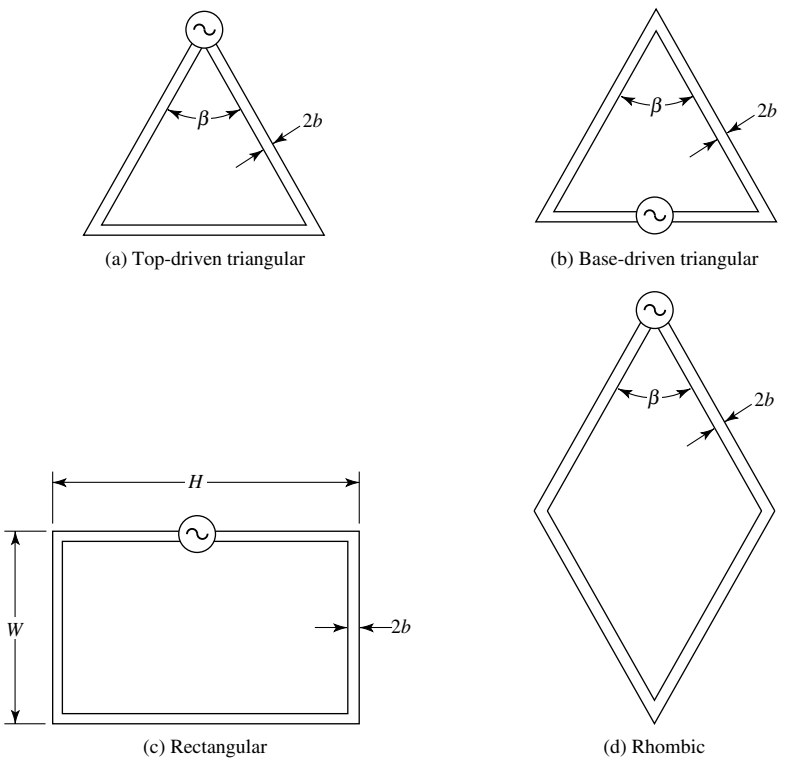

Figure 5.18 Typical configurations of polygonal loop antennas. (SOURCE: T. Tsukiji and S. Tou, "On Polygonal Loop Antennas," *IEEE Trans. Antennas Propagat.*, Vol. AP-28, No. 4, July 1980. © 1980 IEEE).

The parameter β defines the angle of the top corner of the isosceles triangle for the triangular and rhombic loops while $\gamma = W/H$ is used to identify the relative side dimensions of the rectangular loop. The perimeter of each loop is given by P; for the rectangular loop, $P = 2(H + W)$. For all configurations, the radius of the wire is b.

Included in [32] are the input impedance ($Z = R + jX$) variations, as a function of P (in wavelengths), of the four configurations shown in Figure 5.18. The interval between adjacent points on each curve is $\Delta P/\lambda = 0.2$. Depending on the parameters β or γ, the input resistance of polygonal loops near the resonance frequency changes drastically. The reactance goes to zero when a loop approaches a short-circuited $\lambda/2$ long transmission line. In design then, the shape of the loop can be chosen so that the input impedance is equal to the characteristic impedance of the transmission line. Although the curves in [32] are for specific wire radii, the impedance variations of the polygonal antennas as a function of the wire diameter are similar to those of the dipole.

Because the radius of the impedance locus for the $\beta = 60^\circ$ of the top-driven triangular loop [Figure 5.18(a)] is smaller than for the other values of β, the $\beta = 60^\circ$ has the broadest impedance bandwidth compared with other triangular shapes or with the same shape but different feed points. Similar broadband impedance characteristics are indicated in [32] for a rectangular loop with $\gamma = 0.5$ (the side with the feed point is twice as large as the other).

It can then be concluded that if the proper shape and feed point are chosen, a polygonal loop can have broadband impedance characteristics. The most attractive are the top-driven triangular loop with $\beta = 60^\circ$ and the rectangular loop with $\gamma = 0.5$. A 50–70 ohm coaxial cable can be matched with a triangular loop with $\beta = 40^\circ$. Rectangular loops with greater directivities, but with less ideal impedance characteristics, are those with larger values of γ.

The frequency characteristics of a polygonal loop can be estimated by inspecting its current distribution. When the current standing wave pattern has, at its antiresonant frequency, a null at a sharp corner of the loop, the loop has a very low current standing wave and, hence, broadband impedance characteristics.

Radiation patterns for the $\beta = 60^\circ$ top- and base-driven triangular loops and the $\gamma = 4$ rectangular loop, for various values of P (in wavelengths), were also computed [32]. It was noted that for low frequencies near the resonance, the patterns of the top- and base-driven triangular loops were not too different. However, for higher frequencies the base-driven triangular loop had a greater gain than its corresponding top-driven configuration. In general, rectangular loops with larger γ's have greater gains.

5.7 FERRITE LOOP

Because the loss resistance is comparable to the radiation resistance, electrically small loops are very poor radiators and are seldom used in the transmitting mode. However, they are often used for receiving signals, such as in radios and pagers, where the signal-to-noise ratio is much more important than the efficiency.

5.7.1 Radiation Resistance

The radiation resistance, and in turn the antenna efficiency, can be raised by increasing the circumference of the loop. Another way to increase the radiation resistance, without increasing the electrical dimensions of the antenna, would be to insert within

its circumference a ferrite core that has a tendency to increase the magnetic flux, the magnetic field, the open-circuit voltage, and in turn the radiation resistance of the loop [33], [34]. This is the so-called *ferrite loop* and the ferrite material can be a rod of very few inches in length. The radiation resistance of the ferrite loop is given by

$$\frac{R_f}{R_r} = \left(\frac{\mu_{ce}}{\mu_0}\right)^2 = \mu_{cer}^2 \tag{5-72}$$

where

R_f = radiation resistance of ferrite loop
R_r = radiation resistance of air core loop
μ_{ce} = effective permeability of ferrite core
μ_0 = permeability of free-space
μ_{cer} = relative effective permeability of ferrite core

Using (5-24), the radiation resistance of (5-72) for a single-turn small ferrite loop can be written as

$$\boxed{R_f = 20\pi^2 \left(\frac{C}{\lambda}\right)^4 \left(\frac{\mu_{ce}}{\mu_0}\right)^2 = 20\pi^2 \left(\frac{C}{\lambda}\right)^4 \mu_{cer}^2} \tag{5-73}$$

and for an N-turn loop, using (5-24a), as

$$\boxed{R_f = 20\pi^2 \left(\frac{C}{\lambda}\right)^4 \left(\frac{\mu_{ce}}{\mu_0}\right)^2 N^2 = 20\pi^2 \left(\frac{C}{\lambda}\right)^4 \mu_{cer}^2 N^2} \tag{5-74}$$

The relative effective permeability of the ferrite core μ_{cer} is related to the relative intrinsic permeability of the unbounded ferrite material $\mu_{fr}(\mu_{fr} = \mu_f/\mu_0)$ by

$$\mu_{cer} = \frac{\mu_{ce}}{\mu_0} = \frac{\mu_{fr}}{1 + D(\mu_{fr} - 1)} \tag{5-75}$$

where D is the demagnetization factor which has been found experimentally for different core geometries, as shown in Figure 5.19. For most ferrite material, the relative intrinsic permeability μ_{fr} is very large ($\mu_{fr} \gg 1$) so that the relative effective permeability of the ferrite core μ_{cer} is approximately inversely proportional to the demagnetization factor, or $\mu_{cer} \sim 1/D = D^{-1}$. In general, the demagnetization factor is a function of the geometry of the ferrite core. For example, the demagnetization factor for a sphere is $D = \frac{1}{3}$ while that for an ellipsoid of length $2l$ and radius a, such that $l \gg a$, is

$$D = \left(\frac{a}{l}\right)^2 \left[\ln\left(\frac{2l}{a}\right) - 1\right], \qquad l \gg a \tag{5-75a}$$

5.7.2 Ferrite-Loaded Receiving Loop

Because of their smallness, ferrite loop antennas of few turns wound around a small ferrite rod are used as antennas especially in pocket transistor radios. The antenna is

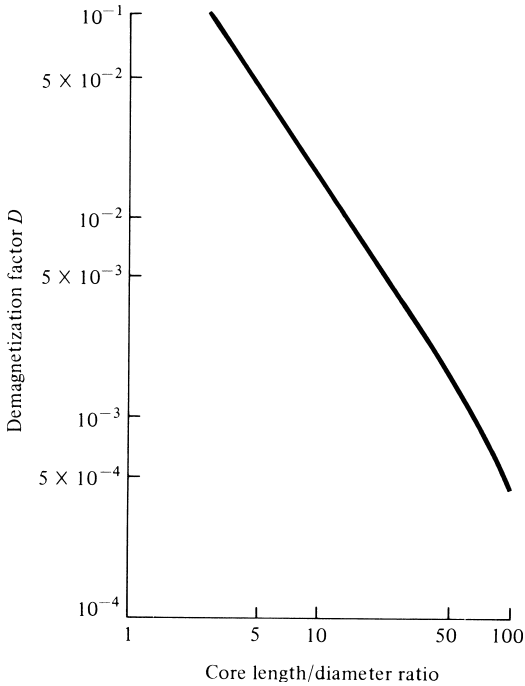

Figure 5.19 Demagnetization factor as a function of core length/diameter ratio. (SOURCE: E. A. Wolff, *Antenna Analysis*, Wiley, New York, 1966).

usually connected in parallel with the RF amplifier tuning capacitance and, in addition to acting as an antenna, it furnishes the necessary inductance to form a tuned circuit. Because the inductance is obtained with only few turns, the loss resistance is kept small. Thus the Q is usually very high, and it results in high selectivity and greater induced voltage.

The equivalent circuit for a ferrite-loaded loop antenna is similar to that of Figure 5.4 except that a loss resistance R_M, in addition to R_L, is needed to account for the power losses in the ferrite core. Expressions for the loss resistance R_M and inductance L_A for the ferrite-loaded loop of N turns can be found in [7] and depend on some empirical factors which are determined from an average of experimental results. The inductance L_i is the same as that of the unloaded loop.

5.8 MOBILE COMMUNICATION SYSTEMS APPLICATIONS

As was indicated in Section 4.7.4 of Chapter 4, the monopole is one of the most widely used elements for handheld units of mobile communication systems. An alternative to the monopole is the loop, [35]–[40], which has been often used in pagers but has found very few applications in handheld transceivers. This is probably due to loop's high resistance and inductive reactance which are more difficult to match to standard feed lines. The fact that loop antennas are more immune to noise makes them more

attractive for an interfering and fading environment, like that of mobile communication systems. In addition, loop antennas become more viable candidates for wireless communication systems which utilize devices operating at higher frequency bands, particularly in designs where balanced amplifiers must interface with the antenna. Relative to top side of the handheld unit, such as the telephone, the loop can be placed either horizontally [36] or vertically [38]–[40]. Either configuration presents attractive radiation characteristics for land-based mobile systems.

The radiation characteristics, normalized pattern and input impedance, of a monopole and vertical loop mounted on an experimental mobile handheld device were examined in [38]–[40]. The loop was in the form of a folded configuration mounted vertically on the handheld conducting device with its one end either grounded or ungrounded to the device. The predicted and measured input impedance of the folded loop, when its terminating end was grounded to the box, are displayed in Figure 5.20(a,b). It is evident that the first resonance, around 900 MHz, of the folded loop is of the *parallel type* (*antiresonance*) with a very high, and rapidly changing versus frequency, resistance, and reactance. These values and variations of impedance are usually undesirable for practical implementation. For frequencies below the first resonance, the impedance is inductive (imaginary part is positive), as is typical of small loop antennas (see Figure 5.13); above the first resonance, the impedance is capacitive (negative imaginary part). The second resonance, around 2,100 MHz, is of the *series type* with slowly varying values of impedance, and of desirable magnitude, for practical implementation. The resonance forms (*parallel* vs. *series*) can be interchanged if the terminating end of the folded loop is ungrounded with the element then operating as an L monopole [38]–[40] and exhibiting the same resonance behavior as that of a monopole mounted on the device (see Chapter 4, Section 4.7.4, Figure 4.21). Even though the radiating element is a loop whose plane is vertical to the box, the amplitude pattern, in both cases (loop and L), is similar and nearly omnidirectional as that of the monopole of Figure 4.21 because the PEC box is also part of the radiating system.

A summary of the pertinent parameters and associated formulas and equation numbers for this chapter are listed in Table 5.1.

5.9 MULTIMEDIA

In the CD that is part of the book, the following multimedia resources are included for the review, understanding, and visualization of the material of this chapter:

a. **Java**-based **interactive questionnaire**, with answers.
b. **Java**-based **applet** for computing and displaying the radiation characteristics of a loop.
c. **Java**-based animation of loop amplitude pattern.
d. **Matlab** and **Fortran** computer program, designated ***Loop***, for computing the radiation characteristics of a loop. A description of the program is found in the READ ME file of the corresponding program in the attached CD.
e. **Power Point (PPT)** viewgraphs, in multicolor.

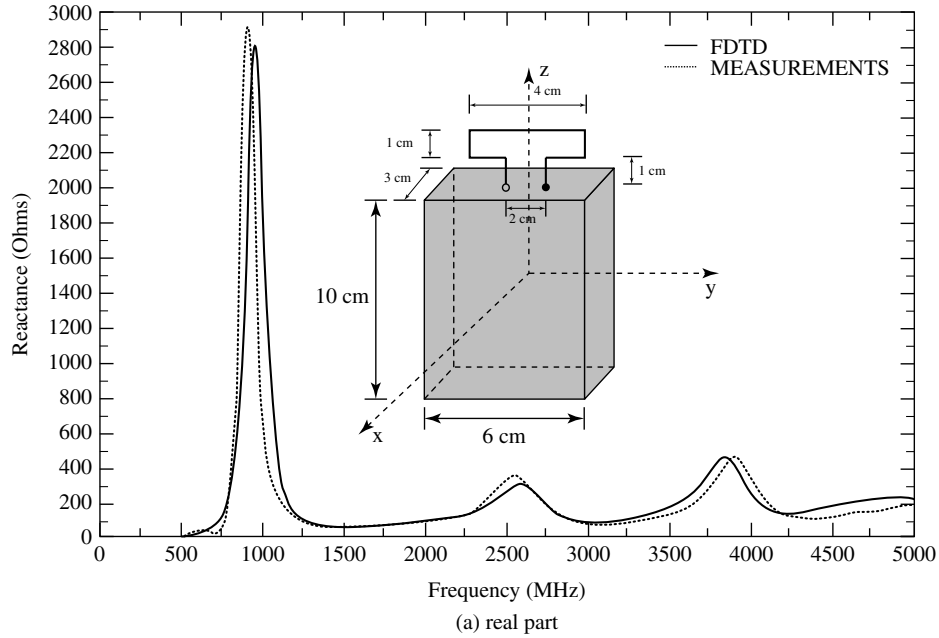

(a) real part

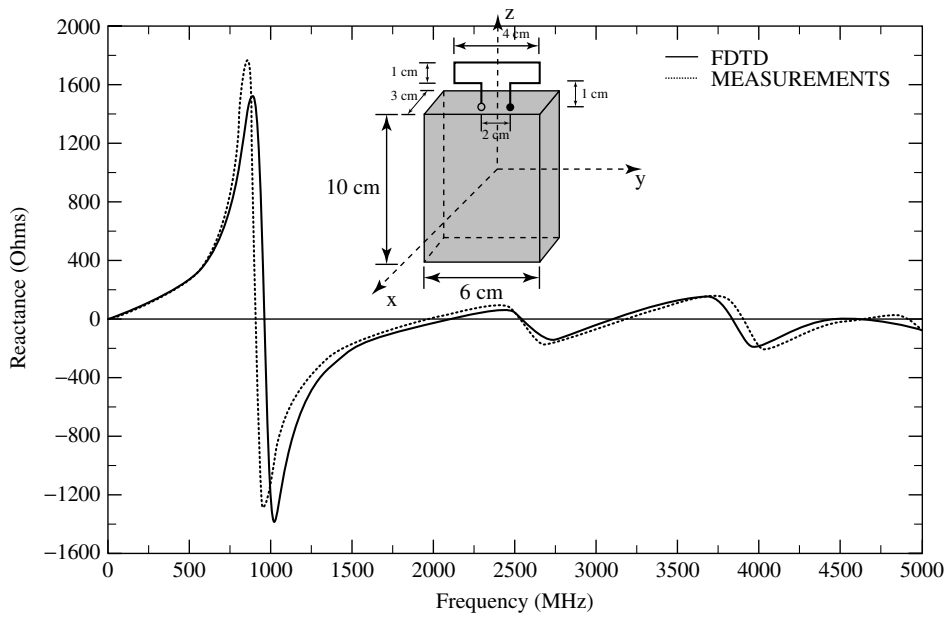

(b) imaginary part

Figure 5.20 Input impedance, real and imaginary parts of a wire folded loop mounted vertically on a conducting mobile hand-held unit (SOURCE: K. D. Katsibas, et. al., "Folded Loop Antenna for Mobile Hand-Held Units," *IEEE Transactions Antennas Propagat.*, Vol. 46, No. 2, February 1998, pp. 260–266. © 1998 IEEE).

TABLE 5.1 Summary of Important Parameters, and Associated Formulas and Equation Numbers for Loop in Far Field

Parameter	Formula	Equation Number
	Small Circular Loop $(a < \lambda/6\pi, C < \lambda/3)$ **(Uniform Current)**	
Normalized power pattern	$U = \lvert E_{\phi n}\rvert^2 = C_0 \sin^2\theta$	(5-27b)
Wave impedance Z_w	$Z_w = -\dfrac{E_\phi}{H_\theta} \simeq \eta = 377 \ \text{Ohms}$	(5-28)
Directivity D_0	$D_0 = \dfrac{3}{2} = 1.761 \ \text{dB}$	(5-31)
Maximum effective area A_{em}	$A_{em} = \dfrac{3\lambda^2}{8\pi}$	(5-32)
Radiation resistance R_r (one turn)	$R_r = 20\pi^2 \left(\dfrac{C}{\lambda}\right)^4$	(5-24)
Radiation resistance R_r (N turns)	$R_r = 20\pi^2 \left(\dfrac{C}{\lambda}\right)^4 N^2$	(5-24a)
Input resistance R_{in}	$R_{in} = R_r = 20\pi^2 \left(\dfrac{C}{\lambda}\right)^4$	(5-24)
Loss resistance R_L (one turn)	$R_L = \dfrac{l}{P}\sqrt{\dfrac{\omega\mu_0}{2\sigma}} = \dfrac{C}{2\pi b}\sqrt{\dfrac{\omega\mu_0}{2\sigma}}$	(2-90b)
Loss resistance R_L (N turns)	$R_L = \dfrac{Na}{b} R_s \left(\dfrac{R_p}{R_0} + 1\right)$	(5-25)
Loop external inductance L_A	$L_A = \mu_0 a \left[\ln\left(\dfrac{8a}{b}\right) - 2\right]$	(5-37a)
Loop internal inductance L_i	$L_i = \dfrac{a}{\omega b}\sqrt{\dfrac{\omega\mu_0}{2\sigma}}$	(5-38)
Vector effective length $\boldsymbol{\ell}_e$	$\boldsymbol{\ell}_e = \hat{\mathbf{a}}_\phi \, j k_0 \pi a^2 \cos\psi_i \sin\theta_i$	(5-40)
Half-power beamwidth	$\text{HPBW} = 90^\circ$	(4-65)

(*continued overleaf*)

TABLE 5.1 (*continued*)

Parameter	Formula	Equation Number
	Large Circular Loop $(a \geq \lambda/2, C \geq 3.14\lambda)$ **(Uniform Current)**	
Normalized power pattern	$U = \lvert E_{\phi n}\rvert^2 = C_1 J_1^2(ka \sin\theta)$	(5-57)
Wave impedance Z_w	$Z_w = -\dfrac{E_\phi}{H_\theta} \simeq \eta = 377 \ \text{Ohms}$	(5-28)
Directivity D_0 $(a > \lambda/2)$	$D_0 = 0.677\left(\dfrac{C}{\lambda}\right)$	(5-63b)
Maximum effective area A_{em} $(a > \lambda/2)$	$A_{em} = \dfrac{\lambda^2}{4\pi}\left[0.677\left(\dfrac{C}{\lambda}\right)\right]$	(5-63c)
Radiation resistance $(a > \lambda/2)$, (one turn)	$R_r = 60\pi^2\left(\dfrac{C}{\lambda}\right)$	(5-63a)
Input resistance $(a > \lambda/2)$, (one turn)	$R_{in} = R_r = 60\pi^2\left(\dfrac{C}{\lambda}\right)$	(5-63a)
Loss resistance R_L (one turn)	$R_L = \dfrac{l}{P}\sqrt{\dfrac{\omega\mu_0}{2\sigma}} = \dfrac{C}{2\pi b}\sqrt{\dfrac{\omega\mu_0}{2\sigma}}$	(2-90b)
Loss resistance R_L (N turns)	$R_L = \dfrac{Na}{b}R_s\left(\dfrac{R_p}{R_0} + 1\right)$	(5-25)
External inductance L_A	$L_A = \mu_0 a\left[\ln\left(\dfrac{8a}{b}\right) - 2\right]$	(5-37a)
Internal inductance L_i	$L_i = \dfrac{a}{\omega b}\sqrt{\dfrac{\omega\mu_0}{2\sigma}}$	(5-38)
Vector effective length $\boldsymbol{\ell}_e$	$\boldsymbol{\ell}_e = \hat{\mathbf{a}}_\phi\, jk_0\pi a^2 \cos\psi_i \sin\theta_i$	(5-40)
	Small Square Loop **(Figure 5.17)** **(Uniform Current, a on Each Side**	
Normalized power pattern (principal plane)	$U = \lvert E_{\phi n}\rvert^2 = C_2 \sin^2\theta$	(5-70)

TABLE 5.1 (*continued*)

Parameter	Formula	Equation Number
Wave impedance Z_w	$Z_w = -\dfrac{E_\phi}{H_\theta} \simeq \eta = 377 \ \text{Ohms}$	(5-28)
Radiation resistance R_r	$R_r = 20\left(\dfrac{2\pi a}{\lambda}\right)^4 = 20\left(\dfrac{C}{\lambda}\right)^4$	
Input resistance R_{in}	$R_{in} = R_r = 20\left(\dfrac{4a}{\lambda}\right)^4 = 20\left(\dfrac{P}{\lambda}\right)^4$	
Loss resistance R_L	$R_L = \dfrac{4a}{P}\sqrt{\dfrac{\omega\mu_0}{2\sigma}} = \dfrac{4a}{2\pi b}\sqrt{\dfrac{\omega\mu_0}{2\sigma}}$	(2-90b)
External inductance L_A	$L_A = 2\mu_0\dfrac{a}{\pi}\left[\ln\left(\dfrac{a}{b}\right) - 0.774\right]$	(5-37b)
Internal inductance L_i	$L_i = \dfrac{4a}{\omega P}\sqrt{\dfrac{\omega\mu_0}{2\sigma}} = \dfrac{4a}{2\pi b\omega}\sqrt{\dfrac{\omega\mu_0}{2\sigma}}$	(5-38)
	Ferrite Circular Loop $(a < \lambda/6\pi, C < \lambda/3)$ **(uniform current)**	
Radiation resistance R_f (one turn)	$R_f = 20\pi^2\left(\dfrac{C}{\lambda}\right)^4 \mu_{cer}^2$ $\mu_{cer} = \dfrac{\mu_{fr}}{1 + D(\mu_{fr} - 1)}$	(5-73) (5-75)
Radiation resistance R_f (N turns)	$R_f = 20\pi^2\left(\dfrac{C}{\lambda}\right)^4 \mu_{cer}^2 N^2$	(5-74)
Demagnetizing factor D	Ellipsoid: $D = \left(\dfrac{a}{l}\right)^2\left[\ln\left(\dfrac{2l}{a}\right) - 1\right]$ $l \gg a$ Sphere: $D = \dfrac{1}{3}$	(5-75a)

REFERENCES

1. P. L. Overfelt, "Near Fields of the Constant Current Thin Circular Loop Antenna of Arbitrary Radius," *IEEE Trans. Antennas Propagat.*, Vol. 44, No. 2, February 1996, pp. 166–171.
2. D. H. Werner, "An Exact Integration Procedure for Vector Potentials of Thin Circular Loop Antennas," *IEEE Trans. Antennas Propagat.*, Vol. 44, No. 2, February 1996, pp. 157–165.
3. D. H. Werner, "Lommel Expansions in Electromagnetics," Chapter in *Frontiers in Electromagnetics*, (D. H. Werner and R. Mittra, eds.), IEEE Press/John Wiley, New York, 2000.

4. E. H. Newman, P. Bohley, and C. H. Walter, "Two Methods for Measurement of Antenna Efficiency," *IEEE Trans. Antennas Propagat.*, Vol. AP-23, No. 4, July 1975, pp. 457–461.
5. G. S. Smith, "Radiation Efficiency of Electrically Small Multiturn Loop Antennas," *IEEE Trans. Antennas Propagat.*, Vol. AP-20, No. 5, September 1972, pp. 656–657.
6. G. S. Smith, "The Proximity Effect in Systems of Parallel Conductors," *J. Appl. Phys.*, Vol. 43, No. 5, May 1972, pp. 2196–2203.
7. J. D. Kraus, *Electromagnetics*, 4th ed., McGraw-Hill Book Co., New York, 1992.
8. G. S. Smith, "Loop Antennas," Chapter 5 in *Antenna Engineering Handbook*, 2nd ed., McGraw-Hill Book Co., New York, 1984.
9. J. E. Storer, "Impedance of Thin-Wire Loop Antennas," *AIEE Trans., (Part I. Communication and Electronics)*, Vol. 75, Nov. 1956, pp. 606–619.
10. S. Adachi and Y. Mushiake, "Studies of Large Circular Loop Antenna," *Sci. Rep. Research Institute of Tohoku University (RITU), B*, Vol. 9, No. 2, 1957, pp. 79–103.
11. S. Ito, N. Inagaki, and T. Sekiguchi, "An Investigation of the Array of Circular-Loop Antennas," *IEEE Trans. Antennas Propagat.*, Vol. AP-19, No. 4, July 1971, pp. 469–476.
12. A. Shoamanesh and L. Shafai, "Properties of Coaxial Yagi Loop Arrays," *IEEE Trans. Antennas Propagat.*, Vol. AP-26, No. 4, July 1978, pp. 547–550.
13. A. Shoamanesh and L. Shafai, "Design Data for Coaxial Yagi Array of Circular Loops," *IEEE Trans. Antennas Propagat.*, Vol. AP-27, September 1979, pp. 711–713.
14. D. DeMaw (ed.), *The Radio Amateur's Handbook*, American Radio Relay League, 56th ed., 1979, pp. 20–18.
15. G. N. Watson, *A Treatise on the Theory of Bessel Functions*, Cambridge University Press, London, 1922.
16. S. V. Savov, "An Efficient Solution of a Class of Integrals Arising in Antenna Theory," *IEEE Antennas Propagat. Mag.*, Vol. 44, No. 5, October 2002, pp. 98–101.
17. J. D. Mahony, "Circular Microstrip-Patch Directivity Revisited: An Easily Computable Exact Expression," *IEEE Antennas Propagat. Mag.*, Vol. 45, No. 1, February 2003, pp. 120–122.
18. J. D. Mahony, "A Comment on Q-Type Integrals and Their Use in Expressions for Radiated Power," *IEEE Antennas Propagat. Mag.*, Vol. 45, No. 3, June 2003, pp. 127–138.
19. S. V. Savov, "A Comment on the Radiation Resistance," *IEEE Antennas Propagat. Mag.*, Vol. 45, No. 3, June 2003, p. 129.
20. I. Gradshteyn and I. Ryzhik, *Tables of Integrals, Series and Products*, Academic Press, New York, 1965.
21. J. E. Lindsay, Jr., "A Circular Loop Antenna with Non-Uniform Current Distribution," *IRE Trans. Antennas Propagat.*, Vol. AP-8, No. 4, July 1960, pp. 438–441.
22. E. A. Wolff, *Antenna Analysis*, Wiley, New York, 1966.
23. H. C. Pocklington, "Electrical Oscillations in Wire," Cambridge Philosophical Society Proceedings, London, England, Vol. 9, 1897, p. 324.
24. R. King, "Theory of Antennas Driven from Two-Wire Line," *J. Appl. Phys.*, Vol. 20, 1949, p. 832.
25. D. G. Fink (ed.), *Electronics Engineers' Handbook*, Section 18, "Antennas" (by W. F. Croswell), McGraw-Hill, New York, pp. 18–22.
26. K. Iizuka, R. W. P. King, and C. W. Harrison, Jr., "Self- and Mutual Admittances of Two Identical Circular Loop Antennas in a Conducting Medium and in Air," *IEEE Trans. Antennas Propagat.*, Vol. AP-14, No. 4, July 1966, pp. 440–450.
27. R. E. Collin and F. J. Zucher (eds.), *Antenna Theory Part 2*, Chapter 23 (by J. R. Wait), McGraw-Hill, New York, 1969.

28. J. R. Wait, "Possible Influence of the Ionosphere on the Impedance of a Ground-Based Antenna," *J. Res. Natl. Bur. Std.* (U.S.), Vol. 66D, September–October 1962, pp. 563–569.
29. L. E. Vogler and J. L. Noble, "Curves of Input Impedance Change Due to Ground for Dipole Antennas," U.S. National Bureau of Standards, Monograph 72, January 31, 1964.
30. D. C. Chang, "Characteristics of a Horizontal Circular Loop Antenna over a Multilayered, Dissipative Half-Space," *IEEE Trans. Antennas Propagat.*, Vol. AP-21, No. 6, November 1973, pp. 871–874.
31. R. W. P. King, "Theory of the Center-Driven Square Loop Antenna," *IRE Trans. Antennas Propagat.*, Vol. AP-4, No. 4, July 1956, p. 393.
32. T. Tsukiji and S. Tou, "On Polygonal Loop Antennas," *IEEE Trans. Antennas Propagat.*, Vol. AP-28, No. 4, July 1980, pp. 571–575.
33. M. A. Islam, "A Theoretical Treatment of Low-Frequency Loop Antennas with Permeable Cores," *IEEE Trans. Antennas Propagat.*, Vol. AP-11, No. 2, March 1963, pp. 162–169.
34. V. H. Rumsey and W. L. Weeks, "Electrically Small Ferrite Loaded Loop Antennas," *IRE Convention Rec.*, Vol. 4, Part 1, 1956, pp. 165–170.
35. K. Fujimoto and J. R. James, *Mobile Antenna Systems Handbook*, Artech House, Norwood, MA, 1994.
36. M. A. Jensen and Y. Rahmat-Samii, "Performance Analysis of Antennas for Hand-Held Transceivers Using FDTD," *IEEE Trans. Antennas Propagat.*, Vol. 42, No. 8, August 1994, pp. 1106–1113.
37. M. A. Jensen and Y. Rahmat-Samii, "EM Interaction of Handset Antennas and a Human in Personal Communications," *Proc. IEEE*, Vol. 83, No. 1, January 1995, pp. 7–17.
38. K. D. Katsibas, C. A. Balanis, P. A. Tirkas, and C. R. Birtcher, "Folded Loop Antenna for Mobile Communication Systems," 1996 IEEE Antennas and Propagation Society International Symposium, Baltimore, MD, July 21–26, 1996, pp. 1582–1585.
39. C. A. Balanis, K. D. Katsibas, P. A. Tirkas, and C. R. Birtcher, "Loop Antenna for Mobile and Personal Communication Systems," IEEE International Vehicular Technology Conference (IEEE VTC '97), Phoenix, AZ, May 5–7, 1997.
40. K. D. Katsibas, C. A. Balanis, P. A. Tirkas, and C. R. Birtcher, "Folded Loop Antenna for Mobile Handheld Units," *IEEE Trans. Antennas Propagat.*, Vol. 46, No. 2, February 1998, pp. 260–266.

PROBLEMS

5.1. Derive

(a) (5-18a)–(5-18c) using (5-17) and (3-2a)

(b) (5-19a)–(5-19b) using (5-18a)–(5-18c)

5.2. Write the fields of an infinitesimal linear magnetic dipole of constant current I_m, length l, and positioned along the z-axis. Use the fields of an infinitesimal electric dipole, (4-8a)–(4-10c), and apply the principle of duality. Compare with (5-20a)–(5-20d).

5.3. A circular loop, *of loop radius* $\lambda/30$ *and wire radius* $\lambda/1000$, is used as a transmitting/receiving antenna in a back-pack radio communication system at *10 MHz*. The wire of the loop is made of copper with a conductivity of 5.7×10^7 S/m. Assuming the antenna is *radiating in free space*, determine the

(a) radiation resistance of the loop;

(b) loss resistance of the loop (*assume that its value is the same as if the wire were straight*);
(c) input resistance;
(d) input impedance;
(e) radiation efficiency.

5.4. A small circular loop with a uniform current distribution, and with its classical omnidirectional pattern, is used as a receiving antenna. Determine the maximum directivity (*dimensionless* and *in dB*) using:
(a) Exact method.
(b) An approximate method appropriate for this pattern. Specify the method used.
(c) Another approximate method appropriate for this pattern. Specify the method used.

Hint: *For the approximate methods, the word omnidirectional is a clue.*

5.5. A *N-turn* resonant circular loop *with a uniform current distribution* and with a *circumference of* $\lambda/4$, is fed by a lossless balanced twin-lead transmission line with a characteristic impedance of 300 ohms. *Neglecting proximity effects*, determine the
(a) *closest integer number* of turns so that the input impedance is nearly 300 ohms;
(b) input impedance of the antenna;
(c) reflection coefficient;
(d) VSWR inside the transmission line.

5.6. A small circular loop with circumference $C < \lambda/20$ is used as a receiving antenna. A uniform plane wave traveling along the x-axis and toward the positive (+) x direction (as shown in the figure), whose electric field is given by

$$\mathbf{E}_w^i = (\hat{\mathbf{a}}_y + \mathbf{2}\hat{\mathbf{a}}_z)e^{-jkx}$$

is incident upon the antenna. Determine the

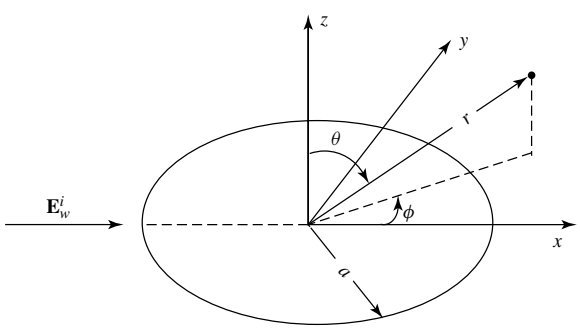

(a) polarization of the incident wave. Justify your answer.
(b) axial ratio of the polarization ellipse of the incident wave.
(c) polarization of the loop antenna toward the x-axis.

(d) polarization loss factor (*dimensionless* and *in dB*).

(e) maximum power at *1 GHz* that can be delivered to a load connected to the antenna, if the power density of the above incident wave is *5 mwatts/cm²*. Assume no other losses.

Hint: $\hat{\mathbf{a}}_\phi = -\hat{\mathbf{a}}_x \sin\phi + \hat{\mathbf{a}}_y \cos\phi$

5.7. Find the radiation efficiency of a single-turn and a four-turn circular loop each of radius $\lambda/(10\pi)$ and operating at 10 MHz. The radius of the wire is $10^{-3}\lambda$ and the turns are spaced $3 \times 10^{-3}\lambda$ apart. Assume the wire is copper with a conductivity of 5.7×10^7 S/m, and the antenna is radiating into free-space.

5.8. Find the power radiated by a small loop by forming the average power density, using (5-27a)–(5-27c), and integrating over a sphere of radius r. Compare the answer with (5-23b).

5.9. For a small loop of constant current, derive its far-zone fields using (5-17) and the procedure outlined and relationships developed in Section 3.6. Compare the answers with (5-27a)–(5-27c).

5.10. A single-turn resonant circular loop with a $\lambda/8\pi$ radius is made of copper wire with a wire radius of $10^{-4}\lambda/2\pi$ and conductivity of 5.7×10^7 S/m. For a frequency of 100 MHz, determine, *assuming uniform current*, the

(a) radiation efficiency (assume the wire is straight);

(b) *maximum gain* of the antenna (*dimensionless* and *in dB*).

5.11. Design a lossless resonant circular loop operating at 10 MHz so that its single-turn radiation resistance is 0.73 ohms. The resonant loop is to be connected to a matched load through a balanced "twin-lead" 300-ohm transmission line.

(a) Determine the radius of the loop (in meters and wavelengths).

(b) To minimize the matching reflections between the resonant loop and the 300-ohm transmission line, determine the closest number of integer turns the loop must have.

(c) For the loop of part b, determine the maximum power that can be expected to be delivered to a receiver matched load if the incident wave is polarization matched to the lossless resonant loop. The power density of the incident wave is 10^{-6}watts/m^2.

5.12. A resonant six-turn loop of *closely spaced turns* is operating at 50 MHz. The radius of the loop is $\lambda/30$, and the loop is connected to a 50-ohm transmission line. The radius of the wire is $\lambda/300$, its conductivity is $\sigma = 5.7 \times 10^7$ S/m, and the spacing between the turns is $\lambda/100$. Determine the

(a) directivity of the antenna (in dB)

(b) radiation efficiency taking into account the proximity effects of the turns

(c) reflection efficiency

(d) gain of the antenna (in dB)

5.13. Find the radiation efficiency (in percent) of an eight-turn circular-loop antenna operating at 30 MHz. The radius of each turn is $a = 15$ cm, the radius of the wire is $b = 1$ mm, and the spacing between turns is $2c = 3.6$ mm. Assume

the wire is copper ($\sigma = 5.7 \times 10^7$ S/m), and the antenna is radiating into free-space. Account for the *proximity effect*.

5.14. A very small circular loop of radius $a (a < \lambda/6\pi)$ and constant current I_0 is symmetrically placed about the origin at $x = 0$ and with the plane of its area parallel to the y-z plane. Find the

(a) spherical **E**- and **H**-field components radiated by the loop in the far zone

(b) directivity of the antenna

5.15. Repeat Problem 5.14 when the plane of the loop is parallel to the x-z plane at $y = 0$.

5.16. Using the computer program of this chapter, compute the radiation resistance and the directivity of a circular loop of constant current with a radius of

(a) $a = \lambda/50$ (b) $a = \lambda/10$ (c) $a = \lambda/4$ (d) $a = \lambda/2$

5.17. A constant current circular loop of radius $a = 5\lambda/4$ is placed on the x-y plane. Find the *two* smallest angles (excluding $\theta = 0^\circ$) where a null is formed in the far-field pattern.

5.18. Design a circular loop of constant current such that its field intensity vanishes only at $\theta = 0^\circ (\theta = 180^\circ)$ and 90°. Find its

(a) radius

(b) radiation resistance

(c) directivity

5.19. Design a constant current circular loop so that its first minimum, aside from $\theta = 0^\circ$, in its far-field pattern is at 30° from a normal to the plane of the loop. Find the

(a) smallest radius of the antenna (in wavelengths)

(b) relative (to the maximum) radiation intensity (in dB) in the plane of the loop

5.20. Design a constant current circular loop so that its pattern has a null in the plane of the loop, and two nulls above and two nulls below the plane of the loop. Find the

(a) radius of the loop

(b) angles where the nulls occur

5.21. A constant current circular loop is placed on the x-y plane. Find the far-field position, relative to that of the loop, that a linearly polarized probe antenna must have so that the polarization loss factor (PLF) is maximized.

5.22. A very small $(a \ll \lambda)$ circular loop of constant current is placed a distance h above an infinite electric ground plane. Assuming z is perpendicular to the ground plane, find the total far-zone field radiated by the loop when its plane is parallel to the

(a) x-z plane

(b) y-z plane

5.23. A very small loop antenna $(a \ll \lambda/30)$ of constant current is placed a height h above a flat, perfectly conducting ground plane of infinite extent. The area plane of the loop is parallel to the interface (x-y plane). For far-field observations

(a) find the total electric field radiated by the loop in the presence of the ground plane

(b) all the angles (in degrees) from the vertical to the interface where the total field will vanish when the height is λ

(c) the smallest nonzero height (in λ) such that the total far-zone field exhibits a null at an angle of 60° from the vertical

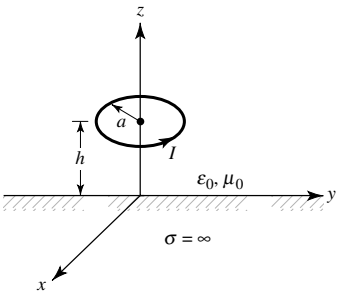

5.24. A small circular loop, with its area parallel to the x-z plane, is placed a height h above an infinite flat perfectly electric conducting ground plane. Determine

(a) the array factor for the equivalent problem which allows you to find the total field on and above the ground plane

(b) angle(s) θ (in degrees) where the array factor will vanish when the loop is placed at a height $\lambda/2$ above the ground plane

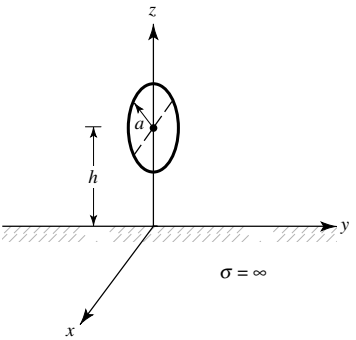

5.25. A small circular loop with its area parallel to the x-z plane is placed at a height h above an infinite perfectly conducting ground plane, as shown in the figure for Problem 5.24. Determine the

(a) array factor for the equivalent problem which will allow you to find the total field *on and above* the ground plane.

(b) two *smallest* heights h (*in* λ) *greater than* $h = 0$ (i.e., $h > 0$) that will form a maximum on the magnitude of the array factor toward $\theta = 0^\circ$.

5.26. For the loop of Problem 5.22(a), find the smallest height h so that a null is formed in the y-z plane at an angle of 45° above the ground plane.

5.27. A small single-turn circular loop of radius $a = 0.05\lambda$ is operating at 300 MHz. Assuming the radius of the wire is $10^{-4}\lambda$, determine the

(a) loss resistance

(b) radiation resistance

(c) loop inductance

Show that the loop inductive reactance is much greater than the loss resistance and radiation resistance indicating that a small loop acts primarily as an inductor.

5.28. Determine the radiation resistance of a single-turn small loop, assuming the geometrical shape of the loop is

(a) rectangular with dimensions a and b ($a, b \ll \lambda$)

(b) elliptical with major axis a and minor axis b ($a, b, \ll \lambda$)

5.29. A one-turn small circular loop is used as a radiating element for a VHF ($f =$ 100 MHz) communications system. The loop is constructed out of a perfect electric conducting wire. The circumference of the loop is $C = \lambda/20$ while the radius of the wire is $\lambda/400$. Determine, using $\sigma = 5.7 \times 10^7$ S/m, the

(a) input resistance of the wire for a single turn.

(b) input reactance of the loop. *Is it inductive or capacitive? Be specific*.

(c) inductance (*in henries*) or capacitance (*in farads*) that can be placed *in series* with the loop at the feed to resonate the antenna at $f = 100$ MHz; choose the element that will accomplish the desired objective.

5.30. Show that for the rectangular loop the radiation resistance is represented by

$$R_r = 31{,}171\left(\frac{a^2b^2}{\lambda^4}\right)$$

while for the elliptical loop is represented by

$$R_r = 31{,}171\left(\frac{\pi^2a^2b^2}{16\lambda^4}\right)$$

5.31 Assuming the direction of the magnetic field of the incident plane wave coincides with the plane of incidence, derive the effective length of a small circular loop of radius a based on the definition of (2-92). Show that its effective length is

$$\boldsymbol{\ell}_e = \hat{\mathbf{a}}_\phi jkS\sin(\theta)$$

where $S = \pi a^2$.

5.32. A circular loop of nonconstant current distribution, with circumference of 1.4λ, is attached to a 300-ohm line. Assuming the radius of the wire is $1.555 \times 10^{-2}\lambda$, find the

(a) input impedance of the loop

(b) VSWR of the system

(c) inductance or capacitance that must be placed across the feed points so that the loop becomes resonant at $f = 100$ MHz.

5.33. A very popular antenna for amateur radio operators is a square loop antenna (referred to as *quad antenna*) whose circumference is one wavelength. Assuming the radiation characteristics of the square loop are well represented by those of a circular loop:

(a) What is the input impedance (real and imaginary parts) of the antenna?

(b) What element (inductor or capacitor), and of what value, must be placed in series with the loop at the feed point to resonate the radiating element at a frequency of 1 GHz?

(c) What is the input VSWR, having the inductor or capacitor in place, if the loop is connected to a 78-ohm coaxial cable?

5.34. Design circular loops of wire radius b, which resonate at the first resonance. Find

(a) four values of a/b where the first resonance occurs (a is the radius of the loop)

(b) the circumference of the loops and the corresponding radii of the wires for the antennas of part (a).

5.35. Using the asymptotic form of (5-59b) for small argument, show that the radiation resistance of (5-64a) for a small loop of uniform current is given by

$$R_r = 20\pi^2(ka)^4 = 20\pi^2\left(\frac{C}{\lambda}\right)^4$$

5.36. Consider a circular loop of wire of radius a on the x-y plane and centered about the origin. Assume the current on the loop is given by

$$I_\phi(\phi') = I_0\cos(\phi')$$

(a) Show that the far-zone electric field of the loop is given by

$$E_\theta = \frac{j\eta ka}{2} I_0 \frac{e^{-jkr}}{r} \frac{J_1(ka\sin\theta)}{ka\sin\theta}\cos\theta\sin\phi$$

$$E_\phi = \frac{j\eta ka}{2} I_0 \frac{e^{-jkr}}{r} J_1'(ka\sin\theta)\cos\phi$$

where

$$J_1'(x) = \frac{dJ_1(x)}{dx}$$

(b) Evaluate the radiation intensity $U(\theta, \phi)$ in the direction $\theta = 0$ and $\phi = \frac{\pi}{2}$ as a function of ka.